SURFACE CHARACTERIZATION AND ADHESION OF PLASMA-MODIFIED POLYIMIDES

by

Joannie W. Chin

Thesis submitted to the Faculty of the
Virginia Polytechnic Institute and State University
in partial fulfillment of the requirements for the degree of :

Master of Science
in
Chemistry

APPROVED:

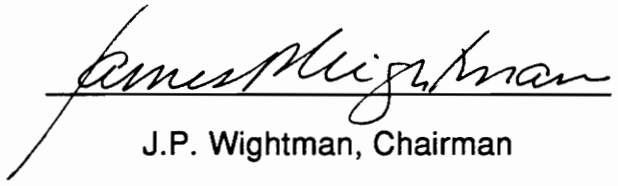

J.P. Wightman, Chairman

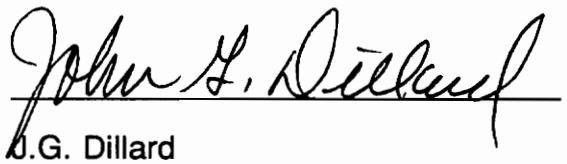

J.G. Dillard

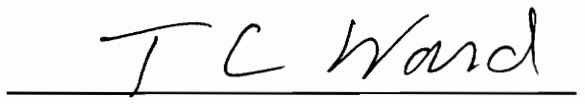

T.C. Ward

August 1991
Blacksburg, Virginia

SURFACE CHARACTERIZATION AND ADHESION

OF PLASMA-MODIFIED POLYIMIDES

by

Joannie W. Chin

Committee Chairman: Dr. James P. Wightman

Chemistry

(ABSTRACT)

LaRC-TPI, an aromatic thermoplastic polyimide, and Kapton®, a poly(pyromellitimide) were exposed to oxygen, argon and ammonia plasmas as pretreatments for adhesive bonding. Chemical changes which occurred in the surface as a result of the plasma treatments were investigated using x-ray photoelectron spectroscopy (XPS) and infrared reflection-absorption spectroscopy (IR-RAS). Water contact angle analysis was utilized to characterize the changes in surface wettability, and the ablative effects of the plasmas were monitored using ellipsometry and high resolution scanning electron microscopy (HR-SEM).

Both XPS and IR-RAS results revealed the formation of polar functional groups at the surface. Contact angle analysis showed enhanced water wettability of the plasma-treated surfaces. As monitored by ellipsometry, oxygen and argon plasmas were seen to be highly ablative, whereas an ammonia plasma was only moderately so. HR-SEM micrographs revealed texturized surfaces in the case of oxygen and argon plasmas, but not in the case of ammonia plasma. Oxygen and argon plasmas appear to react with the polyimides via a fragmentation/oxidation mechanism, forming a loosely attached layer composed of low molecular weight polymer chains. The effect of

ammonia plasma is postulated to be imide ring-opening resulting in the formation of amide functional groups.

The 180° peel test was utilized to determine the receptability of the plasma-treated polyimide surfaces toward bonding with other polymeric materials. Adhesives used were a pressure sensitive acrylate and poly(ether sulfone). The pressure sensitive adhesive, although not representing a realistic bonding situation, does represent a system which presents the least disturbance to the plasma-modified layer, allowing the physical nature of the plasma-treated surface to be probed.

The peel test values of the pressure sensitive adhesive/plasma-treated polyimide systems fell below the level of the non-treated controls, regardless of the plasma treatment used. Peel surface analysis revealed the presence of polyimide on the pressure sensitive adhesive failure surface, indicating failure in the plane of a weak boundary layer created by plasma. The removal of the weak boundary layer by solvent treatment restored the peel values to the level of the controls. Bonding of Kapton® films with poly(ethersulfone) showed an opposite trend; peel strengths of the plasma-treated samples all showed improvements versus the nonplasma-treated control.

Plasma treatments of LaRC-TPI which had been deliberately contaminated with mold release and high density polyethylene illustrated showed that plasma treatments are not always detrimental to adhesion. It was shown that the physical as well as the chemical nature of a polymer surface is critical to the level of adhesion which can be achieved.

Acknowledgements

First and foremost, I would like to thank my advisor, Dr. James P. Wightman, for all of his guidance and support in this work. His insights, enthusiasm and willingness to help have been invaluable. Also contributing to the quality of this M.S. experience has been the many opportunities which have been provided by Dr. Wightman to attend meetings, present papers and meet with renowned scientists in the field of adhesion.

I also thank Dr. J.G. Dillard and Dr. T.C. Ward for serving on my committee and for their helpful suggestions and technical guidance. Thanks also to Dr. J.M. Tanko for his insight into free radical reactions.

The financial support of the National Aeronautics and Space Administration (NASA) as well as the graduate fellowship provided by the Adhesive and Sealant Council, Inc. are gratefully acknowledged. I also thank Dr. Terry St. Clair and Mr. Don Progar from NASA-Langley Research Center for their assistance in providing the LaRC-TPI material and also for their expertise in polyimides.

I also extend my warmest thanks to Frank Cromer, for his patience in training and assisting on the instruments in the surface lab, to Steve McCartney for the high resolution scanning electron micrographs, and to Dr. Dave DIllard and Yong Bao for the use of and training on the slip/peel tester.

Thanks also to my fellow group members, who are never too busy to help, answer questions or just be supportive. A special thanks to Francis Webster for assistance and set-up of the infrared experiments. I would also like to thank the wonderful individuals in the CASS office - Virginia Keller, Katy

Hatfield and Kim Linkous - whom I can always count on to be cheerful, friendly and helpful.

Last, but not least, I would like to thank my husband, Albert, for all of his understanding and support through this sometimes trying period and for spending many evenings alone while I worked; my parents, Dr. and Mrs. Hsien Chang Wang for their encouragement and for engraining in me the value of education; and my sisters, Nancy and Amy, for their love and prayers throughout this endeavor.

Dedication:

To my husband, Albert, and my parents

TABLE OF CONTENTS

		Page
I.	**Introduction**	**1**
II.	**Literature Review**	**4**
	2.1. Polyimides	4
	2.2. Plasma Fundamentals	10
	2.3. Plasma Treatment of Polymers	15
	2.3.1. Plasma Reactions with Solid Surfaces	15
	2.3.2. Application to Polymers	18
	2.3.3. Application to Polyimides	19
	2.4 Theories of Adhesion	21
	2.4.1. Mechanical Adhesion	21
	2.4.2. Diffusion Theory	22
	2.4.3. Electrostatic Theory	23
	2.4.4. Adsorption	24
	2.5. Peel Testing	26
III.	**Experimental**	**30**
	3.1. Materials	30
	3.2. Sample Preparation	31
	3.3 Plasma Treatments	33

Page

3.4. X-ray Photoelectron Spectroscopy (XPS or ESCA) 34

3.5. Infrared Reflection-Absorption Spectroscopy (IR-RAS) 39

3.6. Contact Angle Analysis 40

3.7. Ellipsometry 45

3.8. High Resolution Scanning Electron Microscopy (HR-SEM) 45

3.9. Adhesion Testing 46

3.9.1. Preparation of Adhesive Joints 46
3.9.2. Peel Testing 47
3.9.3. Analysis of Failure Surfaces 49

IV. Results and Discussion 50

4.1. Surface Characterization of Plasma-treated LaRC-TPI 50

4.1.1. Contact Angle Analysis 50
4.1.2. X-ray Photoelectron Spectroscopy (XPS) 52

4.1.2.1. Atomic Composition 52
4.1.2.2. Curve-fitted Results 57
4.1.2.3. Angle Dependent XPS 66
4.1.2.4. Atmospheric Shielding of Argon Plasma-treated LaRC-TPI 70
4.1.2.5. Lithium Fluoride Shielding Experiments 72

4.1.3. Infrared Reflection-Absorption Spectroscopy (IR-RAS) 74
4.1.4. Plasma Etch Rate Studies 82

Page

4.1.5. High Resolution Scanning Electron Microscopy (HR-SEM) 84

4.2. Surface Characterization of Plasma-treated Kapton 87

4.2.1. Contact Angle Analysis 87
4.2.2. X-ray Photoelectron Spectroscopy 89

4.2.2.1. Atomic Composition 89
4.2.2.2. Curve-fitted Results 89
4.2.2.3. Lithium Fluoride Shielding Experiments 96

4.2.3. Plasma Etch Rate Studies 99
4.2.4. High Resolution Scanning Electron Microscopy 101

4.3. Postulated Plasma Reaction Products 103

4.4. Peel Testing 109

4.4.1. Bonding with Scotch Magic Tape 109
4.4.2. Methanol Washing of Plasma-treated Surfaces 119
4.4.3. Fluorine Contamination Experiments 120
4.4.4. Oxygen Plasma Treatment of High Density Polyethylene 124
4.4.5. Kapton Bonding With Poly(ethersulfone) 131

V. Summary 136

VI. References 139

Appendix 151

Vita 155

List of Tables

Table		Page
2.1	Constituents of oxygen, argon and ammonia plasmas.	13
2.2	Comparison of plasma component and bond energies.	16
4.1	XPS analysis of non-imidized, imidized, oxygen plasma, argon plasma and ammonia plasma-treated LaRC-TPI.	53
4.2	Results from curve-fitted C1s, O1s and N1s photopeaks for non-treated and plasma-treated LaRC-TPI.	60
4.3	Angle dependent XPS atomic concentrations for LaRC-TPI.	69
4.4	XPS atomic concentration data for argon plasma-treated LaRC-TPI, exposed and unexposed to atmosphere subsequent to plasma treatment.	71
4.5	XPS atomic concentrations for LiF shielding of plasma-treated LaRC-TPI.	73
4.6	Identification of major bands in IR-RAS spectrum of non-treated LaRC-TPI.	77
4.7	IR-RAS band assignments for plasma-treated LaRC-TPI.	80
4.8	XPS analysis of non-treated, oxygen plasma, argon plasma and ammonia plasma-treated Kapton®.	90
4.9	Results from curve-fitted C1s, O1s and N1s photopeaks for non-treated and plasma-treated Kapton®.	91
4.10	XPS atomic concentrations for LiF shielding of plasma-treated Kapton®.	98
4.11	XPS analysis of LaRC-TPI/Magic Tape peel surfaces, 15° take-off angle.	117
4.12	XPS analysis of Kapton®/Magic Tape peel surfaces, 15° take-off angle.	118
4.13	XPS analysis of Kapton®/PES peel surfaces, 45° take-off angle.	135
A.1	Functional groups and binding energies of XPS standards.	153

List of Figures

Figure		Page
2.1	Synthesis of a polyimide from a dianhydride and diamine.	6
2.2	Structure of the poly(pyromellitimide) Kapton®.	8
2.3	Structure of LaRC-TPI.	9
2.4	Plasma classification by electron energy and density.	11
2.5	ASTM peel testing configurations.	27
3.1	Schematic of x-ray photoelectron spectroscopy (XPS) experiment.	35
3.2	Schematic of angle dependent x-ray photoelectron spectroscopy (AD-XPS) experiment.	37
3.3	Schematic of infrared reflection-absorption (IR-RAS) experiment.	41
3.4	Diagram of Harrick retro-mirror reflection accessory.	42
3.5	Contact angle analysis showing vector resolution of interfacial forces.	44
3.6	180° peel testing configuration.	48
4.1	Results of water contact angle analysis on non-treated and plasma-treated LaRC-TPI.	51
4.2a	Atomic concentrations of C, O and N on LaRC-TPI surface as a function of oxygen plasma exposure time.	54
4.2b	Atomic concentrations of C, O and N on LaRC-TPI surface as a function of argon plasma exposure time.	55
4.2c	Atomic concentrations of C, O and N on LaRC-TPI surface as a function of ammonia plasma exposure time.	56
4.3	Curve-fitted C1s photopeaks for (a) non-imidized and (b) fully imidized LaRC-TPI.	59
4.4	Curve-fitted LaRC-TPI C1s photopeaks for (a) non-treated (b) oxygen plasma (c) argon plasma (d) ammonia plasma.	62
4.5	Hypothetical structure of ammonia plasma-treated LaRC-TPI.	67

		Page
4.6	C1s photopeaks from angle dependent XPS experiments. (a) oxygen plasma (b) ammonia plasma (c) argon plasma.	68
4.7	Reflection-absorption infrared spectra. (a) non-imidized LaRC-TPI (b) fully imidized LaRC-TPI.	76
4.8	IR-RAS difference spectra of plasma-treated LaRC-TPI. (a) oxygen plasma (b) ammonia plasma (c) argon plasma.	79
4.9	Comparison of etch rates of oxygen, argon and ammonia plasmas on LaRC-TPI.	83
4.10	High resolution scanning electron micrographs of 20 minute plasma-treated LaRC-TPI surfaces. (a) oxygen plasma (b) argon plasma (c) ammonia plasma.	86
4.11	Results of water contact angle analysis on non-treated (as-received) and plasma-treated Kapton®.	88
4.12	Curve-fitted Kapton® C1s photopeaks. (a) non-treated (b) oxygen plasma (c) argon plasma (d) ammonia plasma.	92
4.13	Hypothetical structure of ammonia plasma-treated Kapton®.	97
4.14	Comparison of etch rates of oxygen, argon and ammonia plasmas on Kapton® polyimide.	100
4.15	High resolution scanning electron micrographs of 20 minute plasma-treated Kapton® surfaces. (a) oxygen plasma (b) argon plasma (c) ammonia plasma.	102
4.16	Postulated reaction mechanisms for the formation of hydroxyl groups in oxygen plasma-treated materials.	105
4.17	Photoreduction of benzophenone and subsequent plasma reactions to form carboxylic acids, amides and esters.	106
4.18	Formation of carbonate functionality through cleavage of the ether linkage in Kapton® polyimide.	108
4.19	XPS C1s photopeak of Scotch® Magic® Tape.	110
4.20	Peel test results for plasma-treated LaRC-TPI/Magic Tape.	112
4.21	Peel test results for plasma-treated Kapton®/Magic Tape.	113
4.22	Proposed structure of weak boundary layer created by plasma.	116

		Page
4.23	Peel test results for LaRC-TPI/Magic Tape, following plasma treatment and methanol washing.	120
4.24	Peel test results for Kapton®/Magic Tape, following plasma treatment and methanol washing.	121
4.25	C1s photopeaks for (a) non-treated LaRC-TPI (b) oxygen plasma-treated LaRC-TPI (c) oxygen plasma-treated LaRC-TPI followed by methanol wash.	123
4.26	Peel test results for non-treated LaRC-TPI, fluorocarbon-contaminated LaRC-TPI, and fluorocarbon-contaminated LaRC-TPI followed by 20 minute oxygen plasma.	125
4.27	XPS C1s photopeaks of fluorocarbon-contaminated LaRC-TPI following oxygen plasma exposure times of: (a) 0 minutes (b) 1 minute (c) 5 minutes (d) 10 minutes (e) 20 minutes.	126
4.28	Contact angle analysis of as-received, solvent cleaned and oxygen plasma-treated high density polyethylene.	128
4.29	XPS C1s photopeaks for (a) as-received and (b) oxygen plasma-treated high density polyethylene.	129
4.30	Peel test results for as-received and oxygen plasma-treated high density polyethylene.	130
4.31	Chemical structure of poly(ethersulfone).	132
4.32	Peel test results for plasma-treated Kapton®/PES.	133
A.1	Chemical structures of XPS standards.	152

List of Abbreviations

AD-XPS	angle dependent x-ray photoelectron spectroscopy
ASTM	American Society for Testing and Materials
CASING	crosslinking by activated species of inert gases
ESCA	electron spectroscopy for chemical analysis
ESR	electron spin resonance
FTIR	Fourier transform infrared
FWHM	full width at half maximum
HDPE	high density polyethylene
HR-SEM	high resolution scanning electron microscopy
IR-RAS	infrared reflection-absorption spectroscopy
LaRC-TPI	Langley Research Center - thermoplastic polyimide
NMP	N-methyl pyrrolidone
NMR	nuclear magnetic resonance
PES	poly(ethersulfone)
PMDA-ODA	pyromellitic dianhydride-oxydianiline
PSA	pressure sensitive adhesive
RF	radio frequency
STEM	scanning transmission electron microscopy
T_g	glass transition temperature
UV	ultraviolet
VUV	vacuum ultraviolet
WLF	Williams Landel Ferry
XPS	x-ray photoelectron spectroscopy

I. Introduction

The use of polymeric materials has been steadily increasing over the last several decades. A combination of high specific strength, low weight and continually improving mechanical and thermal properties make polymers highly desirable in a myriad of applications. Polyimides, in particular, with excellent dielectric properties and high thermal and chemical resistance, are being widely utilized in structural applications such as composites and adhesives, as well as in microelectronics and electrical components.

Often an application will require that polymers be adhesively bonded to other polymers or metals or be surface coated with materials of different properties. One problem encountered in this process is that polymers, in comparison to metals or ceramics, possess low surface free energies. This property is often an obstacle to effective adhesive bonding or coating, during which a given adhesive or coating must first spread out on and wet the substrate. Any material which does not wet well will not develop intimate molecular contact with the adhering substance and optimum levels of adhesion cannot be achieved.

To overcome this particular problem on polymer surfaces, modification techniques are employed to increase the surface energy/surface wettability, remove contaminant layers and/or increase the surface area available for bonding. The list of techniques used is quite extensive and includes such treatments as abrasion/gritblasting, chemical etching, solvent cleaning, oxidation, heat treatments, additives/sizing agents, high energy radiation and many others. A disadvantage of some of these techniques is that surface

appearance and bulk properties of the treated polymers may be changed in an undesirable manner, not to mention that some of these treatment processes are environmentally unsound and represent workplace hazards.

In recent years, the use of low temperature gaseous plasmas has found widespread utility in the area of adhesion. It has been well-documented that such treatments are capable of inducing significant changes in surface chemistry and wettability without detectable changes in material bulk properties or surface appearance. Also, the use of plasma is a "clean" process which does not release harmful by-products into the workplace or atmosphere.

In this study of surface pretreatment pertaining directly to adhesion, it is important to understand more completely the nature of the modified surface. It is known that polar functional groups are incorporated into polymer surfaces as a result of plasma treatment; however, what is not so well-known is the specific identity of those functional groups and in what way they have been incorporated into the original polymer structure. Such knowledge could lead to the ability to "tailor" treat a polymer surface to give optimum interaction with a given adhesive or coating material.

The objective of this work is two-fold. The first objective is to characterize the chemical and physical changes in the surface of LaRC-TPI and PMDA-ODA polyimides, both commercially important materials, after treatment with oxygen, ammonia and argon plasmas. The primary focus of the second objective is to study the receptability of the plasma-treated surface toward bonding with other polymers. It is proposed that the use of plasma pretreatment will increase the surface energy of the polyimides due to increases in the concentration of surface polar functional groups. This increase in surface polarity should

subsequently increase the degree of interaction with another polar polymer as quantified by peel testing.

II. Literature Review

The major areas covered in this thesis including polyimides, plasma theory, plasma treatment of polymers (particularly polyimides), theories of adhesion and peel testing of thin films, are reviewed in this chapter. An understanding of each of these areas is necessary in order to understand surface modification and adhesive bonding of polyimides.

2.1. Polyimides

Due to an attractive combination of dielectric, mechanical, chemical and thermal properties, aromatic polyimides are being increasingly utilized in microelectronics, electrical and aerospace applications. The availability of numerous monomers makes it possible to produce a seemingly infinite variety of polyimides. Specific applications in electronics include such uses as insulators for printed circuit boards, motors, wire and cable, passivation coatings, alpha particle barriers, planarization coatings, interlayer dielectrics and photoresists [1,2]. Polyimides are also frequently utilized as high performance composite matrix resins [3-6].

Polyimides are synthesized in a condensation reaction between a dianhydride and diamine, with the specific dianhydride and diamine dictated by the desired backbone structure and ultimate end-use. Due to the insolubility of high molecular weight polyimides, it is necessary to utilize a two-step synthesis. In the first step, an amidation reaction is carried out under mild conditions (~70°C) in a polar solvent, yielding a high molecular weight poly(amic-acid). At

this point, the polymer is still soluble and processable. Cyclization or imidization is then carried out in the second step at temperatures > 150°C, sometimes exceeding 300°C, yielding water as a by-product of the reaction. This mechanism is illustrated in Figure 2.1. It is also possible to chemically imidize the polymer in dehydrating agents such as acetic anhydride/pyridine [2,7,8]. A wide variety of aliphatic, aromatic, linear and crosslinked polyimides have been synthesized and studied [1,7,9].

Polyimides synthesized from aromatic dianhydrides and aromatic diamines exhibit particularly outstanding thermal and chemical resistance. Most aromatic polyimides are insoluble in common organic solvents after complete imidization. Other properties which make polyimides high performance engineering materials include high values of toughness, impact strength, modulus and excellent tensile, flexural and compressive strengths. Glass transition temperatures (T_g) of aromatic polyimides are strongly dependent on structure and have been found to be as high as 400°C for certain poly(pyromellitimides). Flexible units in the backbone such as ether, thioether, or aliphatic carbons are known to decrease the T_g [7]. Since the T_g determines both the maximum use temperature as well as ease of processability, compromises between high temperature performance and processability are often necessary.

One of the better known aromatic polyimides is poly(N,N'-p,p"-oxydiphenylene-pyromellitimide), also recognized in film form under the tradename Kapton®. It is synthesized from pyromellitic dianhydride and oxydianiline, to yield a linear, para-oriented polymer with a T_g of 360-420°C and no solubility in any known organic solvent. The chemical structure of

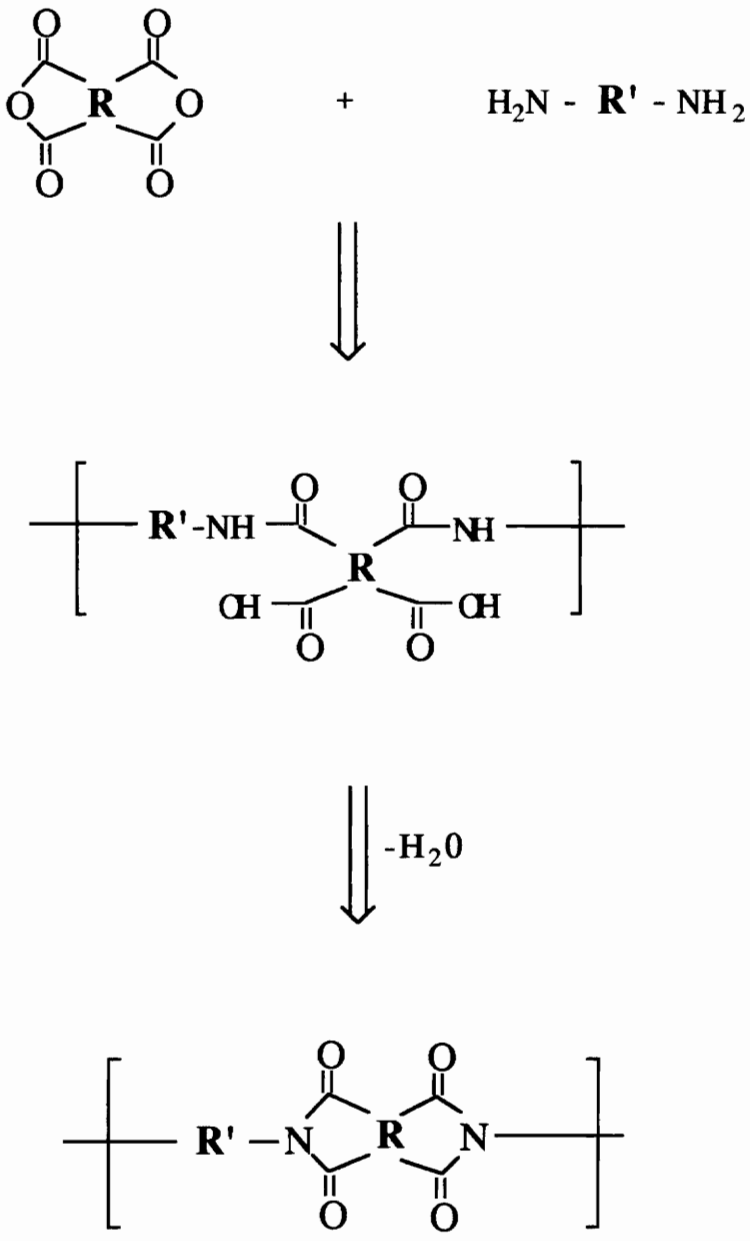

Figure 2.1: Synthesis of a polyimide from a dianhydride and diamine.

Kapton® is shown in Figure 2.2. Kapton® was developed in the 1960s by researchers at the DuPont Company and has been studied extensively and well-characterized [10-16]. Kapton® films are used in wire/cable insulation, flexible circuitry, transformer and capacitor insulation; its excellent physical, chemical and dielectric properties are well-documented [17]. It shows little crystallinity, presumably due to the immobility of the chains at processing temperatures and exhibits no melting or softening transitions [1].

The demand for improved processability has led to the development of thermoplastic polyimides. One of the first of this new class was LaRC-TPI (Langley Research Center-Thermoplastic Polyimide), pioneered by researchers at NASA-Langley Research Center [18-20]. Unlike the early polyimides which were intractable after imidization, LaRC-TPI can be de-volatilized and imidized at relatively low temperatures and then further melt processed. This new method of processing also eliminates problems associated with trapped water of imidization which can lead to voids in fabricated parts.

LaRC-TPI is synthesized from diaminobenzophenone and benzophenone-tetracarboxylic dianhydride. The resulting polymer has a meta-oriented backbone structure as seen in Figure 2.3, which lowers the Tg and results in improved melt processability, while retaining thermo-oxidative stability. LaRC-TPI has been found to be potentially useful in the areas of films, fibers, moldings, structural adhesives and composite matrix resins [21-23].

LaRC-TPI has a glass transition temperature in the range of 230-260°C, dependent on processing conditions. A transient form of crystallinity has been detected in the molding powder, but it has been found that high temperature thermal treatment decreases the degree of crystallinity and creates an

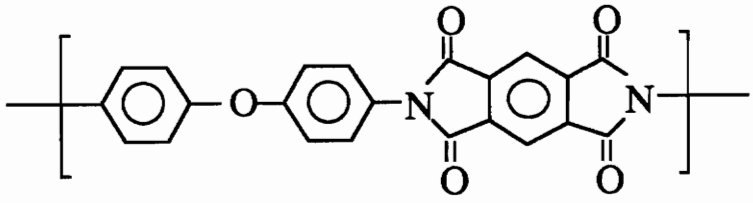

Figure 2.2: Structure of the poly(pyromellitimide) Kapton®.

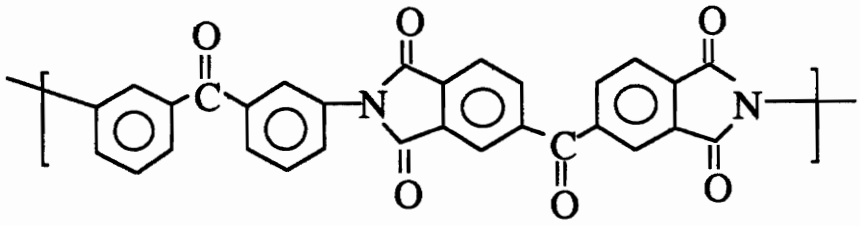

Figure 2.3: Structure of LaRC-TPI.

amorphous polymer [24]. Recent work has shown that LaRC-TPI can be thermally conditioned so that crystallinity can be regenerated [25]. Still more recent work has focused on replacing the mutagenic diaminobenzophenone monomer by developing an isomeric LaRC-TPI synthesized from isophthaloyldiphthalic anhydride and metaphenylenediamine [26].

2.2. Plasma Fundamentals

A plasma is defined as a partially ionized gas composed of ions, electrons and neutral species. In a macroscopic sense, it is spatially neutral, consisting of an equal concentration of positive and negative species. The degree of ionization can range from being very low, as in this particular case of interest, to high, such as in thermonuclear reactions [27].

Plasmas can be man-made or naturally occurring, and are categorized by particle density and energy, as shown in Figure 2.4. In the radio frequency-generated (RF) plasmas of interest in this work (also termed "cold" plasmas), the average electron energy ranges from 1 to 10 eV and electron density from 10^9 to $10^{12}/cm^3$. Energy sources capable of generating plasmas include chemical energy, electrical discharges, electro-magnetic fields, photons and shock waves, to name just a few [28].

In an RF plasma, the free electrons in a gas are accelerated in an RF field between two electrodes and increase in energy. This energy is then transferred to gas molecules through collisions which result in ionization and the subsequent formation of ions, radicals and metastable species. Electrons released from the ionization process are further accelerated, causing further

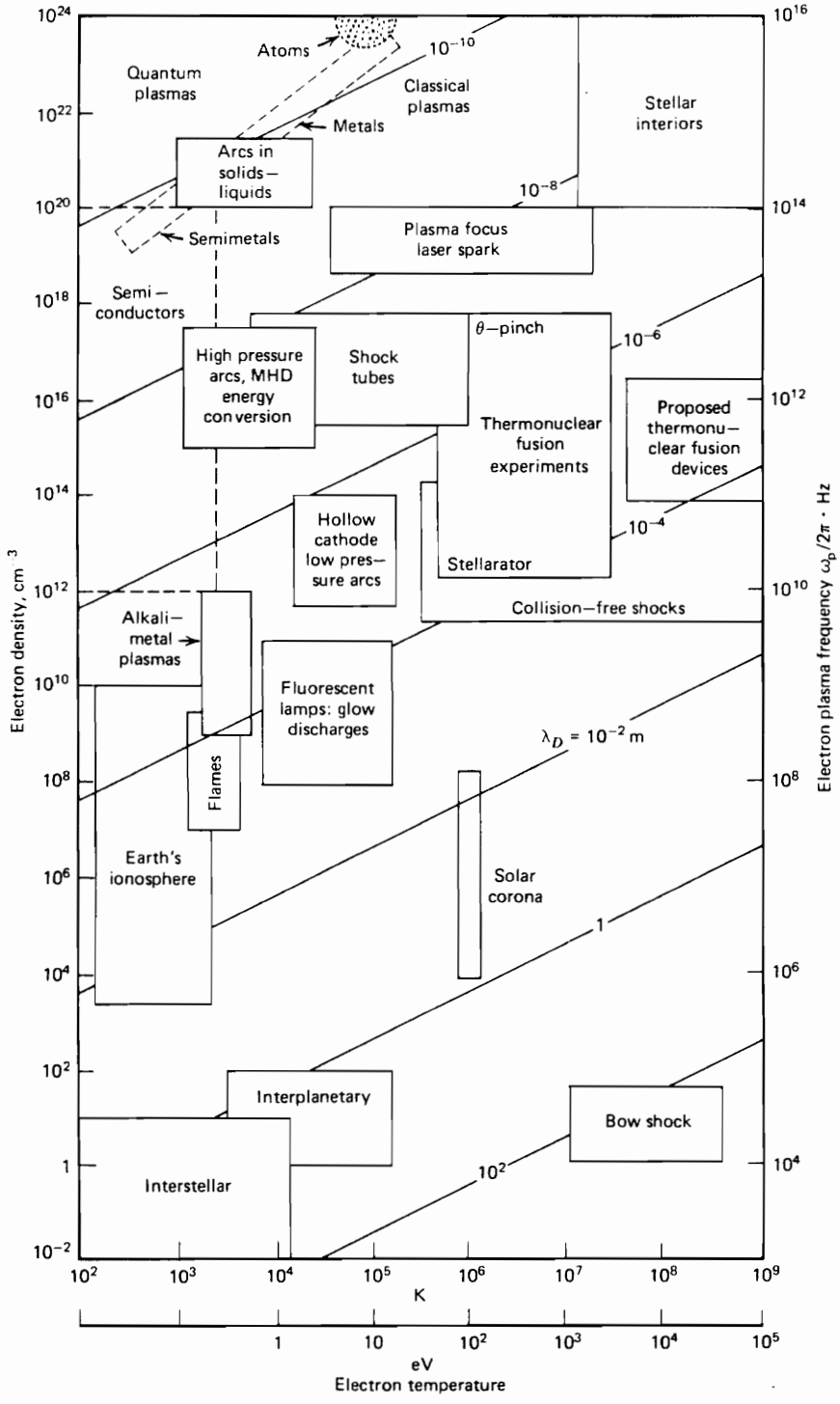

Figure 2.4: Plasma classification by electron energy and density.

ionization which continues until extensive breakdown of the gas occurs. As this continues, the current within the gas rises, and the discharge is considered to be established. At this point, there is an equilibrium between the rate of formation and rate of recombination of ions and electrons [29,30]. The recombination of dissociated species in a plasma causes energy to be given off in the form of photons. It is these photons which create the characteristic visible glow seen in many plasmas; this property gives rise to the alternative name "glow discharge" [31].

RF plasmas consist of a few parts per million ions and between 2-20% free radical species, the remainder being made up of neutral and excited state species. As stated above, plasmas are also excellent sources of ultraviolet (UV) and vacuum ultraviolet (VUV) radiation, which are also sufficiently energetic to induce reactions in organic materials. The wavelengths of the UV and VUV photons are dependent on the particular gas used in the discharge [30,32].

The known species contained in the three plasmas utilized in this work - oxygen, argon and ammonia - are listed in Table 2.1 [27,30,33,34]. Oxygen plasma contains a variety of species, including atomic(radical) species, atomic ions, molecular ions and metastable excited state species. In an argon plasma are contained positive ions, electrons and the relatively long-lived metastable species Ar^*. It has been observed that argon plasma-modified fluoropolymers are strikingly similar to samples bombarded by low energy Ar ions at low current. This suggests that the outermost surface reactions are dominated by direct energy transfer from Ar^+ and Ar^* species [33]. The situation within an ammonia plasma has not been well-characterized. It is postulated that the active species are the radical, positive and negative ionic forms of N, H, NH and

Table 2.1: Constituents of oxygen, argon and ammonia plasmas.

Plasma	**Constituents**
Oxygen	O_2^+, O_2^-, O^+, O^-, $O\cdot$, O_3, O_2^* (metastable)
Argon	Ar^+, Ar^*(metastable)
Ammonia	N, H, NH, NH_2. (cationic, anionic and radical forms)

NH_2. NH_2· is thought to be particularly reactive, especially with aromatic ring systems [34].

Due to differences in mass, the various species in an RF discharge differ widely in kinetic energy and hence temperature (through the relation E = kT). Electrons are approximately two orders of magnitude greater in temperature than ions and neutral species, which are roughly at ambient temperature. This absence of thermal equilibrium allows the existence of highly energetic electrons, capable of inducing chemical reactions, in a gas which is at ambient temperature. It is this property of an RF plasma which makes it ultimately useful for the processing of thermally labile materials, such as polymers [27,30].

The actual physical and chemical properties of a particular plasma are greatly dependent on the type of gas or gases used, the geometry of the reactor and electrodes, operating power and pressure, gas flow rate and temperature [31]. RF plasmas are usually generated in the pressure range between 0.1 and 10 torr. If the pressure is too low, the electron mean free path is too long for significant collisions with gas molecules to occur; if the pressure is too high, the mean free path is short and the formation of localized conduction pathways can occur, resulting in no discharge [27].

A study by Bell and Kwong involving an oxygen plasma showed that the conversion and yield of atomic oxygen was determined primarily by electric field strength (power), gas pressure and gas flow rate [35]. Other studies have shown a dependence on other factors such as contact or residence time, surface characteristics of the reactor, moisture content of inlet oxygen gas and shunt impedance of the discharge [36,37].

2.3. Plasma Treatment of Polymers

2.3.1. Plasma Reactions with Solid Surfaces

When an organic material is exposed to an RF plasma, essentially all significant reactions which occur are based on free radical chemistry, initiated by both chemically active species and UV/VUV radiation [27,32]. These surface free radicals are detectable by such methods as electron spin resonance spectroscopy (ESR) [38].

Both the particle flux as well as the vacuum ultraviolet radiation in a plasma are capable of reacting with solid surfaces. A comparison of organic bond energies with energies of the species contained in plasmas is made in Table 2.2. It is evident that plasmas contain more than sufficient energy to homolytically cleave organic bonds [27]. Energy can be transferred to surfaces and dissipated through radiation, neutral particle fluxes (metastable and radical species) and ionic particle fluxes. All of these energetic species lead to formation of radical species in the surface as well as moderate substrate heating effects [30]. It has been suggested by Clark and Dilks that the topmost surface reactions are dominated by particle fluxes while VUV radiation dominates reactions further into the bulk of the material. However, both effects were observed to result in the same types of free radical species [33].

The formation of free radicals results in the abstraction of atoms or molecular fragments, which can then further react to form volatile species which are ultimately removed by the vacuum system. Surface radicals may also react with gas species and/or adjacent surface free radicals. These free radical reactions lead to surface molecular weight changes - chain scission,

Table 2.2: Comparison of plasma component and bond energies.

	Energy (eV)
Plasma Species	
Electrons	0-20
Ions	0-2
Metastables	0-20
UV/visible radiation	3-40
Organic Bonds	
C-H	4.3
C-N	2.9
C-Cl	3.4
C-F	4.4
C=O	8.0
C-C	3.4
C=C	6.1

crosslinking, branching - dependent on the particular polymer and the plasma gas used. Almost always, dramatic changes in surface wettability, reactivity and chemical composition are observed after plasma exposure [30-32].

Plasma etching can also occur in certain materials. This effect can result in increases in surface roughness, especially in semi-crystalline materials in which differences in density between the crystalline and amorphous regions cause differential etching to occur. It is generally observed that ablation is primarily a property of polymers containing hetero-atoms such as oxygen in the backbone, which can act as active sites for chain scission. Fluorocarbon and hydrocarbon-based polymers are not observed to undergo chain scission or ablation to any great extent. This ablative effect is also useful in removal of low molecular weight organic contamination or weakly attached layers on both organic and inorganic surfaces [27,30,32].

Although plasmas can be extremely aggressive toward an organic surface, their reactions are limited only to the topmost molecular layers. Hence, the bulk physical properties and visual appearance of a material remain undisturbed while significant changes are occurring in the surface properties. This allows for selective tailoring of the surface while retaining desired bulk properties. Improvements in surface wettability and increases in surface energy, often due to both surface cleaning effects and increases in the concentration of polar groups, are all factors which may lead to improved adhesion of various organic or inorganic coatings, inks, adhesives and other materials [30-32].

2.3.2. Application to Polymers

Plasma treatments have been widely used with polymers in a variety of areas, ranging from products encountered in everyday usage to highly technical and sophisticated applications. Polymers, in general, possess low energy surfaces and usually must be surface pretreated in some manner to increase surface free energy and improve practical adhesion.

Fluorine-based polymers are perhaps the best example of this property. The use of plasma treatments in place of corrosive chemical etches on fluoropolymers such as polytetrafluoroethylene has shown great promise [39-42]. Polyolefins, or hydrocarbon-based polymers, also possess low surface free energies and poor wettability. Plasma treatment with inert gases, a process known as CASING (Crosslinking by Activated Species of Inert Gases) appears to be particularly effective in modifying the surface chemistry by crosslinking low molecular weight surface molecules (postulated to have been excluded from the crystallization process) to form a strong adherent layer [43-46]. Treatment with reactive plasmas such as oxygen, nitrogen and nitrous oxide have also been observed to improve wettability and printability on polyolefin surfaces [47-50].

Other polymers such as polycarbonate, poly(methylmethacrylate) [51,52], poly(phenylene sulfide) [53], poly(ethylene terephthalate) [54-57], polyoxymethylene, cellulose acetate, polyacrylonitrile, and polyamide [50] have also been plasma treated and studied extensively by a variety of techniques.

Polymers used in biomedical applications need to be surface-modified in order to function effectively in the various physiological environments which may be encountered. It has been found that protein and blood platelet

adsorption can be enhanced or inhibited on various polymeric substrates depending on the plasma treatment employed [58-60]. Grafting of anti-clotting substances such as heparin onto the surfaces of implant materials can be accomplished by first activating the surface with plasma [34]. Plasmas can also be utilized to create hydrophobicity gradients on surfaces to serve as diagnostic screening tools for blood and tissue compatibility evaluations [61].

Plasma treatment of natural and synthetic fibers has been used to improve dyeability, chemical and thermal resistance, and adhesion to matrix resins [62-65]. In particular, the use of graphite fibers in advanced composite materials has necessitated the investigation of plasma treatment of the fibers [66-69].

Adhesive bonding of fiber-reinforced polymer composites is still the only viable method of joining composite sections. Plasma treatment has been studied as a method of surface preparation for bonding both thermoplastic and thermoset matrix composites [70-72]. Plasma treatments have been found not only to incorporate additional polar groups into the surface, but to serve as an effective cleaning process for removal of fluoropolymer release cloth residues [73].

2.3.3. Application to Polyimides

High performance polyimide materials are commonly used in two major categories: advanced structural materials and microelectronics/electrical applications. Plasma treatment is often used as a processing step in each of these two categories. Other techniques utilized for surface pretreatment of

polyimides include reactive ion beam etching and wet chemical treatments [74-77].

Moyer and Wightman have shown that the use of plasma on LaRC-160 (thermosetting polyimide)/graphite composites is an effective way to remove fluoropolymer release cloth residue as well as a way to increase surface polar groups. Oxygen plasma was found to be particularly effective in removing the fluoropolymer residue as demonstrated by surface characterization data as well as results from lap shear and Boeing wedge test studies [73]. Stancil et al. have shown interesting results following oxygen plasma treatment of composites composed of polyetherimide and a LaRC-TPI/polyethersulfone blend. It was found that oxygen plasma was able to simulate atomic oxygen exposure in low earth orbit (LEO) environments. Both ablative effects and loss of tensile properties were observed after prolonged exposure [78]. Other studies concerned with the impact of atomic oxygen in LEO have been carried out on Kapton® [79]. Changes in adhesion properties were also studied for plasma-treated polyetherimides [48].

In the electronics area, polyimide materials are commonly used as dielectric substrates in Very Large Scale Integration (VLSI) packaging technology. Metals used as interconnecting circuitry must form reliable and durable bonds to the underlying polyimide. Metals used for circuitry are often vapor-deposited or sputtered onto the surface of the polyimide. Enhancement of metal film adhesion is accomplished by exposure to oxygen, argon or nitrogen plasmas [80-83]. Researchers have also studied the surface texturing and etching of the polyimide substrates by plasma [84,85], as well as the effect

of the UV and VUV radiation given off in a plasma reactor on polyimide surface chemistry [86].

2.4. Theories of Adhesion

The term *adhesion* can be defined as the bonding together of two similar or dissimilar materials into one homogeneous structure. A number of theories have been proposed to explain adhesion-related phenomena; however, at the present time, there is no general or unified theory which applies to all situations. Although the heart of any adhesive joint lies in the interface, or more properly, the interphase region, other factors can also have an effect on bond strength. The following discussion will focus on the surface or interfacial aspects of adhesion and leave the structural and mechanical aspects to be discussed in the following section.

2.4.1. Mechanical Adhesion

Mechanical interlocking of a liquid or molten adhesive into the interstices of a rough, irregular substrate is perhaps the easiest theory to visualize. Many studies have shown the importance of surface roughness on increasing joint strength. As early as the 1940s, adhesion between rubber and textiles was explained by the embedment of the fiber ends into the rubber phase [87]. The adhesion of electrolessly-deposited metals to polymers is significantly increased if etching or roughening of the substrate has taken place, resulting in pits and pores [88]. Adhesion of polymers to a variety of metals, including

aluminum, copper and titanium, is also known to increase if the metal surface is anodized, nodularized or otherwise roughened [89-92].

Bikerman hypothesized that the main cause of joint failure is mechanical failure through weakly bound layers on adherend surfaces. These so-called weak boundary layers are often due to contamination resulting from poor surface preparation and other factors [93]. A properly prepared joint should not fail in the interphase region, but should exhibit cohesive failure in the adhesive or adherend. Removal of weak boundary layers by a variety of methods has been shown to improve bond strength [94-96]. A criticism of the weak boundary layer theory has been presented by Good, who states that little experimental evidence has been found in support of this principle, and that experimental data which does appear to support it is open to alternative explanations [97].

Although many examples exist in which mechanical interlocking appears to play a predominant role in adhesion, examples exist in which good adhesion to smooth surfaces such as mica or glass can still occur [88,98]. Thus, it is generally accepted that mechanical interlocking alone cannot explain the mechanism of adhesion, but does provide an enhancement to other theories.

2.4.2. Diffusion Theory

The diffusion theory, originally proposed by Voyutskii, states that when two polymers above their respective Tg's are in contact, interdiffusion of the chains across the interface can occur. This is obvious in situations involving autohesion, defined as the adhesion of a material to itself, such as seen in the self-tack of pressure sensitive adhesives, heat sealing of plastics, drying of emulsions and solvent-bonding of polymer pairs [99]. Voyutskii was able to

demonstrate that, as the interdiffusion between polymer pairs increased, the peel strength also increased [100].

When two dissimilar materials are involved, the situation becomes more complicated in that the thermodynamic compatibility of the two materials must be considered. Thermodynamic compatibility can be quantified through the use of the polymers' solubility parameters. Polymers with similar solubility parameters are more thermodynamically compatible [87]. For two polymers in contact in the presence of a solvent, the degree of interpenetration can be calculated by considering the average effective segment length of each polymer and the interaction parameters [101].

More quantitative treatments have been developed by Campion and Vasenin by working with theories of diffusion in liquids. Campion modified the Kauzmann-Eyring theory of diffusion in liquids to allow for segmental movement of polymer chains in vacancies. By calculations based on free volume, packing densities and cross-sectional areas for diffusion, it was possible to rate a series of hydrocarbon rubbers in order of their known autohesive behavior. Starting from Fick's first law of diffusion, Vasenin established the dependence of polymer interdiffusion on the concentration and nature of the diffusing molecule [87].

2.4.3. Electrostatic Theory

The electrostatic theory postulates that adhesion arises from charge transfer at the interface between two dissimilar materials, giving rise to electrical double layers. The double layers can be likened to two plates of a capacitor

and work is done in separating the two layers. Derjaguin and coworkers have been the principal proponents of this particular theory [102].

Particle adhesion to surfaces is electrostatic in nature; also, electrical discharges have been observed during the peeling of pressure sensitive adhesives from glass and metal substrates [87,103,104]. Contact charging between polymers and vapor-deposited metal layers is thought to arise from electron transfer [88]. The concept of ionic bonds, such as between metals and their oxides, is also generally accepted. Some researchers have observed that the application of external electromagnetic fields can result in increased bond strength [105]. However, the general consensus concerning this particular theory is that while electronic interactions are known to be present in adhesion, their contribution toward the total bonding force is small.

2.4.4. Adsorption

The main idea behind the theory of adsorption is that molecular interactions can occur across an interface. These interactions can be primary in nature, involving formation of covalent or ionic bonds, or secondary, such as in dipole/dipole, dipole/induced dipole, dispersion forces, acid-base interactions and hydrogen bonding interactions. Of these, only the dispersion forces are universal [87]. Evidence for primary bonding has been seen in studies involving rubber/brass bonding, in which cupric sulfide bonds were postulated, in interfacial reactions involving reactive functional groups, and in the use of silane and other organo-metallic coupling agents, to name just a few [87,88].

In the case of secondary interactions, in accordance with the theory of Fowkes, all polymers (except saturated hydrocarbons) are either acidic or basic

in a Lewis sense and their interactions with solvents, plasticizers, fillers, fibers, other polymers and inorganic surfaces are dominated by acid-base interactions [106-108]. Hydrogen bonding interactions are encompassed in this category, and what are commonly called "polar" interactions (dipole/dipole, dipole/induced dipole) are considered to be insignificant. The strength of acid/base interactions can be quantified through heats of interaction measured relative to test acid and base materials, by such techniques as calorimetry, inverse gas chromatography, contact angle analysis and FTIR/NMR spectral shifts [107].

Since it is known that dispersion forces vary with the inverse seventh power of the intermolecular distance and other forces decay even more quickly [109], adsorption interactions can only be significant if intimate molecular-level contact is made between adhesive and adherend. This can be accomplished if good wetting of the substrate occurs. According to the Young-Dupre equation,

$$W_A = \gamma_{lv} (1 + \cos \theta) \qquad (2.1)$$

the work of adhesion W_A is maximized if the contact angle θ of a material on a substrate is zero. An adhesive material will spontaneously spread and wet on a substrate only if the surface free energy γ_{lv} of the adhesive is less than or equal to the surface energy of the substrate. This is usually a problem since most polymer surfaces have low surface free energies and the adhesives used on them are higher in energy. Hence, surface pretreatment of polymers is usually necessary to improve surface energetics [110].

2.5. Peel Testing

When one or both adherends in an adhesive joint are flexible members, joint strength can be evaluated by peel testing. A variety of peel tests are in use, including the T-peel test, climbing drum peel, floating roller peel and 180° peel. A method to test the durability of peel joints in various hostile environments also exists. The geometries of these tests and their governing ASTM test standards are shown in Figure 2.5 [111-113].

Peel testing is a widely used test method which is relatively simple to carry out and represents a mode of failure under service conditions for certain geometries. It is a controlled rate test and forces measured in peel testing are also considered to be direct measurements of the work of detachment [114,115]. Anderson et al. have shown that peel testing can be used to calculate adhesive fracture energy values [112]. Other features which make the peel test useful from an analytical point of view are that the dependence of the peel strength on the peel angle allows investigation of the influence of stress geometry, and that approximate analyses of stress distributions and work of peeling can be performed [116]. Finally, because peel testing, like the Boeing wedge test, concentrates stresses at the interface, durability effects will be observed more readily and greater sensitivity toward environmental attack can be demonstrated [117].

Stress analysis of peel joints has been approached in various ways. Bikerman, DeBruyne, Kaelbe and Jouwersma have studied cases involving small strains and elastic deformation only. Since most practical adherends and adhesives undergo at least small amounts of plastic deformation and owe part of their success to their ability to undergo deformation, analyses have been

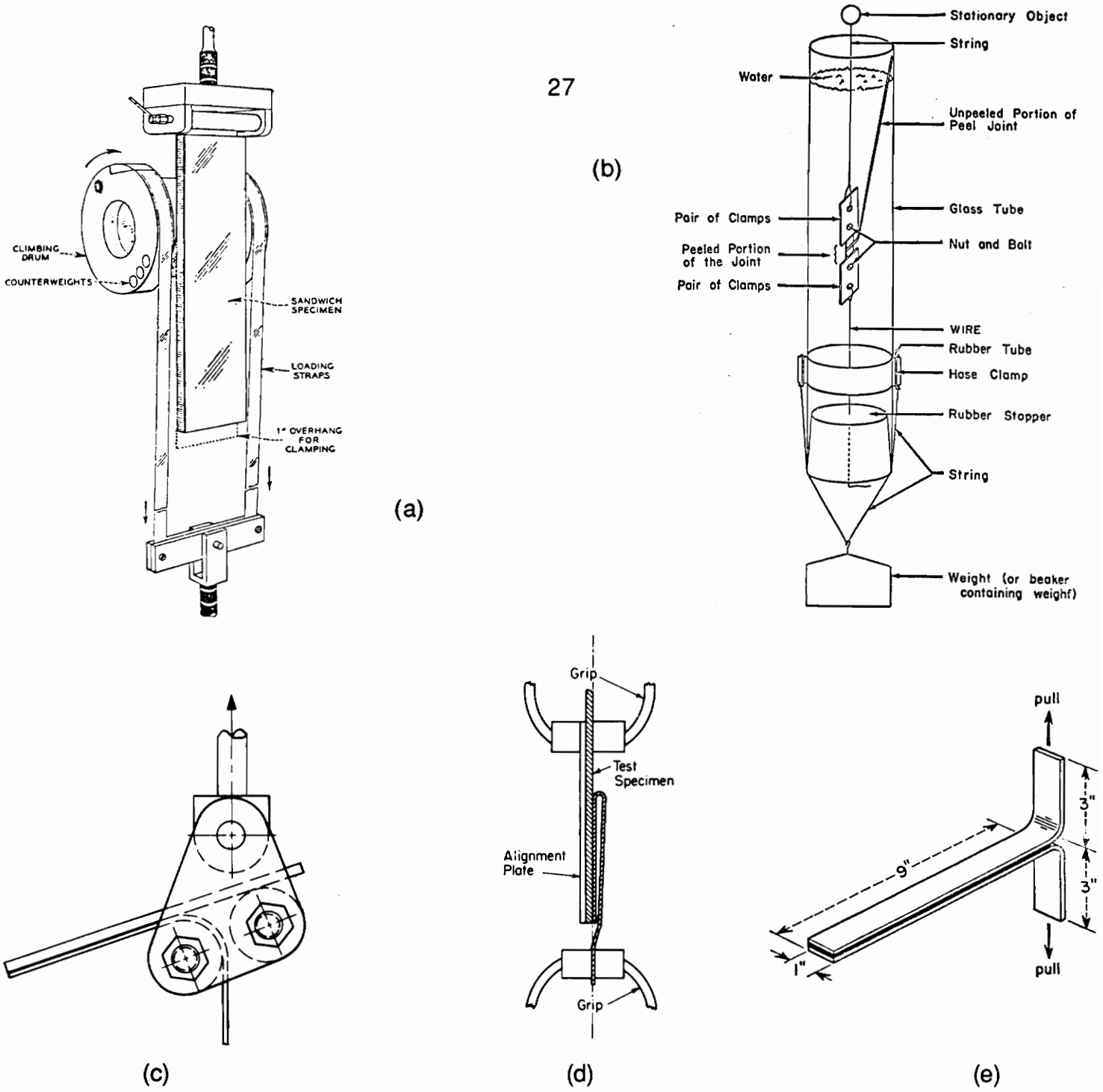

Figure 2.5: ASTM peel testing configurations: (a) D 1781 - climbing drum peel test (b) D 2918 - durability of adhesive joints stressed in peel (c) D 3167 - floating roller peel (d) D 903 - peel/stripping strength test (e) D 1876 - T-peel test.

extended to include large and small degrees of plastic deformation [116]. Analysis methods involving energy conservation can be applied to adhesive joints; this approach seeks to account for total work done in detaching the adherend [114,118,119]. Peeling processes can also be explained in terms of fracture mechanics and crack propagation, since the degree of mode I or mode II loading can be varied with the peel angle [112,120].

In peel testing, tensile stresses are concentrated at the peel front with a region of compressive stress immediately following. Since there is no dependence on the debonded length, peel strength is measured as a force per unit width. In some instances, there is a sharp initial spike in the peel force, after which a lower average value is seen. Other systems may exhibit erratic "slip-stick" behavior throughout testing. Shear stresses are more predominant in the adhesive layer from a zero degree peel angle to about 30-50°. From this point to 90°, more cleavage or opening mode stresses come into play. From 90° to 180°, cleavage stresses become increasingly dominant [87,112].

There are a number of uncertainties associated with peel testing. Much of the controversy lies in the question of whether or not the peel test is a true test of interfacial properties. Interpretation of peel data can be confusing because of the influence of many factors. It is well known that adhesive thickness, adherend thickness and the angle of peel all affect the measured peel strength [87,114-116,121,122]. Gent and Kaang have found that a peel angle of 45° minimizes bending moments and deformation of the adherend [115]. Other factors which affect peel strengths include modulus, yield strength and strain hardening coefficient of the adherend film, as well as the compliance

of the substrate. Furthermore, the locus of failure in the peel joint does not necessarily occur at the interface [120].

The rate and temperature at which peel testing is carried out are critical, as most adhesives and some adherends are polymeric materials, which are known to be viscoelastic in nature [123,124]. As the peel rate increases, polymers behave in a more glassy manner; as the peel rate decreases, the chains have time to "follow" the stress and thus behave in a more rubber-like fashion. This effect can cause the locus of failure in a joint to shift as peel rate increases [116]. Gent and Hamed have shown that peel strengths are proportional to the amount of energy dissipation in a material. The exact effect depends on the rheological character of the adherends/adhesives, and the rate dependence can be related to the stress/strain response [122]. For predictive purposes, it is not appropriate to extrapolate test data performed at a single arbitrary rate and temperature. Instead, WLF plots and master curves can be constructed for peel joints tested within a range of temperatures and rates, such as often done in the case of bulk polymers tested in creep or stress relaxation [125-127].

Some researchers have concluded that peel testing represents practical adhesion, or engineering strength, and does not measure true interfacial adhesion. The actual measured values also include work expended in plastic deformation and bending moments [87,119,120]. However, it is possible to use peel test results to compare the relative effects of adhesives and surface preparation on adhesion [112]. If the properties of materials utilized in a peel joint are known, interfacial adhesion values can be extracted from a Universal Peel Diagram for a given adherend/adhesive pair [120].

III. Experimental

3.1. Materials

LaRC-TPI utilized in this study was produced by the Mitsui Toatsu Chemical Company (New York, New York) and supplied by researchers at NASA-Langley Research Center (Hampton, Virginia) as a 30% w/w poly(amic-acid) solution in diglyme (2-methoxyethylether). Solutions were stored in a refrigerator until needed. Reagent grade diglyme used for diluting the LaRC-TPI solution was obtained from Fisher Scientific.

Poly(pyromellitimide) derived from pyromellitic dianyhydride and oxydianiline was obtained as 0.125 mm (5-mil) and 0.05 mm (2-mil) thick films from the E.I. DuPont de Nemours Co., Inc. (Wilmington, Delaware), under the trade names Kapton® 500 HN and 200 HN, respectively. The poly(amic-acid) precursor solution was supplied under the trade name PI 2545, also from DuPont, as a 14% w/w solution in a solvent solution composed primarily of N-methyl pyrrolidone (the exact solvent composition is proprietary). Reagent grade N-methyl pyrrolidone for diluting the PI 2545 solution was obtained from Fisher Scientific.

Commercial ferrotype photographic plates were used as substrates for the LaRC-TPI and PI 2545 thin coatings and were obtained from Apollo Metals (Bethlehem, Pennsylvania). These plates consist of a 0.5 mm steel base plated with nickel and an approximately 80 nm thick outermost layer of chromium oxide.

Oxygen and argon gases used for the plasma treatments were obtained from Airco, Inc. (Radford, Virginia). Semi-conductor grade ammonia gas was

obtained from Matheson Gas Products (East Rutherford, New Jersey). Purities of the gases are listed as follows: Oxygen - 99.95%, Argon - 99.995%, Ammonia - 99.999%.

1.9 cm (3/4 inch) wide Scotch® Magic® Tape, a pressure sensitive adhesive composed of polyacrylates and acrylic acid, was obtained from the 3M Company (St. Paul, Minnesota). 0.1 mm (4-mil) thick polyethersulfone film was obtained from ICI Industries. (Wilmington, Delaware), under the trade name Stabar® S100.

3.2. Sample Preparation

For XPS characterization and contact angle analysis, LaRC-TPI solution was diluted to a 24% w/w solution with additional diglyme. The solution was spin-coated at room temperature onto a 2.5 cm x 2.5 cm (1 in x 1 in) ferrotype plate which had been pre-cleaned with methanol and acetone. Stepwise imidization was carried out in a circulating air oven at 100°C, 200°C and 300°C, holding for 30 minutes at each temperature setting. The samples were cooled to room temperature before removal from the oven. Coating thicknesses as measured by a digital micrometer ranged from 5-8 μm.

Contact angle analysis was carried out on the coated 2.5 cm x 2.5 cm plates. 0.5 cm (3/16 in.) diameter discs were punched out from the coated 2.5 cm x 2.5 cm plates for plasma treatment and XPS analysis. 3.8 cm x 3.8 cm (1.5 in x 1.5 in) specimens for tape adhesion testing were prepared as described above, then sheared into 3.8 cm x 1.9 cm (1.5 in x .75 in) strips.

Kapton® film samples were cleaned with methanol prior to plasma treatment. 1 cm x 1 cm (0.4 in x 0.4 in) sections of the 5-mil films were cut for XPS analysis; contact angle analysis was carried out on 2.5 cm x 2.5 cm (1.0 in x 1.0 in) samples of the 5-mil film. For tape adhesion testing, 5-mil films were cut into 2.5 cm x 5.0 cm (1.0 in x 2.0 in) strips. For bonding with polyethersulfone films, 5.0 cm x 7.5 cm (2.0 in x 3.0 in) strips of both the 5-mil and 2-mil Kapton® films were used. Prior to plasma treatment and bonding, Kapton® and PES films were cleaned with methanol and dried in a 120°C oven for 24 hours .

IR-RAS and ellipsometric analysis required thinner coatings in the 25-50 nm range. In a thin coating, the plasma-modified region represents a larger percentage of the total coating thickness, thus greatly enhancing the surface sensitivity of the IR technique. Thin LaRC-TPI coatings were obtained by further diluting the LaRC-TPI solution with diglyme to 2.5% w/w. Both the LaRC-TPI solution and the diglyme were cooled in an ice bath to prevent the resin from precipitating out of solution. Unused solutions were refrigerated. 3.8 cm x 3.8 cm (1.5 in x 1.5 in) ferrotype plates were cleaned in an oxygen plasma for 20 minutes, then scrubbed with deionized distilled water and acetone prior to coating. Spin-coating and imidization were carried out as described above.

Thin PMDA-ODA films for ellipsometry were obtained by diluting the PI 2545 solution with additional NMP to obtain a 1% w/w solids solution. Solutions were stored in a refrigerator until needed. Due to the poor affinity of NMP for the ferrotype substrate, the plates were cleaned as described above for the thin LaRC-TPI coatings immediately prior to the spin coating operation in order to obtain good wetting. Spin-coating was carried out as described above;

coatings were thermally imidized at 100, 200, 300 and 350°C, holding 30 minutes at each temperature setting.

3.3. Plasma Treatments

Plasma treatments were carried out in a March Instruments Plasmod® unit (Concord, California), at 13.56 MHz and 50 watts. Gas lines were purged with the gas of interest for 30-60 seconds before use. The pressure inside the unit during its operation was approximately 1 torr. Care was taken to pump down and purge the treatment chamber for at least 10 minutes prior to activating the RF field. All subsequent surface analyses or bonding treatments were performed within 5 minutes of plasma treatment, to minimize the possibility of surface molecular rearrangement and/or contamination by the atmosphere.

Experiments were carried out to determine whether surface composition changes following exposure to noble gas plasmas (such as argon) were induced by the plasma or by post-plasma atmospheric exposure. These experiments were accomplished by sealing the entire plasma unit in a polyethylene glove bag, which was then purged with argon. A sample box to hold the sample and an XPS mount were also placed into the glove bag. Plasma treatment in an argon plasma was performed as described above. The sample was removed from the plasma reaction chamber, secured onto the XPS mount and sealed into the sample box. The sample box was then removed from the glove bag and placed into another purged glove bag surrounding the introduction chamber of the spectrometer. The plasma-treated sample was not removed the sample box until the glovebag surrounding the introduction

chamber was fully purged with argon. XPS analysis was then carried out with the sample not having been exposed to the atmosphere from the time of treatment to the time of analysis.

In order to isolate the effect of vacuum ultraviolet radiation from the plasma on the polyimide surfaces, plasma treatments were carried out with the sample sandwiched between two lithium fluoride (LiF) windows. Circular LiF windows 3 cm in diameter and 1 mm thick were obtained from Optovac, Inc. (North Brookfield, Massachusetts).

3.4. X-ray Photoelectron Spectroscopy (XPS or ESCA)

In this work, XPS was used extensively to characterize the chemical changes which occurred as a result of plasma treatment, as well as to analyze the failure surfaces of peeled specimens. XPS, also known as ESCA (Electron Spectroscopy for Chemical Analysis), is ideal for polymer surface analysis due to its non-destructive nature, compared to ion or electron bombardment techniques, and its shallow sampling depth.

Figure 3.1 shows a schematic of the XPS experiment. A sample surface is irradiated with a monoenergetic beam of x-rays, which are absorbed by the atoms in the sample. Each absorption of an x-ray photon leads to the emission of a photoelectron. All electrons with binding energy less than the x-ray energy can be excited, though not with equal probability. Conservation of energy principles require that:

$$\text{Binding energy} = h\nu - KE + \phi_s \qquad (3.1)$$

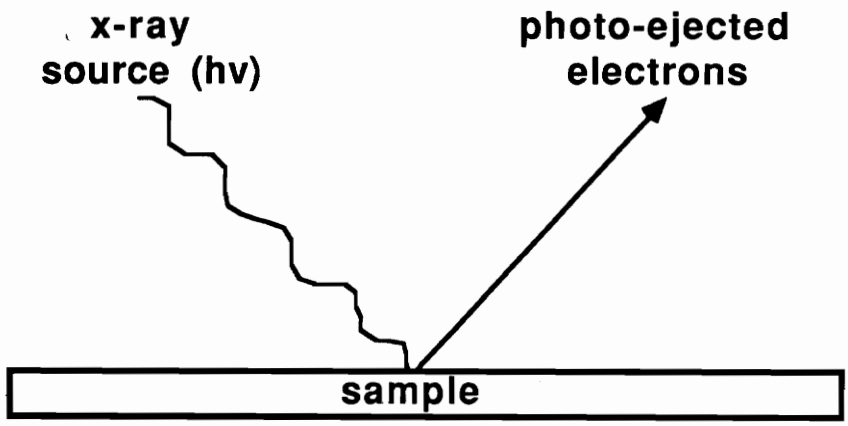

Figure 3.1: Schematic of x-ray photoelectron spectroscopy (XPS) experiment.

where hν is the x-ray energy, KE is the kinetic energy of the photoelectron and $ø_s$ is the spectrometer work function [128].

Since the atomic structure of each element in the periodic table is distinct from the others, measurement of binding energies allows the qualitative identification of elements present at the surface. Quantitative information can also be obtained from area intensities of photopeaks along with consideration of the mean free path of the photoelectron of interest as well as the efficiency of x-ray absorption for that particular subshell.

XPS is also capable of providing valuable information on oxidation state and molecular bonding through the phenomenon of *chemical shift.* A decrease in electron density in the valence region around an atom produces an increase in the binding energy of the core level electrons. Changes in electron density are due primarily to changes in oxidation state or substituent effects. In the analysis of organic materials, the C1s level is particularly sensitive to changes in substitutent electronegativity and hence structural information can be inferred from careful curve-fitting and analyses of peak positions. Chemical shift effects are dependent primarily on atoms attached directly to a particular atom and to a much lesser extent on atoms further removed [129,130].

Although x-ray photons have deep penetrating power, the short mean free paths of photoelectrons allow information to be obtained only from the topmost ~100Å of the surface. The depth of analysis can be varied through a technique known as Angle Dependent XPS (AD-XPS). A schematic of the AD-XPS experiment is shown in Figure 3.2. The depth of analysis d as a function of the take-off angle θ and electron mean free path λ is given by the relationship $d = 3\lambda\cos\theta$, where values of θ generally range from 10-90° [131].

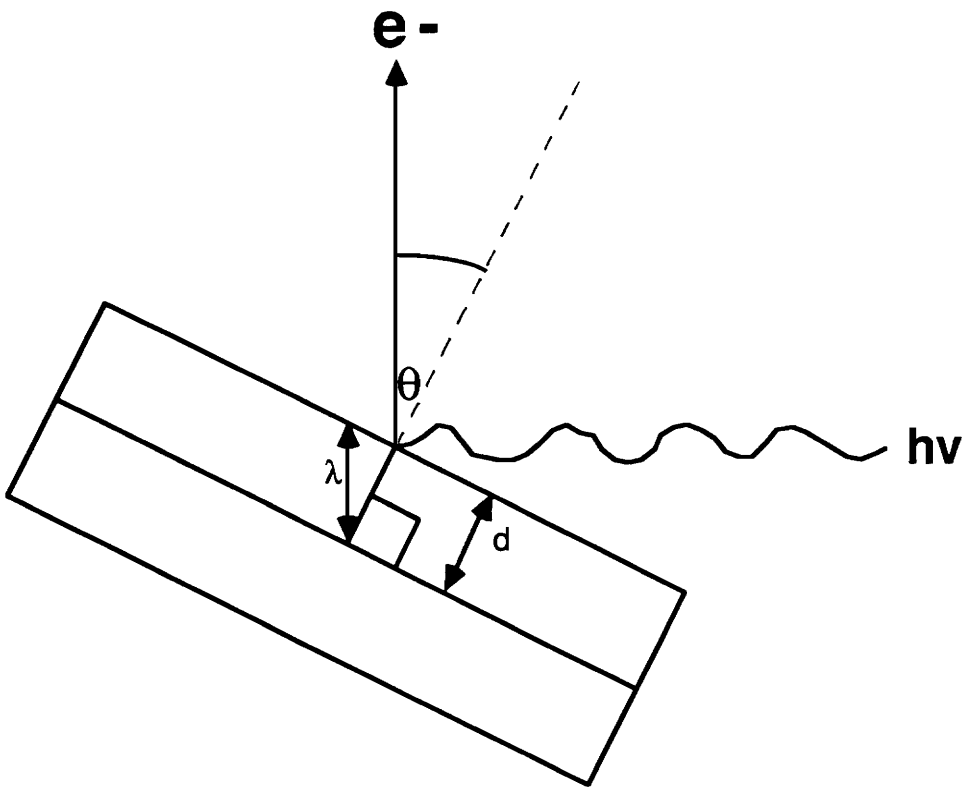

Figure 3.2: Schematic of angle dependent x-ray photoelectron spectroscopy (AD-XPS) experiment.

XPS analysis was performed on a Perkin-Elmer PHI 5300 spectrometer with a Mg K_α achromatic X-ray source (1253.6 eV), operating at 15 keV and 400 watts with an emission current of 30 mA. The spectrometer was calibrated to the the $4f_{7/2}$ photopeak of gold and the $2p_{3/2}$ photopeak of copper. Pressure inside the analysis chamber was held below 5×10^{-7} torr during analysis. Samples were mounted onto the spectrometer probe with double-sided tape. Dimensions of the analyzed areas on the samples were typically 1 mm x 3 mm. No neutralization with the electron gun was necessary, since only minimal charging effects were present.

For each sample analyzed, a survey scan encompassing the region of 0-1100 eV was first taken. Multiplex scans of all significant peaks seen in the survey were then run. Binding energies for all observed photopeaks were referenced to the value for hydrocarbon species at 284.6 eV. Atomic concentration calculations and curve-fitting were carried out by use of the PHI software, version 2.0. Atomic concentrations were determined by the following formula:

$$\text{Atomic \% for element X} = \frac{\frac{I_x}{S_x T_x}}{\sum_{i=1}^{n} \frac{I_i}{S_i T_i}} \qquad (3.2)$$

where I = the area of the photopeak, S = sensitivity factor, T = total acquisition time for each data point and n = the number of photopeaks considered.

Photopeaks of interest were fitted with Gaussian curves, varying both the peak intensity and position while holding the full width at half maximum (FWHM) at 1.7 ± 0.1 eV. The curve-fitting routines in the PHI software utilize the error mean square as a measure of the goodness-of-fit of the fitted peaks; this value

is minimized given a starting set of parameters. Between 3-5 samples were run for each plasma treatment and the curve-fitted values were averaged in order to obtain a statistical sampling.

To obtain information on the depth of plasma treatment, angle dependent XPS (AD-XPS) was carried out by analyzing the treated samples at take-off angles of 15°, 45° and 90°.

3.5. Infrared Reflection-Absorption Spectroscopy (IR-RAS)

In order to obtain molecular information on the plasma-treated surfaces, IR-RAS experiments on the thin LaRC-TPI coatings were performed. The theory of infrared analysis and the applications of the technique to organic structural analysis are well-known [132,133]. The term "reflection-absorption spectroscopy" was coined by Greenler et al., who utilized it to study thin organic films on metal substrates. In IR-RAS, an absorption spectrum is obtained through reflections. When the reflection is made at a near-normal incidence angle, the technique is termed "specular reflectance"; IR-RAS is more correctly reserved for experiments in which a near-grazing angle of incidence is utilized. The increased path length due to grazing angle incidence increases sensitivity for the study of thin films [134].

The basic principles of the technique involve the reflection of electromagnetic waves at an interface. Reflection will always occur at an interface if there is a difference in the refractive indices between the two contacting materials. For unpolarized radiation, the incident and reflected waves usually combine to form a standing wave, which has a very small electric

field amplitude at the surface. Only minimal interaction between the electromagnetic radiation and the surface film occurs. However, when parallel polarized radiation is incident on the substrate at grazing angle incidence, the electric field amplitude and the intensity of absorption is maximized. This is due to the fact that parallel polarized radiation has a finite amplitude at all angles of incidence except very close to 90°, whereas the perpendicular component of the radiation destructively interferes with itself at any incidence angle [135,136].

Experiments were performed on a Nicolet 510 Fourier transform infrared spectrometer, utilizing a Harrick retro-mirror reflection accessory and p-polarized radiation at an incident grazing angle of 85° measured from the surface normal, as seen in Figure 3.3. A diagram of the retro-mirror accessory is shown in Figure 3.4. The spectrometer bench was purged with dry nitrogen prior to analysis. 1000 scans were collected and averaged at a resolution of 4 cm^{-1}. A clean, uncoated ferrotype plate served as a suitable background. Difference spectra were obtained by subtracting the untreated LaRC-TPI spectrum from the spectrum of the plasma-treated sample, utilizing Nicolet software for interactive subtraction.

3.6. Contact Angle Analysis

The technique of contact angle analysis is an important one in the field of surface science. Through the use of a simple, inexpensive apparatus, the topmost molecular layers of surfaces can be probed, and measurements which are made can be correlated directly to theories of surface thermodynamics.

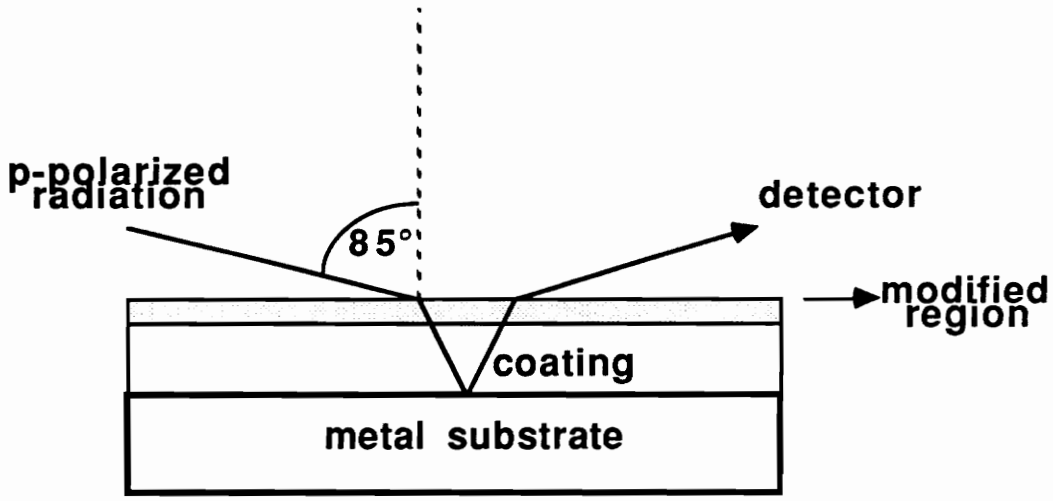

Figure 3.3: Schematic of infrared reflection-absorption (IR-RAS) experiment.

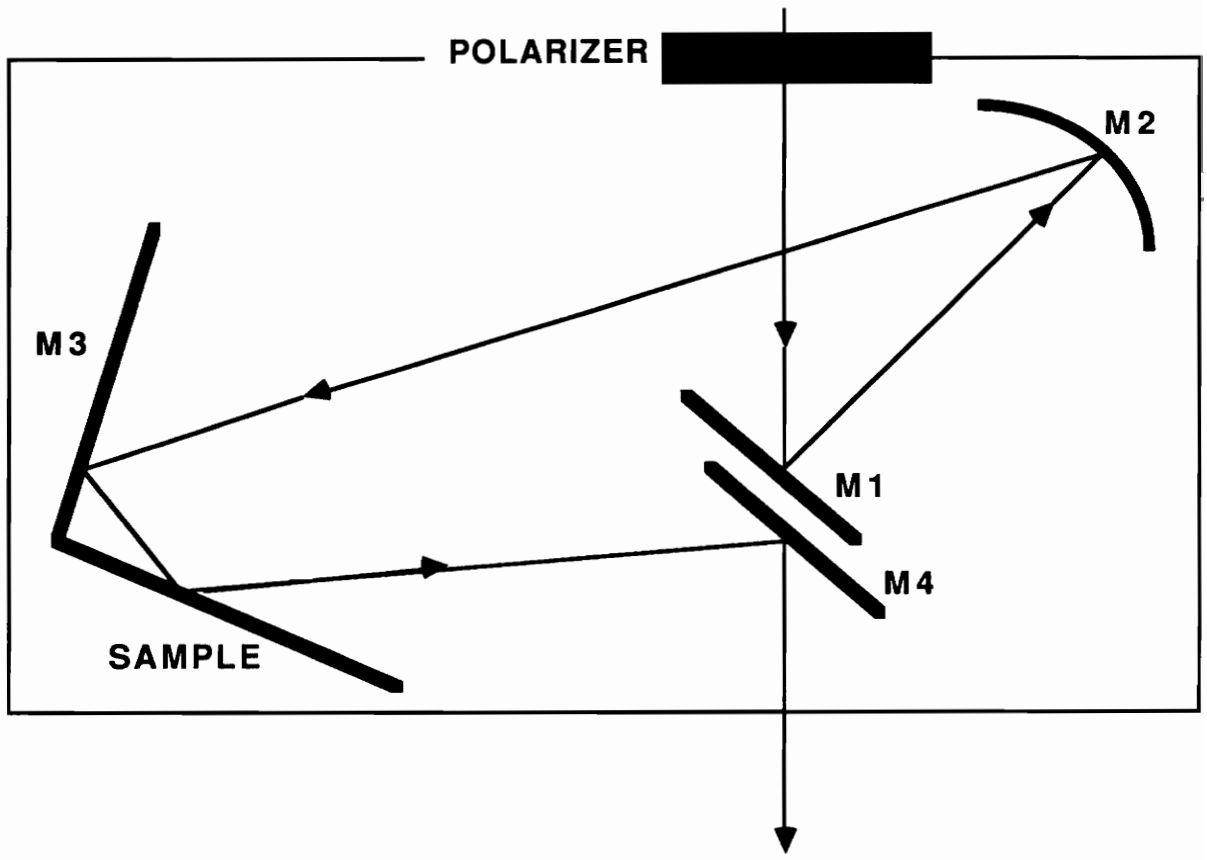

Figure 3.4: Diagram of Harrick retro-mirror reflection accessory.

When a drop of liquid is placed on a solid, usually the drop will not completely wet the substrate but will retain a definite shape and angle of contact on the solid. A force balance can be derived for the vectors corresponding to the various interfacial forces involved, as shown in Figure 3.5. This yields:

$$\gamma_{sl} - \gamma_{sv} + \gamma_{lv} \cos \theta + \pi = 0 \qquad (3.3)$$

where π is the equilibrium spreading pressure, a quantity which arises from the difference between the true γ_s and γ_{sv}, the surface free energy of a solid in equilibrium with liquid vapor. In most applications, π is considered to negligible. Since the thermodynamic work of adhesion between two phases is defined as:

$$W_A = \gamma_{sv} + \gamma_{lv} - \gamma_{sl} \qquad (3.4)$$

This yields an expression for the work of adhesion as a function of contact angle:

$$W_A = \gamma_{lv} (1 + \cos \theta) \qquad (3.5)$$

This is known as the Young-Dupre equation. Generally speaking, if the contact angle is greater than 90°, the liquid is said not to wet the solid. If the contact angle is close to zero, the solid is considered to be wetted. Wetting will usually occur if the surface energy of the substrate is greater than or equal to the surface energy of the probe liquid [109,137]. Thus, contact angle measurements can yield a semi-quantitative determination of surface free energy.

To determine the water wettability of the plasma-treated surfaces, contact angle analysis was carried out with a Rame-Hart 100-00 115 NRL contact angle goniometer. 4 ul drops of deionized distilled water were carefully placed on the substrate with a microliter syringe held in an upright position. Both the left and right sides of at 3 to 5 drops were measured and averaged.

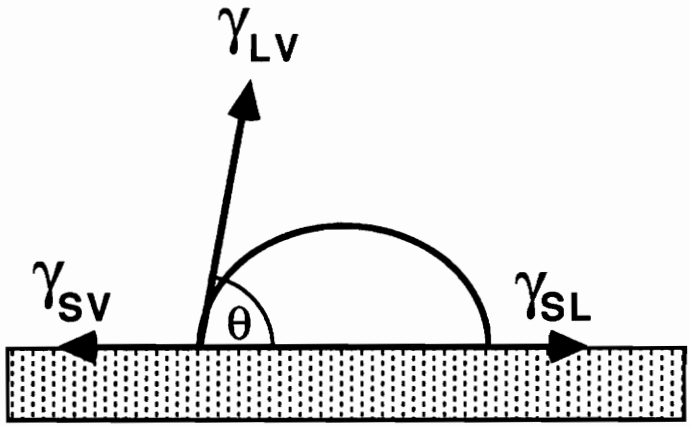

Figure 3.5: Contact angle analysis showing vector resolution of interfacial forces.

3.7. Ellipsometry

Ellipsometry was utilized to study plasma etch rates by monitoring the thickness of the thin polyimide films as a function of plasma exposure time. Ellipsometric measurements were performed using a Gaertner L116A dual mode automatic ellipsometer. A 1 mW helium-neon laser (632.8 nm) was used as a light source at an incident angle of 70°. The analysis area is a circular area approximately 1 mm in diameter. Between 5-8 separate measurements were made over the entire area of the plasma-treated sample and averaged.

A value of 1.70 was used for the refractive index of the polyimide film, which is in the range of literature values given for imide-containing polymers [77,138]. The refractive index and absorption coefficient of the cleaned chromium oxide substrate was measured to be 3.6 and -4.1, respectively.

3.8. High Resolution Scanning Electron Microscopy (HR-SEM)

HR-SEM photomicrographs were taken of the polyimide surface topography before and after exposure to plasma. Samples were sputtered with approximately 7-9 nm of gold to reduce charging and destruction of the surface by the electron beam, then mounted with silver paint onto the microscope probe. Photomicrographs were taken on a Philips EM-420T scanning transmission electron microscope (STEM).

3.9. Adhesion Testing

3.9.1. Preparation of Adhesive Joints

LaRC-TPI-coated Ferrotype plate and 5-mil Kapton® film were cleaned with acetone and methanol and treated in the plasma chamber for 1 minute and 20 minutes in each plasma. Magic® Tape was placed on the surfaces with firm pressure within seconds of removal from the plasma chamber. A fresh section of tape which had not previously been exposed to air was used. Samples were stored for a minimum of 24 hours and a maximum of 72 hours in a desiccator prior to peel testing.

In a separate experiment, plasma-treated samples were rinsed with methanol, scrubbed with a Kim-wipe® soaked in methanol, then rinsed again with methanol and blown dry with nitrogen. Tape was then applied as described above after the drying step.

Kapton® /PES joints were fabricated by heat sealing the PES film between the plasma-treated 5-mil and 2-mil Kapton® films in a Carver Model C laboratory press. The samples were sandwiched between mold release-treated stainless steel plates and inserted into the press platens. The platens were closed and a pressure of 0.7 MPa (100 psi) was applied when the temperature reached 260°C. The temperature was then increased to 320°C and maintained for 30 minutes. The plates were removed from the press when the temperature had dropped to 200°C; samples were cooled to 150°C before the plates were dismantled.

Annealing of the Kapton/PES samples was accomplished by heating the samples at 240°C for 30 minutes in a Blue M oven, then allowing the oven to

cool down slowly to 25°C over a period of 18 hours before removing the samples.

0.16 cm (1/16 in)high density polyethylene (HDPE) obtained from Atlantic Plastics Company (Roanoke, Virginia) was cut into 2.5 cm x 5.0 cm (1.0 in x 2.0 in) strips, treated in an oxygen plasma and bonded with Magic® Tape as a comparison to the polyimide materials. Contact angle and XPS analysis were also carried out on the oxygen plasma-treated samples.

To determine the effectiveness of plasma as a cleaning process, LaRC-TPI samples were intentionally contaminated with a mold release agent prior to plasma treatment. The mold release was obtained from the Miller-Stephenson Chemical Company (Danbury, Connecticut) and consists of a mixture of fluorocarbons. The mold release material was sprayed onto the samples and allowed to dry. Any excess mold release was removed by wiping. Both XPS analysis and peel testing were carried out on the contaminated and plasma-cleaned surfaces.

3.9.2. Peel Testing

An Instrumentors Inc. slip-peel tester was used for the peel testing of samples adhered with Magic® Tape as well as the Kapton®/PES samples. The load cells were calibrated electronically prior to peel testing. Samples were clamped to the instrument and the adherends peeled off at an 180° angle by a hook attached to a load cell as shown in Figure 3.6. A peel rate of 25 cm/min (10 in/min) was utilized; this ensured that cohesive failure within the adhesives would not occur. The peel strength is calculated as the average force divided by the width of of the specimen peeled. All peel strengths are reported in

Figure 3.6: 180° peel testing configuration.

newtons/meter (N/m). At least 3 peel specimens for each plasma treatment condition were tested for each individual experiment.

For the LaRC-TPI and Kapton® samples bonded with Magic® tape, the tape was the adherend which was peeled off. In the case of the Kapton®/PES laminates, the 2-mil Kapton® film was peeled off as the adherend. It is known that a thinner adherend film would contribute less to the bending moment of the measured peel force [120].

3.9.3. Analysis of Failure Surfaces

Failure surfaces of the peeled specimens were analyzed utilizing x-ray photoelectron spectroscopy at both 45° and 15° take-off angles. Both sides of the peel specimen were analyzed to make a determination of the average failure plane. Nitrogen was used as a tag element in the the Magic® tape samples, since Magic® tape does not contain nitrogen. In the Kapton®/PES samples, both sulfur and nitrogen were used as tags.

IV. Results and Discussion

4.1. Surface Characterization of Plasma-treated LaRC-TPI

This section will discuss the surface analysis of plasma-treated LaRC-TPI with a variety of surface-sensitive techniques. Both chemical as well as physical changes induced in the surface by the plasma treatment will be characterized. Oxygen was chosen as one of the plasma treatments due to its well-known oxidizing effect and ability to create polar functional groups. Argon, although generally considered to be an inert gas, is also known to produce similar oxidative effects as oxygen. The use of an ammonia plasma was intended to introduce nitrogen-containing functional groups into the LaRC-TPI surface; groups such as amino or amide could have potential reactivity toward materials such as epoxies.

4.1.1. Contact Angle Analysis

The technique of sessile drop contact angle analysis is a simple and convenient method for evaluating surface wettability of polymer films by a variety of liquids. Water was chosen as the probe liquid because it is a high surface free energy, polar compound and can be used to semi-quantitatively assess the degree of surface polarity or increases in surface energy of a polymer film.

The contact angle of water on the untreated, imidized LaRC-TPI surface is on the order of 73°, as shown in Figure 4.1. Wiping with a Kimwipe® tissue soaked in acetone resulted in a decrease in contact angle to approximately 58°. It is noted that all three plasmas - oxygen, argon and ammonia - greatly

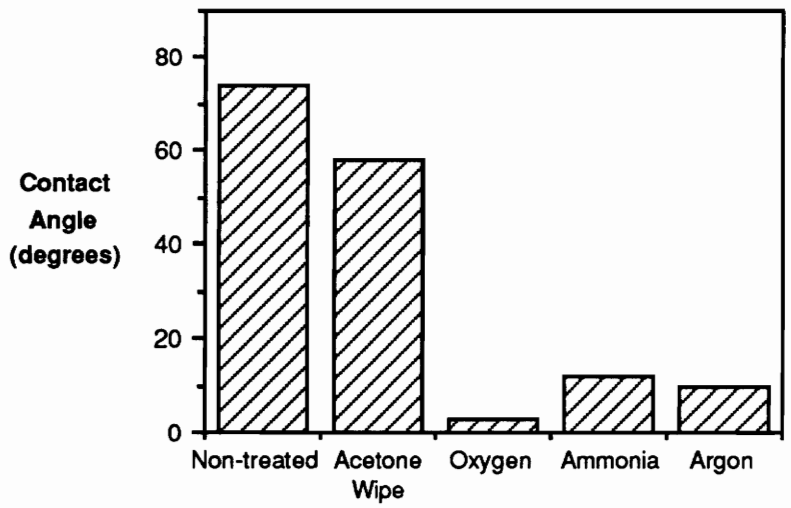

Figure 4.1: Results of water contact angle analysis on non-treated and plasma-treated LaRC-TPI.

decrease the water contact angle on the LaRC-TPI surface. In the case of the oxygen plasma-treated surface, the contact angle is essentially zero, whereas for argon and ammonia a slightly higher angle is observed. The enhanced wettability of the plasma-treated surface is indicative of higher surface free energy.

4.1.2. X-ray Photoelectron Spectroscopy (XPS)

4.1.2.1. Atomic Composition

XPS analysis of the non-imidized and imidized/non-plasma treated LaRC-TPI surfaces was performed to obtain a baseline by which to compare the plasma-treated surfaces. Atomic concentrations are listed in Table 4.1. The non-imidized surface, prepared by drying the spin-coated film at 160°C, was shown to have an atomic composition of 76.4% C, 18.9% O and 4.7% N, which compares well with the bulk stoichiometry for the poly(amic-acid) precursor of 75% C, 20% O and 5% N. Also, as seen in Table 4.1, the imidized, non-treated surface shows a surface composition of 80.3 % C, 14,1% O and 5.6% N. These results are again in good agreement with the bulk atomic composition for LaRC-TPI of 79% C, 16% O and 5% N, indicating that complete imidization of the film has occurred.

Changes in surface atomic composition as a function of plasma exposure time are detailed in Figures 4.2a-4.2c. It is seen that all three plasmas cause significant changes in the atomic concentrations of carbon, oxygen and nitrogen to occur. These changes in chemical composition take place in less than 30 seconds of treatment, after which the atomic concentrations remain constant.

Table 4.1: XPS analysis of non-imidized, imidized, oxygen plasma, argon plasma and ammonia plasma-treated LaRC-TPI.

	Atomic Concentration (%)		
	Carbon	**Oxygen**	**Nitrogen**
Non-imidized	76.4	18.9	4.7
Imidized	80.3	14.1	5.6
Oxygen plasma	58.7	36.1	5.2
Argon plasma	70.1	23.3	6.6
Ammonia plasma	73.2	14.0	12.8

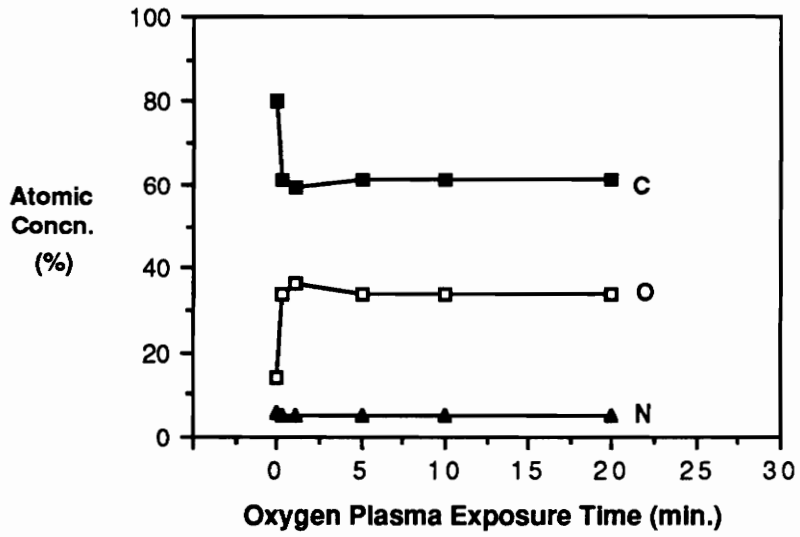

Figure 4.2a: Atomic concentrations of C, O and N on LaRC-TPI surface as a function of oxygen plasma exposure time.

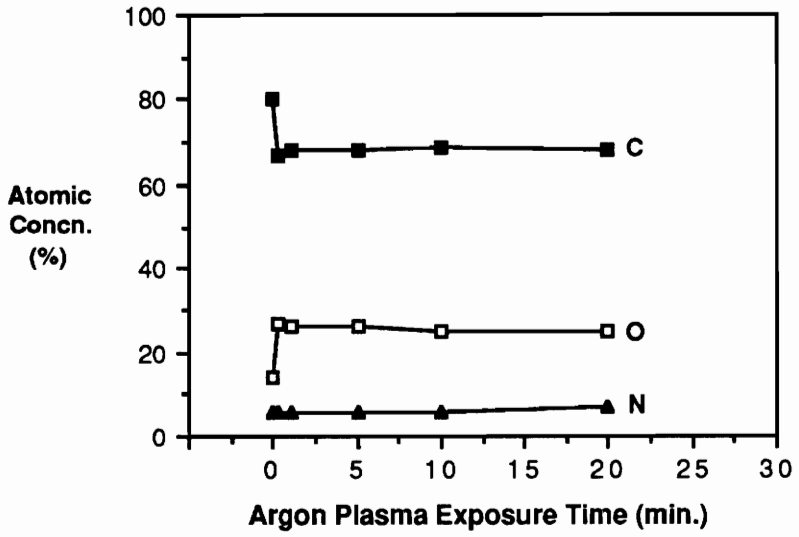

Figure 4.2b: Atomic concentrations of C, O and N on LaRC-TPI surface as a function of argon plasma exposure time.

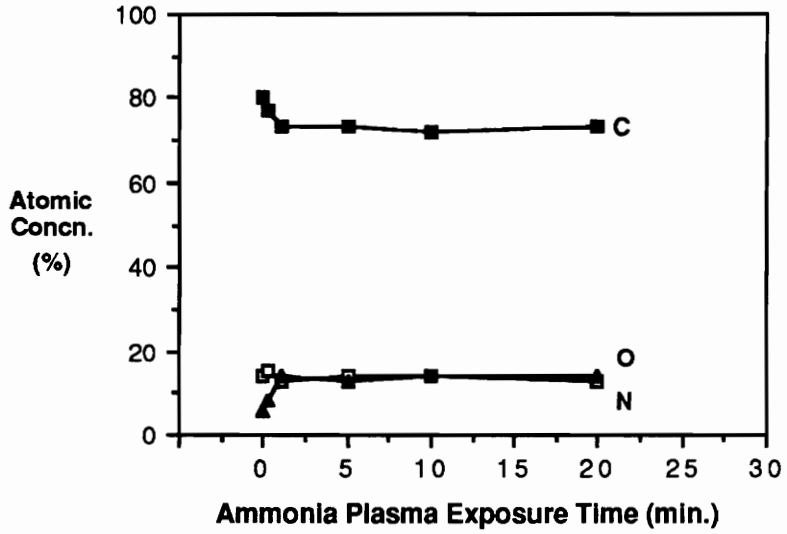

Figure 4.2c: Atomic concentrations of C, O and N on LaRC-TPI surface as a function of ammonia plasma exposure time.

The steady-state atomic concentrations are listed and compared to the non-treated surface in Table 4.1. Further treatment beyond the first 15-30 seconds does not create any further changes in surface chemical composition. Thus, the action of plasma is extremely rapid.

Treatment in oxygen plasma causes an increase in surface oxygen concentration from the original value of 14 to 36%. Carbon concentration correspondingly decreases and no change is observed for the concentration of surface nitrogen. The result of argon plasma exposure shows similar results, with an increase in oxygen concentration to 23% and a slight increase in nitrogen concentration. Ammonia plasma is somewhat different, causing no change in oxygen concentration but instead increasing the nitrogen concentration from about 6% to 13%. All XPS atomic concentration values were reproducible and consistent within $\pm$2%. This indicates that plasma reactions are not simply random, but follow a distinctive pattern or mechanism.

4.1.2.2. Curve-fitted Results

Curve-fitting of the C1s, O1s and N1s photopeaks was carried out to obtain more detailed chemical information on the LaRC-TPI surfaces. The C1s photopeak, in particular, is sensitive to substituent effects [130]. Hence, the identity and concentration of surface functional groups can be inferred through an analysis of binding energies and intensities of the constituent peaks within the photopeak envelope. The shift in the C1s binding energy is dependent upon the electronegativity of the substituent atom(s). A general rule of thumb states that there is an upward shift in binding energy away from the main hydrocarbon peak (referenced to 284.6 eV) of 1.5$\pm$.3 eV for every bond made to

oxygen. For example, C-O species exhibit a 1.5 eV shift, C=O is shifted by 3.0 eV and O-C=O by 4.5 eV. Work with model compounds is necessary for exact identifications to be made. The XPS binding energies of a number of polymeric as well as low molecular weight compounds are detailed in the Appendix.

The sensitivity of XPS to changes in chemical bonding is first illustrated by its ability to distinguish between non-imidized and imidized LaRC-TPI. Figure 4.3 shows the curve-fitted C1s photopeak for non-imidized LaRC-TPI, compared to the C1s photopeak for the completely imidized sample. The peaks at 287.4 and 288.6 eV in the C1s photopeak of the non-imidized surface correspond to the amide and carboxylic acid functionality, respectively. After imidization is complete, these two peaks are seen to coalesce into the single peak at 288.0 eV corresponding to imide and benzophenone carbonyls. Similar results have been observed by other researchers [139-142].

The curve-fitted peaks in the imidized, non-treated surface are assigned as shown in Table 4.2. Referenced to the hydrocarbon peak at 284.6 eV, peaks at 286.5 eV, 288.0 eV and 290.5 eV are resolved from the C1s envelope and are assigned to C-N, C=O (imide and benzophenone) and C-C shake-up satellite, respectively. It is noted that the atomic concentration of C-N linkages (5.6%) is identical to the total atomic concentration of nitrogen, thus supporting the assignment of the 286.5 eV peak as C-N versus possibly C-O. The presence of the shake-up satellite is indicative of aromaticity in LaRC-TPI [128].

The major constituent of the O1s photopeak at 531.6 eV shown in Table 4.2 is assigned to carbonyl oxygen and the main N1s peak at 400.1 eV is assigned to nitrogen in the imide ring. The percentage of carbonyl oxygen at 11.3% is roughly equal to the concentration of carbonyl carbon at 9.4%. It is

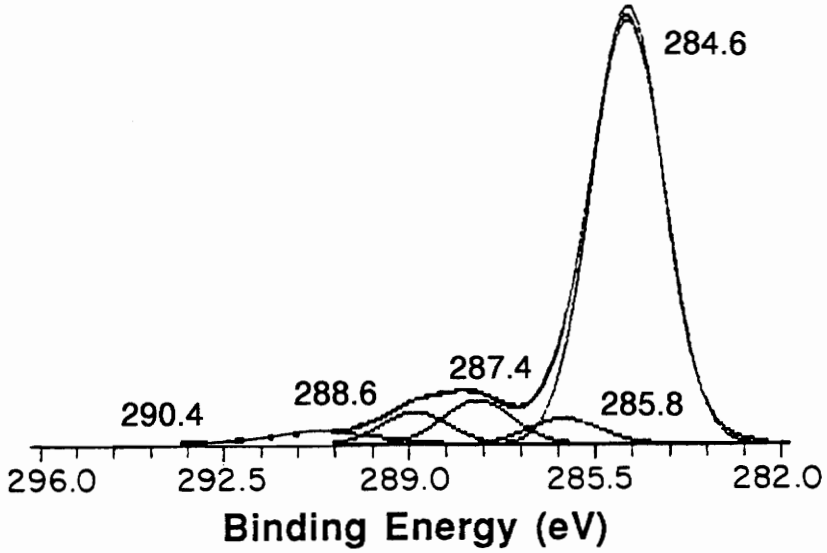

(a)

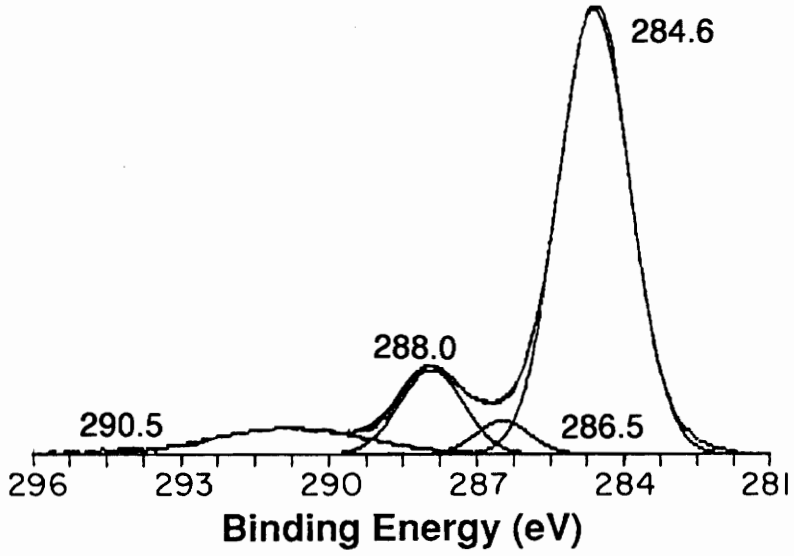

(b)

Figure 4.3: Curve-fitted C1s photopeaks for (a) non-imidized and (b) fully imidized LaRC-TPI.

TABLE 4.2: Results from curve-fitted C1s, O1s and N1s photopeaks for non-treated and plasma-treated LaRC-TPI

Photopeak		NON-TREATED BINDING ENERGY (eV)	NON-TREATED ATOMIC CONCN. (%)	OXYGEN BINDING ENERGY	OXYGEN ATOMIC CONCN.	AMMONIA BINDING ENERGY	AMMONIA ATOMIC CONCN.	ARGON BINDING ENERGY	ARGON ATOMIC CONCN.
C1s	C-C	284.6	61.9	284.6	23.2	284.6	51.7	284.6	47.5
	C-O			286.0	4.8				
	C-N	286.5	5.6	286.8	9.2	286.1	9.9	286.4	6.4
	C=O	288.0	9.4	288.3	15.7	287.8	11.6	288.0	13.0
	O=C-O			289.2	4.6			289.8	2.3
	shake-up	290.5	3.4	290.4	1.2			291.8	0.9
			80.3		**58.7**		**73.2**		**70.1**
O1s		530.4	0.7			530.1	0.5		
				531.0	2.3				
	O=C	531.6	11.3	531.8	10.1	531.5	11.4	531.6	14.7
				532.6	11.1	532.7	2.1	532.8	5.9
	O-C	533.1	2.1	533.4	8.7			533.8	2.7
				534.3	3.9				
			14.1		**36.1**		**14.0**		**23.3**
N1s						398.6	2.8		
	O=C-N-	400.1	5.6	400.2	5.2	399.7	10.0	400.0	6.6
			5.6		**5.2**		**12.8**		**6.6**

observed that there is a stoichiometric deficiency of surface C=O groups compared to the expected bulk composition - this finding has also been documented by other researchers [139,143,144]. It has been postulated that this carbonyl deficiency may be due to the presence of iso-imide formation or molecular shielding of carbonyl groups at the surface [139].

Both Table 4.2 and Figure 4.4 clearly show that the effect of plasma treatment is to create additional peaks within the C1s envelope, indicative of new surface species. The C1s photopeak for oxygen plasma-treated LaRC-TPI shows new peaks at 286.0, 286.8 and 289.2 eV. The peak at 286.5 eV in the non-treated LaRC-TPI corresponding to C-N linkages disappears, and the binding energy of the imide carbonyl increases from 288.0 to 288.3 eV. Although it appears that the two peaks at 286.0 and 286.8 eV can be combined into one single peak, performing this operation does not lead to a satisfactory fit due to the unreasonable breadth (>2.0 eV) of the single peak which would be needed to fit this region. By running 3-5 independent XPS experiments and curve-fits, sufficient statistical information can be gathered to make a distinction between peaks at 288.0 eV and 288.3 eV; the standard deviations in binding energy for both of these peaks are <0.1 eV.

The disappearance of the C-N peak at 286.5 eV, coupled with the increase in imide carbonyl binding energy to 288.3 eV is good evidence for chain scission at the C-N bond, resulting in the formation of phthalimide structures from the original imide rings. Phthalimide run as an XPS standard also exhibited no peak at 286.5 eV, as would be expected, but showed an imide carbonyl peak with a binding energy of 288.3 eV (see Table A.1). It has been shown that succinimidyl radical, similar in structure to phthalimide, is extremely

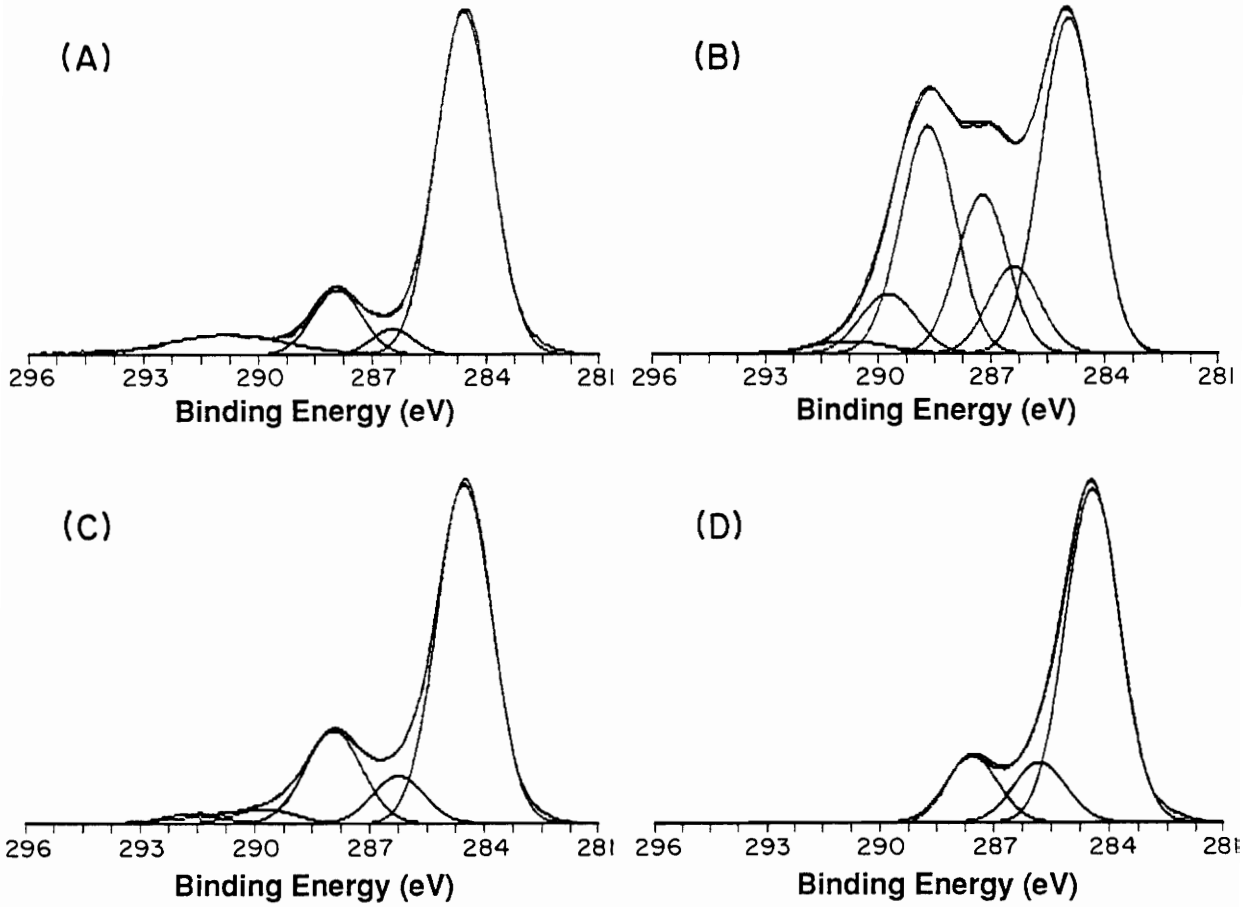

Figure 4.4: Curve-fitted LaRC-TPI C1s photopeaks. (A) non-treated (B) oxygen plasma (C) argon plasma (D) ammonia plasma.

stable due to extensive pi delocalization of the unpaired electron [145]. The formation of a stable radical species would serve as a driving force for chain scission at the C-N linkage.

New peaks at 286.0 and 286.8 eV can be assigned to C-O-C or C-OH structures, based both on reported literature values and XPS analysis of model compounds (Appendix). Peaks in the vicinity of 286.0 eV corresponding to C-O linkages were also found in bisphenol A polycarbonate, poly(methyl methacrylate), phenyl benzoate and poly(vinyl phenol). The peak at 286.8 eV was not found in any standards which were analyzed; however, the PHI handbook reports one type of acrylate polymer to have a C-O peak at 286.6 eV [146]. The new peak at 289.2 eV could be identified as either an ester or carboxylic acid species. Materials such as terephthalic acid and phenyl benzoate also display peaks ~289.0 eV corresponding to O-C=O species (see Table A.1).

A significant observation in the curve-fitted C1s photopeak is that there is an increase in the intensity of the original imide carbonyl peak. Imide functional groups are not known to be created within the free radical environment of an RF plasma. Thus, the only way in which the concentration of species at 288.3 eV can be increased is if selective etching or fragmentation of the original LaRC-TPI structure has occurred, leading to an apparent enrichment of imide groups at the surface. Using diffuse reflectance infrared spectroscopy, Stancil et al. in fact observed an increase in imide ring concentration in the surface of a LaRC-TPI composite after atomic oxygen exposure [78]. This mechanism will be further discussed in a later section describing plasma etch rate experiments.

No changes in imide nitrogen binding energy are observed as a result of oxygen plasma exposure. The absence of high binding energy nitrogen species precludes the formation of oxidized nitro compounds. A weak shake-up satellite can be still be fitted to the C1s envelope after plasma treatment, showing that aromatic ring structures are still present in the plasma-treated surface. Possible reaction mechanisms for the formation of the observed species will be discussed in a later section.

In the case of argon plasma, examination of the curve-fitted C1s photopeak in Figure 4.4c and the tabulated data in Table 4.2 reveals that, overall, there is essentially very little change in the binding energies of the original curve-fitted peaks. The C1s photopeak can be fitted with a new component at 289.8 eV and the O1s photopeak contains two new components at 532.8 and 533.8 eV. These are assigned to the formation of an ester or carbonate species, with the two O1s components corresponding to the doubly and singly-bonded oxygens of the ester/carbonate, respectively. Again, the presence of a weak shake-up satellite is indicative of surface aromaticity. The lack of any shift in the binding energy of the N1s photopeak again precludes the formation of oxidized nitrogen functional groups.

As seen in the case of oxygen plasma, the atomic concentration of the imide group in the argon plasma-treated surface is again increased. This is possibly another case of fragmentation/oxidation as observed with the oxygen plasma. Because argon is considered to be an inert gas, no components of the plasma are capable of reacting with the free radicals which are generated in the LaRC-TPI surface. Thus, all active free radicals persist until they are exposed to the outside atmosphere, at which time reaction with molecular oxygen, carbon

dioxide, moisture and other such species can occur. The most likely site for fragmentation and subsequent free radical formation would be at the benzophenone linkages. Benzophenone groups are known to be excellent chromophores and have the potential to undergo photoreduction by ionizing radiation, such as that found in the high energy ultraviolet/vacuum ultraviolet component of plasma [147].

In contrast to oxygen and argon XPS results, no additional curve-fitted peaks are observed in any photopeak for the ammonia plasma-treated LaRC-TPI surface. Instead, binding energy shifts are observed. The imide carbonyl peak, originally at 288.0 eV has decreased in binding energy to 287.8 eV, the binding energy of the C-N bond has also shifted downward to 286.1 eV. The imide nitrogen 1s peak is also shifted to lower binding energy, moving from 400.1 eV to 399.7 eV. As in the case of oxygen plasma, these small shifts in binding energies are reproducible through repeated XPS experiments and curve-fitting. Another significant observation is that the shake-up satellite can no longer be fitted in the high binding energy region of the C1s photopeak; this could be indicative of loss of aromaticity as a result of ammonia plasma attack.

XPS analysis of Kevlar® (poly(imino-1,4-phenylene imino terephthaloyl)) and nylon 6,6 standards reveals that there are very close matches between these standards and the ammonia plasma-treated LaRC-TPI surface; indicating the possibility of amide formation (see Table A.1). Both poly(amide) standards show an amide nitrogen peak at ~399.7 eV. Nylon 6,6 also exhibits a C-N peak at 285.7 eV and an amide carbonyl peak at 287.6 eV; Kevlar® has a C-N peak at 286.1 eV and an amide carbonyl peak at 287.9 eV.

A direct conversion of imide and benzophenone carbonyl to amide groups is suggested by the fact that the intensity of the peak at 288.0 eV and the intensity of the shifted peak at 287.8 eV are almost identical; also, the O1s peak at 531.5 eV is essentially equal in intensity to the O1s peak for the non-treated film. Also, the atomic concentration of carbonyl carbon (11.6%) and carbonyl oxygen (11.4%) is roughly equal to the total concentration of nitrogen (12.8%).

It is postulated that direct attack of ammonia plasma species such as NH· or NH_2· at the carbonyl carbon position leads to the formation of amide groups. This hypothetical product is illustrated in Figure 4.5. The replacement of each C=O group with an amide group results in a theoretical atomic composition of 71.4% C, 14.3% O and 14.3% N. This compares extremely well with the experimentally observed atomic concentrations of 73.2% C, 14.0% O and 12.8% N.

4.1.2.3. Angle Dependent XPS

By performing the XPS experiment at different take-off angles, the vertical homogeneity of the plasma-modified region can be studied. Figure 4.6 shows the C1s photopeaks for oxygen plasma, argon plasma and ammonia plasma-treated LaRC-TPI, obtained at take-off angles of 15°, 45° and 90°. Atomic concentrations for each plasma and take-off angle are listed in Table 4.3.

It is evident from the shape of the photopeaks for oxygen and argon plasmas that the composition throughout the analysis region is not homogeneous. As the take-off angle approaches 90°, the intensity of the high binding energy region decreases and the photopeak shape begins to approach that of the non-treated LaRC-TPI (see Figure 4.4a). This suggests that as the

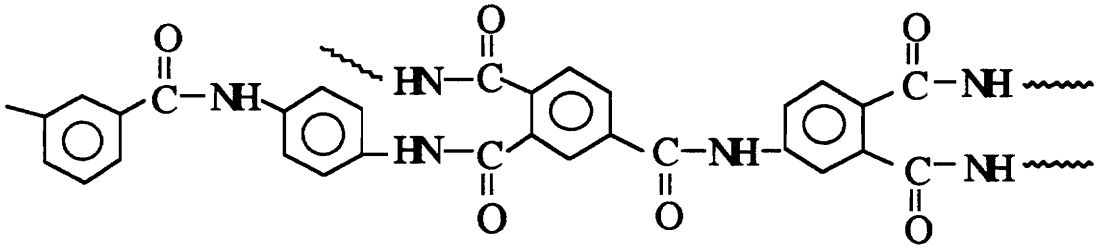

Figure 4.5: Hypothetical structure of ammonia plasma-treated LaRC-TPI.

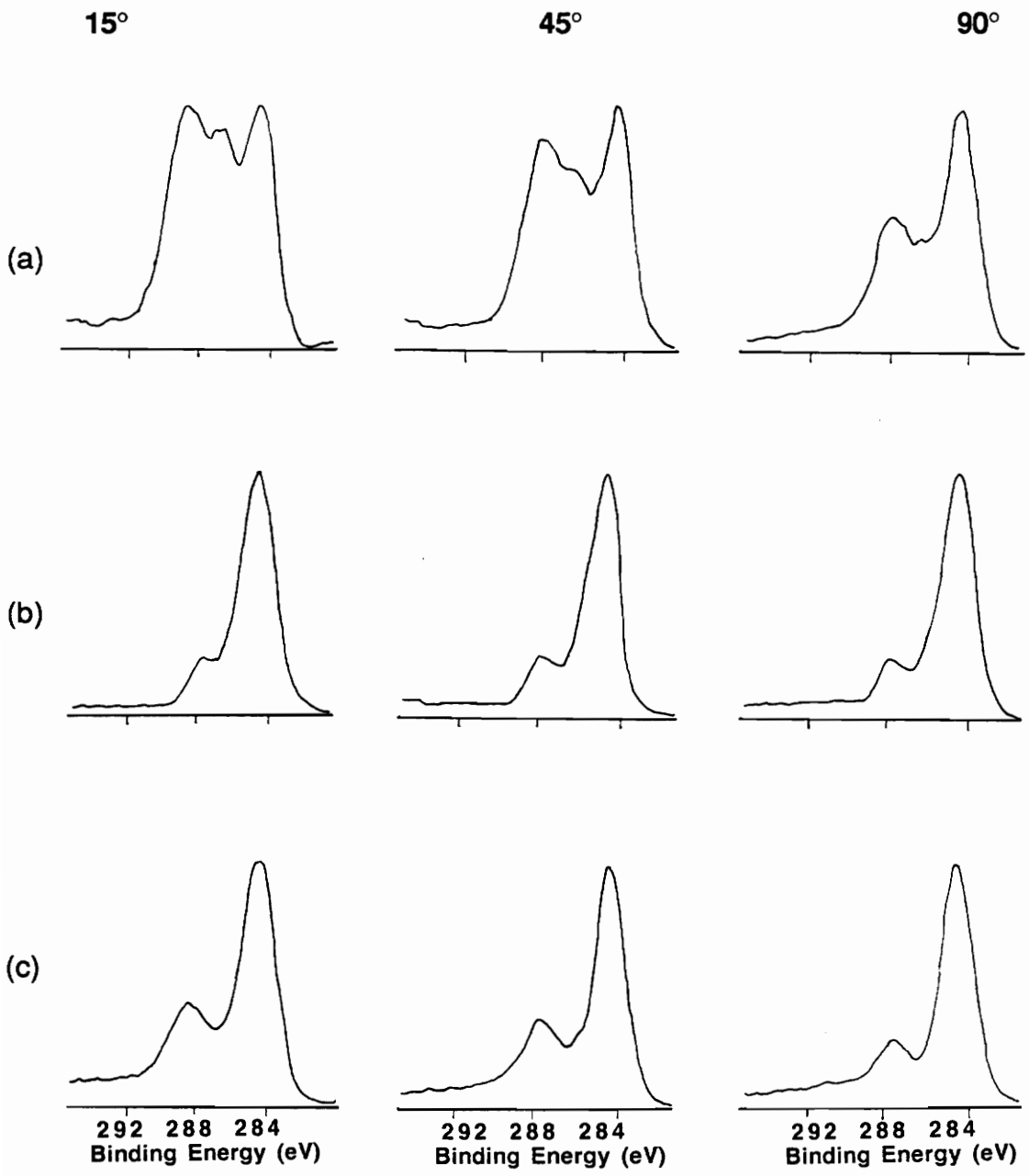

Figure 4.6: C1s photopeaks from angle dependent XPS experiments. (a) oxygen plasma (b) ammonia plasma (c) argon plasma.

Table 4.3: Angle dependent XPS atomic concentrations for LaRC-TPI.

A. Oxygen Plasma

Photopeak	15°	45°	90°
C1s	55.9%	55.8%	62.3%
O1s	39.0	38.7	32.3
N1s	5.1	5.5	5.4

B. Argon Plasma

Photopeak	15°	45°	90°
C1s	65.8%	68.2%	72.3%
O1s	28.5	25.9	22.0
N1s	5.7	6.0	5.7

C. Ammonia Plasma

Photopeak	15°	45°	90°
C1s	72.9%	72.4%	74.8%
O1s	11.2	13.0	12.5
N1s	15.9	14.6	12.7

sampling depth increases, the regions beyond the plasma-treated layer are being included in the analysis. The spectra following ammonia plasma shows no changes in the intensity of the high binding energy shoulder as the angle changes, suggesting a more uniformly modified or thicker layer.

XPS atomic concentrations listed in Table 4.3 confirm the photopeak shape analysis. For oxygen and argon plasmas, the relative concentration of carbon increases about 7% while the oxygen concentration decreases ~6-7% as the take-off angle is changed from 15° to 90°. The nitrogen concentration does not change significantly for either oxygen or argon plasma-treated LaRC-TPI as a function of take-off angle. In the case of ammonia plasma, the changes in atomic concentration are much less in going from 15° to 45° to 90°. This atomic composition data is also supported by the lack of shape or intensity changes seen in the C1s photopeak for samples treated in ammonia plasma (see Figure 4.6b). Overall, it can be stated that the plasma-modified regions are contained in the near-surface regions and the depth which can be probed at the take-off angle of 90° is not vertically homogeneous.

4.1.2.4. Atmospheric Shielding of Argon Plasma-treated LaRC-TPI

Table 4.4 shows the XPS results of the glove bag experiments in which argon plasma-treated LaRC-TPI was protected from the atmosphere and compared to samples prepared without regard to atmospheric exposure. There are essentially no differences seen in the samples prepared by the two different methods. The possibility exists that some leakage or residual air was present in the glove-bag(s) although care was taken to purge thoroughly. To be certain of eliminating atmospheric contact between plasma treatment and XPS analysis, it

Table 4.4: XPS atomic concentration data for argon plasma-treated LaRC-TPI, exposed and unexposed to atmosphere subsequent to plasma treatment.

	Atmospheric Exposure		No Atmospheric Exposure	
Photopeak	**Binding Energy** (eV)	**Atomic Conc.** (%)	**Binding Energy** (eV)	**Atomic Conc.** (%)
C1s	284.6, 288.1	69.4	284.6, 288.0	69.2
O1s	531.5	24.5	531.7	23.7
N1s	399.9	6.1	400.0	7.1

would be best to connect the plasma reactor directly to the XPS unit, through a series of vacuum interlocks.

4.1.2.5. Lithium Fluoride Shielding Experiments

The lithium fluoride (LiF) windows utilized in the shielding experiments have the lowest ultraviolet transmission limit of any known material, with a lower limit cut-off of 104 nm [148]. This is well into the vacuum ultraviolet region; radiation of these wavelengths is well-represented in plasmas [32]. It was critical in performing these experiments to let as much vacuum ultraviolet and ultraviolet radiation as possible pass through to the sample surface. Thus, the only effect of shielding the samples would be to prevent direct contact with particle fluxes.

The atomic concentrations of plasma-treated LaRC-TPI which was shielded with LiF windows during plasma exposure are shown in Table 4.5. The atomic concentrations of the oxygen and argon plasma-treated samples differ only slightly from the atomic concentrations listed in Table 4.1 for unshielded samples. On the other hand, the atomic concentrations of C, O and N for the shielded ammonia plasma-treated samples are quite different from the values for the samples treated without shielding and in fact, are essentially identical to the values for the non-treated LaRC-TPI surface.

It appears that in the case of oxygen and argon plasmas, shielding the surface from the particle flux has no effect due to the high intensity of the radiative component of the plasmas. Bond breakage and changes in the surface composition still can occur, leading to changes in surface chemistry. However, in the case of ammonia plasma, the particle flux is critical in initiating

Table 4.5: XPS atomic concentrations for LiF shielding of plasma-treated LaRC-TPI.

	Photopeak		
	C1s	O1s	N1s
Non-treated LaRC-TPI	80.3%	14.1%	5.6%
Oxygen Plasma/LiF	61.5	32.6	5.9
Argon Plasma/LiF	72.0	22.4	5.6
Ammonia Plasma/LiF	81.5	13.6	4.9

change in surface chemistry. It was stated earlier that the attack of ammonia plasma species at the carbonyl carbons results in the formation of amide functional groups. The results of this shielding experiment appear to lend support to this mechanism, since blocking the reactive species from the surface apparently results in no reaction.

The effects of vacuum UV radiation on polyimides have been documented by Lazare and Srinivasan. In their studies, polyimide films were bombarded with a high energy pulse output from a mercury vapor lamp, where the predominant radiation wavelength is 185 nm. It was found that when the samples were exposed to air after the radiation treatment, the polyimide surface was both ablated and oxidized and the relative atomic concentration of oxygen on the polyimide surface was also increased. Therefore, it can be concluded that the effect of UV radiation alone can induce significant changes in polyimide surface chemistry [149].

4.1.3. Infrared Reflection-Absorption Spectroscopy (IR-RAS)

The use of IR-RAS, a molecular technique, in the analysis of the plasma-modified surfaces was intended to complement the results obtained by XPS, which yields primarily atomic information. IR-RAS is not generally considered to be a surface sensitive technique in the same sense as XPS, since the entire thickness of a sample film is probed by the infrared beam. However, by keeping the total sample thickness less than 50 nm, the modified surface regions represent a more significant percentage of the entire sample. The IR spectrum of the surface regions can then be extracted by conventional spectral subtraction techniques without significant loss of signal/noise. Assignment of IR

bands, unless otherwise stated, was made by consulting textbooks and handbooks on IR analysis of organic compounds [150-154].

The thicknesses of LaRC-TPI coatings on Ferrotype used in these experiments were measured by ellipsometry to be 25-30 nm. Figure 4.7 shows the IR-RAS spectra of non-imidized and imidized LaRC-TPI. These spectra were obtained to understand the IR absorption characteristics of nonplasma-treated samples. The band at 1535 cm^{-1} in the non-imidized film corresponds to the amide group in the poly(amic-acid) precursor and is not observed in the spectra of the imidized film [155]. Assignments of the major peaks in the imidized sample are listed in Table 4.6 [156,157]. Characteristic imide bands include those at 1780 and 1710 cm^{-1}, which are assigned to the imide C=O stretching modes. The weak band around 1852 cm^{-1} is a feature observed only in the case of LaRC-TPI; it has been suggested that it corresponds to residual anhydride, isoimide or other intermediate products. Benzophenone C=O stretch is observed around 1675 cm^{-1}. Bands at 1370 and 1100 cm^{-1} correspond to imide C-N stretching.

Surface changes resulting from plasma exposure were observed by subtracting the spectrum of the imidized, non-plasma treated LaRC-TPI from the spectrum of the plasma-treated sample. The resulting difference spectrum contains only bands which are associated with changes induced by plasma. Positive peaks correspond to new species whereas negative peaks reflect species which are no longer present. Due to the low absorbances of the peaks in the difference spectra (usually 10^{-3} absorbance units), the presence of even small quantities of water or water vapor is extremely detrimental to the quality of

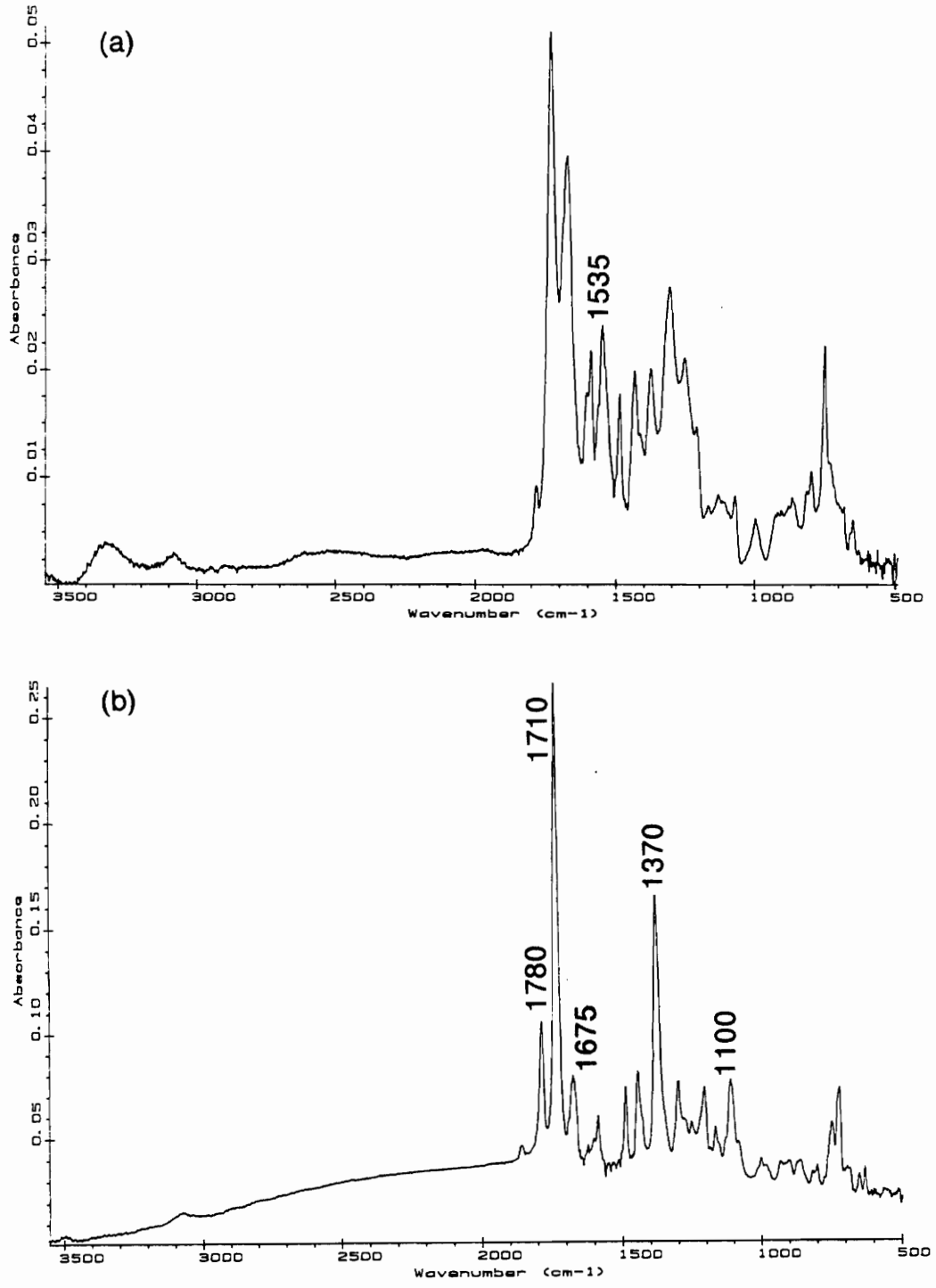

Figure 4.7: Reflection-absorption infrared spectra. (a) non-imidized LaRC-TPI (b) fully imidized LaRC-TPI.

Table 4.6: Identification of major bands in IR-RAS spectrum of non-treated LaRC-TPI.

Frequency(cm^{-1})	**Assignment**
3500	O-H stretch (acid)
3070	Aromatic C-H stretch
1852	C=O stretch (intermediate products)
1780	C=O stretch (imide)
1710	C=O stretch (imide), ø-N stretch
1675	C=O stretch (benzophenone and acid))
1585,1485,1443	Substituted C=C stretch
1370	Imide C-N stretch
1300	Aromatic C-H bend
1275,1250	CH, CH_2, CH_3 bend
1200	ø-N bend
1100	ø-N-C bend
900,930	O=C-ø-H stretch
720	O=C-N bend

the spectra. It was necessary to purge the spectrometer bench for several hours with dry nitrogen to remove all traces of the water peaks from the spectrum.

The difference spectra from the plasma-treated LaRC-TPI films are shown in Figure 4.8. The major peaks are tabulated in Table 4.7. A comparison of all three plasma treatments reveal new species in regions of the IR spectrum associated with C=O stretching and C-O or C-N stretching. The spectra for oxygen and ammonia plasma-treated LaRC-TPI spectra also show weak broad absorbances in the O-H or N-H stretching regions. This IR information is complementary to the XPS results, which showed that new species containing C-O and/or O-C=O groups were formed from plasma treatment.

All three plasmas also show negative peaks at 2930 and 2860 cm^{-1}, corresponding to aliphatic C-H stretching. It is postulated that these bands result from carbonaceous contamination acquired during the high temperature imidization of the LaRC-TPI coatings. Subsequent plasma treatment removes this thin layer of contamination, causing the peaks to be seen as negative.

The IR spectrum for the oxygen plasma-treated surface shows new bands in the C=O stretching region at 1770 and 1725 cm^{-1}, which could be assigned to carboxylic acid or ester functionality, as also observed from the XPS curve-fitted data. A weak broad band at 3332 cm^{-1} could be indicative of O-H stretching from carboxylic acids and/or hydroxyl groups. Further evidence for ester or hydroxyl groups is provided by the presence of bands associated with C-O stretching observed at 1390 and 1205 cm^{-1}. The band at 1205 cm^{-1} could also correspond to C-O-H bending. The breadth of all the peaks in the difference spectra makes any assignments strictly speculative.

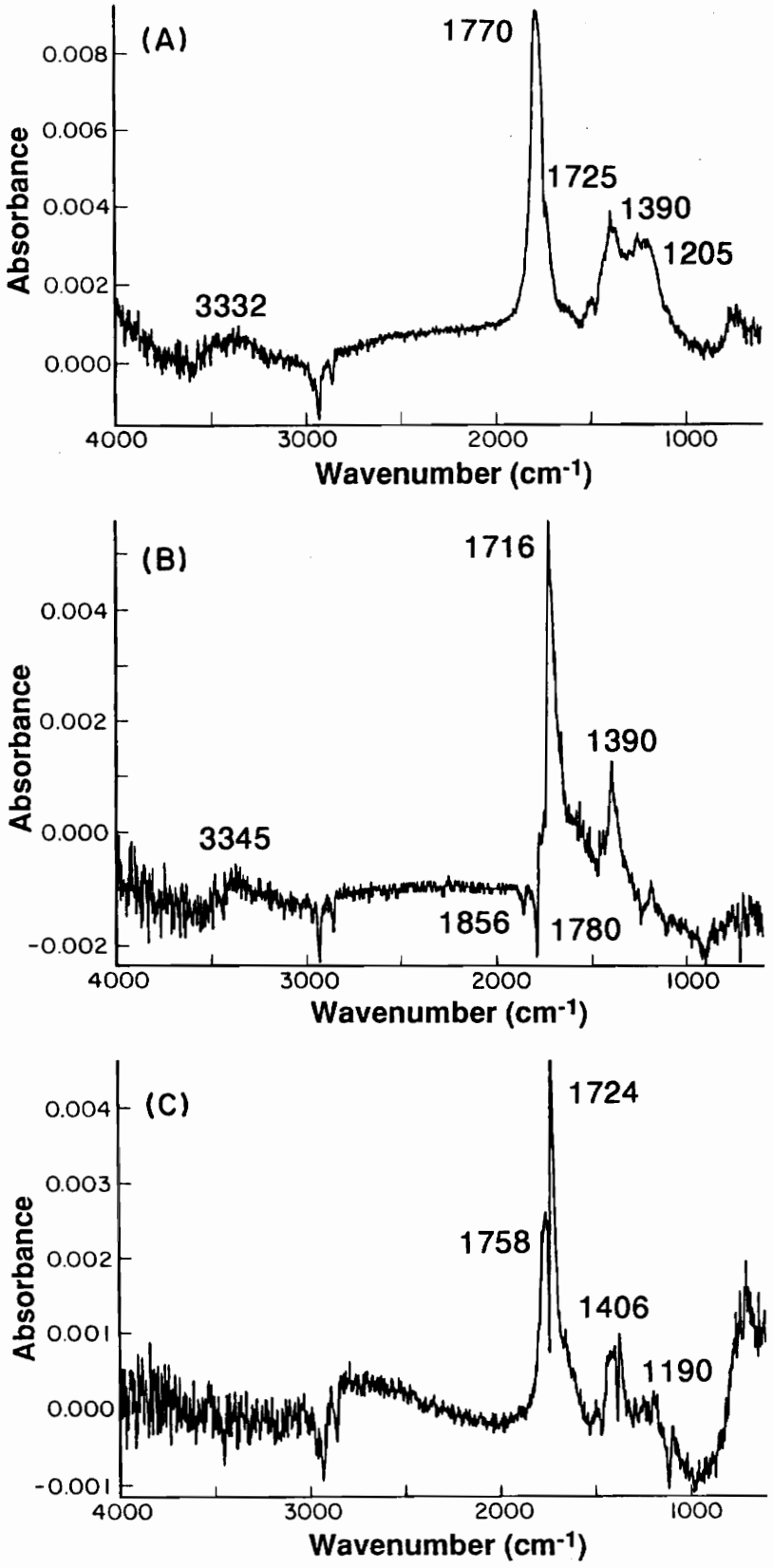

Figure 4.8: IR-RAS difference spectra of plasma-treated LaRC-TPI. (A)

Table 4.7: IR-RAS band assignments for plasma-treated LaRC-TPI.

Plasma	Frequency (cm^{-1})	Assignment
Oxygen	3332	O-H stretch
	1770	C=O stretch (ester)
	1725 (shoulder)	C=O stretch (acid)
	1390	C-O stretch
	1205	C-O-H bend
Ammonia	3345	N-H stretch
	1716	C=O stretch (amide)
	1390	C-N stretch
	1856 (negative)	C=O stretch (imide)
	1780 (negative)	
Argon	1758	C=O stretch
	1724	C=O stretch
	1406	C-C=O bend (ketone)
	1190	C-O stretch

Dunn et al. studied changes in the IR-RAS spectrum of poly(pyromellitimide) after oxygen plasma treatment and have also reported increases in the intensity of bands in the 1575-1830 cm^{-1} C=O stretching region and in the 1050-1250 cm^{-1} C-O stretching region. It was suggested that the C=O groups may arise from the formation of aldehydes, ketones, esters or carboxylic acids, and that the C-O groups are due to the presence of ether, alcohol/phenol or esters [158].

The IR-RAS spectrum for argon plasma-treated LaRC-TPI shows new bands at 1758 and 1724 cm^{-1}, which appear to correspond to ester, carbonate or ketone species. Results of the XPS curve-fit analysis also suggested the presence of ester or carbonate (see Section 4.1.2.2). Ketone groups could be formed during photoreduction or cleavage reactions centered around the benzophenone group. The absence of a resolvable band in the high-frequency region of the spectrum precludes the presence of carboxylic or hydroxyl functional groups. Bands at 1190 and 1406 cm^{-1} are assigned to C-O stretching and ketone C-C=O bending modes, respectively.

In the IR-RAS spectrum for the ammonia plasma-treated sample, shown in Figure 4.8b, two additional negative peaks are observed at 1856 and 1780 cm^{-1}. These peaks are assigned to imide ring vibrations which are observed in the spectra of non-treated LaRC-TPI, as discussed above. The negative orientation of these peaks provides strong evidence that imide ring chemistry is altered during exposure to ammonia plasma. It was also observed by XPS (see Section 4.1.2.2) that imide functionality appeared to be converted to amide functionality; again, the two techniques are seen to be complementary in nature. The IR-RAS spectrum also shows evidence for amide formation. Bands at

1716, 1390 and 3345 cm^{-1} correspond to the amide I carbonyl stretching mode, C-N stretching and N-H stretching of amides, respectively. The amide I band falls into the high end of the amide range; more appropriately, it could be assigned to a lactam or fused amide structure.

The possibility of nitrogen from the ammonia plasma being incorporated into amine groups as opposed to amide groups is also a possibility, but a less likely one. Not only would the C-N stretch for amines be observed at a lower frequency than 1390 cm^{-1}, but amine formation would also not account for the intense C=O absorption, since the XPS atomic concentration data showed that no additional oxygen was incorporated as a result of plasma treatment.

4.1.4. Plasma Etch Rate Studies

Through the study of polymer ablation rates, it is possible to obtain information on the physical mechanism of the plasma reaction. For ablation to occur, successive fragmentation of surface chains must first occur, leading eventually to the formation of volatile, low molecular weight species which are subsequently pumped out of the plasma system. Thus, when ablative effects are observed, chain scission must necessarily be occurring. The largest ablation rates are primarily observed with oxygen or other hetero-atom-containing polymers, mainly due to the fact that groups such as C=O are known to serve as active sites for initiation of molecular weight changes [30].

Figure 4.9 shows a comparison of etch rates of LaRC-TPI in oxygen, argon and ammonia plasmas. It can be seen that oxygen is the most ablative plasma, followed closely by argon. Oxygen and argon etch rates at 50 watts are estimated to be 30-50 Å/min. Ammonia plasma is so slow as to be almost

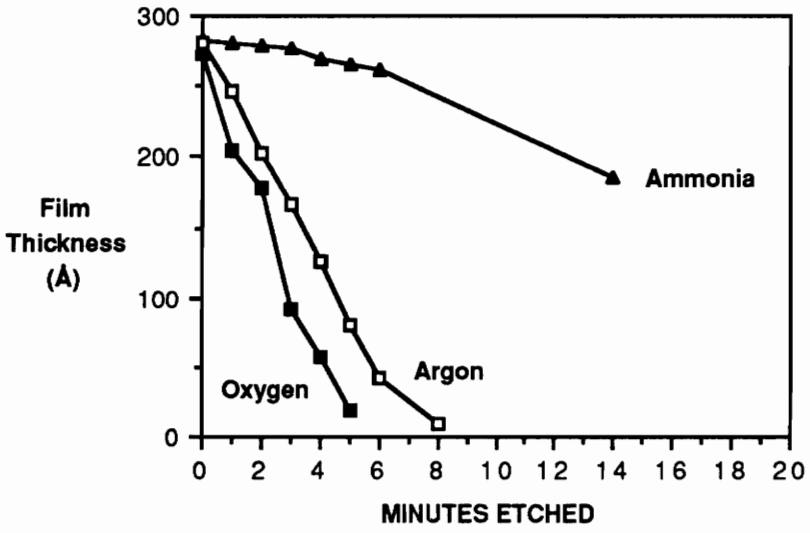

Figure 4.9: Comparison of etch rates of oxygen, argon and ammonia plasmas on LaRC-TPI.

negligible in the early stages of etching. It can be implied from this study that different mechanisms in plasma reactions are operative for oxygen and argon plasmas versus ammonia plasma.

These results can also be correlated with the information obtained from the curve-fitted XPS C1s photopeaks. It was reported in Section 4.1.2.2 that increases in the intensity of the imide carbonyl peak were observed for oxygen and argon plasmas, but not for an ammonia plasma. The earlier conclusion was that selective ablation/chain fragmentation was occurring to create an enrichment of imide-containing segments at the surface. Since no changes in imide intensity were seen following ammonia plasma exposure, it was also concluded that no significant chain scission was taking place. The etch rate experiments exactly parallel the XPS results, in that the two plasmas that are seen to be the most ablative in the etch rate experiments have also shown evidence of causing chain scission as observed by XPS curve-fitting.

4.1.5. High Resolution Scanning Electron Microscopy (HR-SEM)

Due to possible ablative effects of certain plasmas as evidenced by the results of the previous section, it should be possible to observe changes in surface topography induced by a given plasma. It is well known that in the plasma treatment of semi-crystalline polymers, density differences between the crystalline and amorphous components cause surface texturing to develop [27]. In plasma etching of polyimides, significant nodularization of the surface can be seen after treatment with oxygen, argon and fluorine containing plasmas [158]. Other researchers have concluded that the "hills" seen by SEM after plasma

treatment are the nothing more than lumps of low molecular weight degradation products [30].

Figure 4.10 shows HR-SEM photomicrographs of LaRC-TPI surfaces subjected to oxygen, argon or ammonia plasma for 20 minutes. Samples treated for 1 minute were identical in appearance to the control non-treated surface, that is, flat and featureless and are therefore not shown. It is seen that an oxygen plasma creates a definite surface texture, whereas argon texturing is weaker but still visible and the ammonia plasma-treated surface demonstrates no change in surface topography whatsoever. Again, this result correlates with the results of etch rate experiments and the XPS spectroscopic evidence for chain scission. The ablative effects of oxygen and argon plasmas lead to the development of visible surface topography whereas the non-ablative ammonia plasma does not disturb the original surface morphology even after a 20 minute exposure.

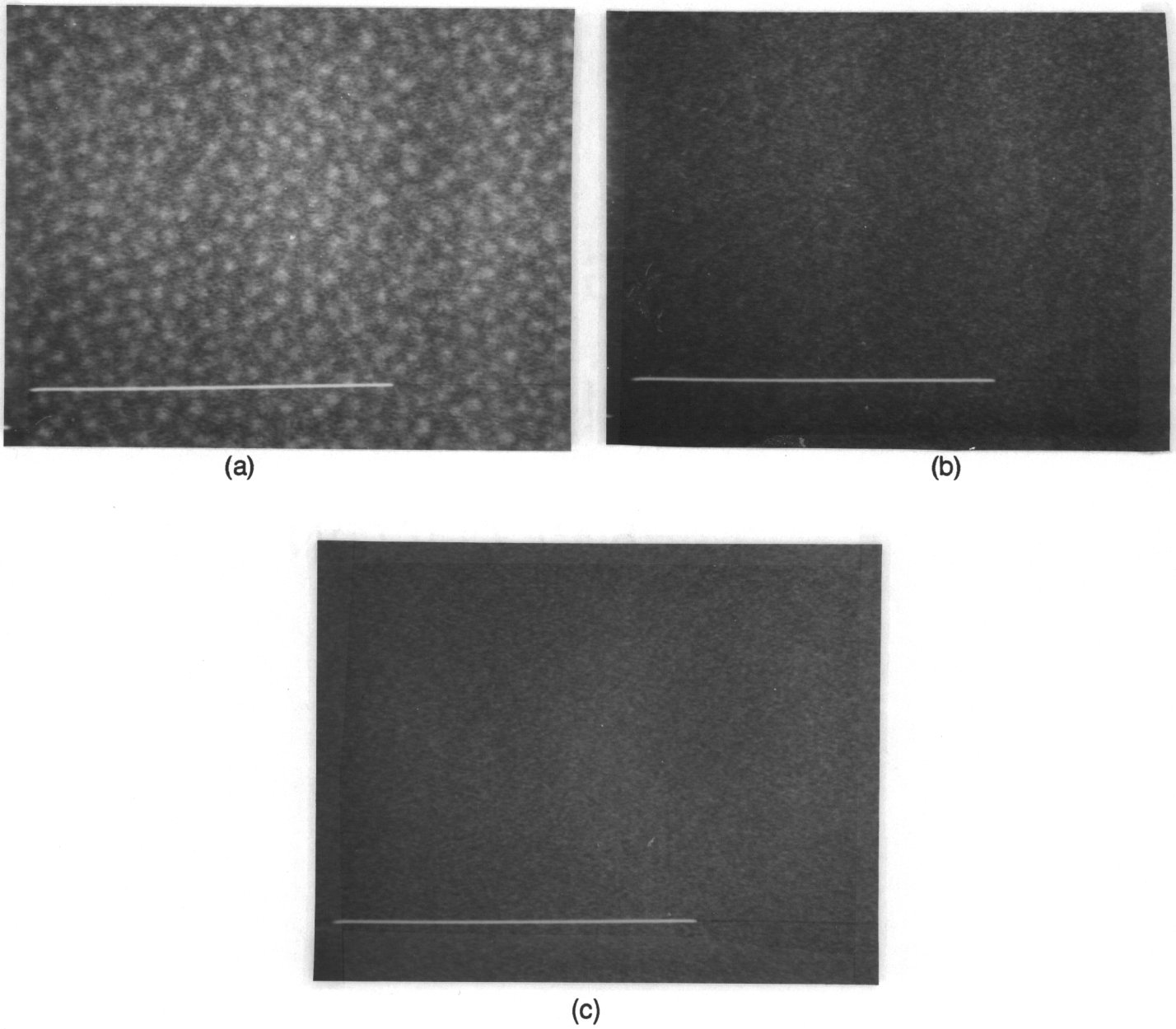

Figure 4.10: High resolution scanning electron micrographs of 20 minute plasma-treated LaRC-TPI surfaces. (a) oxygen plasma (b) argon plasma (c) ammonia plasma. (_____ = .5 μm)

4.2. Surface Characterization of Plasma-treated Kapton®

Kapton® polyimide film was plasma-treated and characterized in order to provide a comparison to the work performed on LaRC-TPI. Although both are linear, uncrosslinked polyimides, Kapton® is an insoluble, intractable polymer in contrast to LaRC-TPI, which is a thermoplastic. The two polyimides also differ in chemical structure, having been synthesized from two different sets of dianhydrides and diamines. There is also a large body of literature on the plasma treatment of poly(pyromellitimides) to which comparisons can be drawn.

4.2.1. Contact Angle Analysis

The results of contact angle analysis on Kapton® are displayed in Figure 4.11. The contact angle of water on non-treated Kapton® is approximately 70°. Following an acetone wipe, the contact angle decreases to just below 50°. As in the case of LaRC-TPI, the plasma treatments decrease the water contact angle significantly below the level of the control (see Figure 4.1). These results point to the formation of a more polar, higher energy surface. The contact angle on the oxygen plasma-treated surface is approximately 10° while that of the argon plasma-treated surface is around 12°. As observed in the case of LaRC-TPI, the ammonia plasma-treated surface exhibits a higher contact angle around 20°.

The contact angles for the non-treated surface and for the oxygen plasma-treated Kapton® film show good agreement with reported literature values of 70° and 10°, respectively [81]. It has also been reported for Kapton® that the polar component of the surface free energy increases after exposure to oxygen plasma [159].

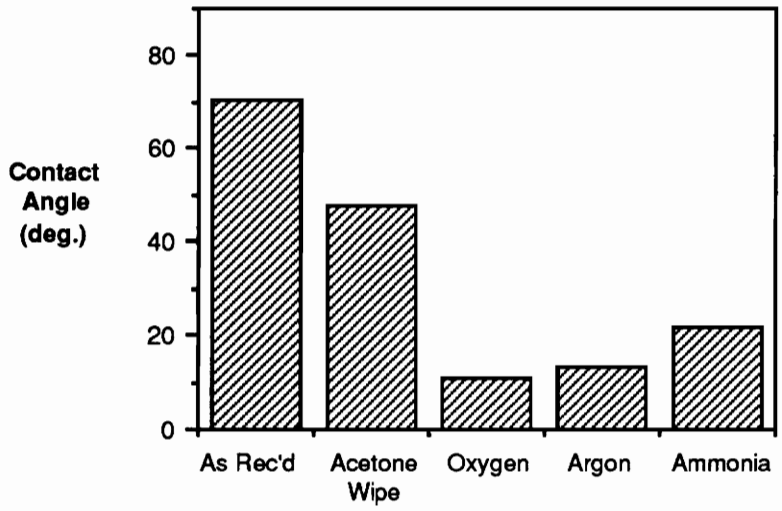

Figure 4.11: Results of water contact angle analysis on non-treated (as-received) and plasma-treated Kapton®.

4.2.2. X-ray Photoelectron Spectroscopy

4.2.2.1 Atomic Composition

The XPS atomic concentrations measured for the as-received and plasma-treated Kapton® films are listed in Table 4.8. The theoretical atomic composition of Kapton® is 75.9% C, 17.2% O and 6.9% N, which compares closely with the experimentally observed results of 78.4% C, 15.6% O and 6.0% N. The atomic compositions of the plasma-treated Kapton® films show trends which are similar to those observed for the plasma-treated LaRC-TPI surfaces. These values were obtained from samples which were plasma-treated for 1 minute. Both oxygen and argon plasma increase the surface atomic concentration of oxygen, while ammonia plasma is again seen to increase the concentration of surface nitrogen. As seen with LaRC-TPI, a small increase in nitrogen concentration is observed in the case of argon plasma, whereas the nitrogen concentration essentially does not change after oxygen plasma treatment. Similarly, the concentration of surface oxygen does not change after exposure to ammonia plasma.

4.2.2.2. Curve-fitted Results

Curve-fitting of the major photopeaks was carried out to extract additional information from the XPS experiments. Table 4.9 contains the binding energy and atomic concentrations of the constituent peaks for the C1s, O1s and N1s photopeaks; the C1s photopeaks are shown in Figure 4.12.

In the spectrum of the non-treated Kapton® film, four major peaks are resolved from the C1s envelope. The peaks at 284.6 and 291.3 eV are

Table 4.8: XPS analysis of non-treated, oxygen plasma, argon plasma and ammonia plasma-treated Kapton®.

	Atomic Concentration(%)		
	Carbon	**Oxygen**	**Nitrogen**
Non-treated	78.4	15.6	6.0
Oxygen plasma	63.0	30.8	6.2
Argon plasma	67.9	24.5	7.6
Ammonia plasma	71.6	15.8	12.6

TABLE 4.9: Results from curve-fitted C1s, O1s and N1s photopeaks for non-treated and plasma-treated Kapton®

Photopeak		NON-TREATED BINDING ENERGY (eV)	NON-TREATED ATOMIC CONCN. (%)	OXYGEN BINDING ENERGY	OXYGEN ATOMIC CONCN.	AMMONIA BINDING ENERGY	AMMONIA ATOMIC CONCN.	ARGON BINDING ENERGY	ARGON ATOMIC CONCN.
C1s	C-C	284.6	35.3	284.6	19.7	284.6	49.4	284.6	23.9
	C-O/C-N	285.7	28.6	285.7	14.4	285.8	9.3	285.6	21.4
	C-O			286.9	8.4			286.8	4.2
	C=O	288.5	10.9	288.6	17.0	287.8	12.9	288.5	14.0
	carbonate			290.1	2.6			290.0	2.8
	shake-up	291.3	3.6	292.2	0.9			292.3	1.6
			78.4		**63.0**		**71.6**		**67.9**
O1s	O=C	532.1	10.1	532.3	16.3	531.6	11.7	532.2	16.3
	O-C	533.5	5.5	533.4	10.3	532.7	4.1	533.4	6.8
	carbonate			534.2	4.2			534.4	1.4
			15.6		**30.8**		**15.8**		**24.5**
N1s	N-C=O	400.6	**6.0**	400.6	**6.2**	399.6	**12.6**	400.5	**7.6**

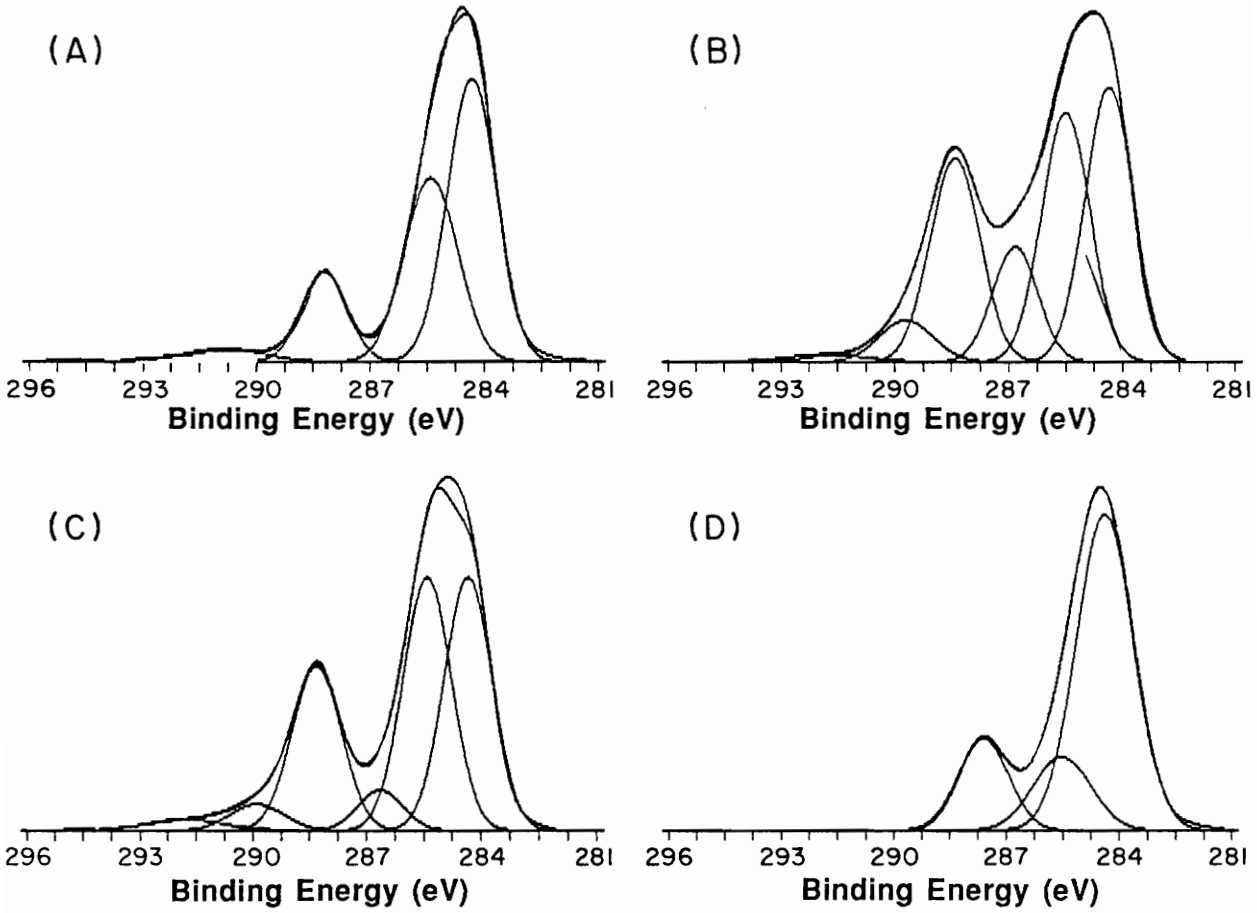

Figure 4.12: Curve-fitted Kapton® C1s photopeaks. (A) non-treated (B) oxygen plasma (C) argon plasma (D) ammonia plasma.

assigned to carbons from the aromatic rings and the aromatic C-C shake-up satellite, respectively. The peak at 285.7 is assigned to the ether C-O linkages and imide C-N linkages, and the peak at 288.5 eV is representative of the imide carbonyl group. This is in full agreement with the curve-fitted values reported in the literature [81,139,140,144,160].

Careful analysis of the peak intensities within the C1s photopeak for the non-treated surface reveals a nonstoichiometric situation. It was noted by Buchwalter and Baise that the peak at 285.7 eV, corresponding to C-O and C-N linkages, is too intense in comparison to theoretical values. The total percentage of atoms singly bonded to oxygen and nitrogen in this particular poly(pyromellitimide) should only be 10.3%, however, it is seen to be 28.6%. This anomaly was accounted for by postulating that the benzene ring carbons directly attached to the imide ring are rendered electron deficient by conjugation with the imide functional group. Thus, these ring carbons are also included in the peak at 285.7 eV rather than being included with the hydrocarbon species at 284.6 eV. This effect is only observed when there are three or more imide groups attached directly to an aromatic ring. This assumption, proven out by model compound studies, apparently solves the stoichiometry problem [144].

Following treatment with oxygen plasma, two new species at 286.9 and 290.1 eV can be fitted to the C1s photopeak. No major shifts or disappearances of any peaks are observed. The O1s photopeak contains a new component at 534.2 eV. No change in binding energy or intensity is observed for the N1s photopeak, as also observed for oxygen plasma-treated LaRC-TPI.

On the basis of being shifted +5.5 eV from the hydrocarbon peak, the peak at 290.1 eV is most likely a carbonate species. This is supported by the

peak at 534.2 eV in the O1s photopeak which also corresponds to the singly-bonded oxygen of a carbonate group. Analysis of bisphenol A polycarbonate reveals peaks at 290.4 and 534.3 eV for the carbonate functional group (see Table A.1). As in the situation of LaRC-TPI, the peak at 286.9 eV was not found in any XPS standards which were analyzed. However, other studies of oxygen plasma-treated Kapton® also report the presence of this peak after exposure to plasma and its assignment has been made as a type of plasma-induced C-O bond, possibly through atomic oxygen addition to the unsaturated benzene rings [81,140,159].

The concentration of the imide carbonyl at 288.6 eV in the oxygen plasma-treated surface increases from 10.9 to 17.0%. This increase in imide concentration after oxygen plasma treatment was also observed for LaRC-TPI and can again be proposed to originate from the selective fragmentation of the Kapton® polyimide, resulting in ablation and surface enrichment of imide functionality.

Similar results are obtained for the argon plasma-treated Kapton®. New peaks are observed at 286.8, 290.0 and 534.4 eV, pointing to the presence of carbonate and C-O containing species. The curve-fitted data for the oxygen and argon plasma-treated surfaces are essentially identical, except for differences in peak intensities. This is in contrast to LaRC-TPI, in which differences were observed between the oxygen and argon plasma-treated surfaces.

Also as observed with the oxygen plasma-treated Kapton® and both oxygen and argon plasma-treated LaRC-TPI, an increase in the concentration of imide is observed from 10.9 to 14.0% for the argon plasma-treated Kapton®

films. The repeated observation of increases in imide intensity is indicative of the fact that chain scission occurs for polyimide materials. It is unlikely that the increase in concentration is due to plasma-induced reactions, as stated in Section 4.1.2.2. It is also unlikely that the increase is actually due to ester or acid species which just happen to have the same binding energy as the original imide carbonyl. It would be an unlikely coincidence that for both types of polyimide studied, new ester or acid species would have the identical C=O binding energies as the original polyimide. This surface chain scission which can be spectroscopically inferred plays an important role in the adhesion of the the two polyimide surfaces, as demonstrated subsequently.

In the case of samples treated in ammonia plasma, results similar to those obtained for LaRC-TPI are seen. Shifts to lower binding energy are observed for the imide carbonyl and the imide N1s peaks. The carbonyl peak at 287.8 eV resembles the binding energy for the nylon 6,6 carbonyl at 287.6 eV and Kevlar® amide carbonyl at 287.9 eV (see Table A.1). The imide N1s peak at 399.6 eV corresponds to the values of 399.6 and 399.7 eV for the nylon 6,6 and Kevlar® N1s photopeaks. This evidence further points to the formation of amide functional groups, as observed with the ammonia plasma-treated LaRC-TPI. As with LaRC-TPI, no shake-up satellite can be fitted to the C1s photopeak after plasma treatment with ammonia.

In the case of LaRC-TPI, it was postulated that the ammonia plasma species attacked carbonyl groups to form amide groups. Thus, in the ammonia plasma-treated LaRC-TPI surface, the oxygen concentration was seen to be equivalent to the nitrogen concentration. This is because all oxygen in LaRC-TPI is in the form of carbonyl groups and each carbonyl group is changed into

an amide group in a 1:1 transformation. However, in Kapton®, only 4 out of 5 (80%) oxygens are contained in carbonyl functional groups, the remaining oxygen (20%) is an ether oxygen. Experimentally, it is observed that the ratio of nitrogen to oxygen in the ammonia plasma-treated Kapton® surface is also 4/5. Therefore, this finding is consistent with the proposed mechanism of ammonia plasma attack in that only carbonyl groups are converted to amide groups.

The replacement of imide C=O with amide functional groups results in the hypothetical molecule shown in Figure 4.13. The calculated atomic composition of this species is 71.0% C, 16.1% O and 12.9% N. As for LaRC-TPI (see Section 4.1.2.2), this compares closely to the experimentally observed values of 71.6% C, 15.8% O and 12.6% N for the ammonia plasma-treated surface.

4.2.2.3. Lithium Fluoride Shielding of Plasma-treated Kapton®

Table 4.10 shows the results from lithium fluoride (LiF) shielding of the Kapton® samples during plasma treatment. It is observed that surface chemistry changes occur for the oxygen plasma and argon plasma-treated surfaces in spite of the shielding, whereas in the case of ammonia plasma, there is essentially no change in the atomic concentration.

These findings are essentially identical to the results for LiF shielded LaRC-TPI samples (see Table 4.5) in which oxygen and argon plasma were able to modify the surface chemistry with the UV/VUV component alone but ammonia plasma was incapable of inducing any surface compositional changes when the LiF windows covered the sample. This again points to the capability of the UV/VUV component of oxygen and argon plasmas to induce

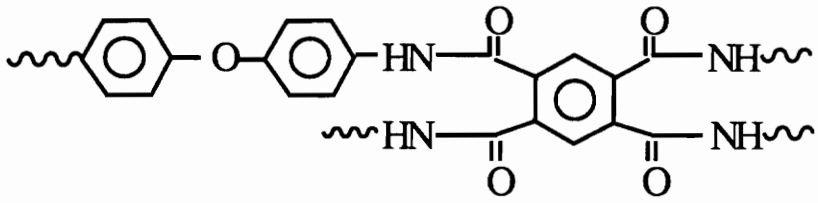

Figure 4.13: Hypothetical structure of ammonia plasma-treated Kapton®.

Table 4.10: XPS atomic concentrations for LiF shielding of plasma-treated Kapton®.

	Photopeak		
	C1s	**O1s**	**N1s**
Non-treated Kapton®	78.4%	15.6%	6.0%
Oxygen Plasma/LiF	57.6	35.9	6.5
Argon Plasma/LiF	65.1	28.0	6.9
Ammonia Plasma/LiF	78.9	14.5	6.6

surface changes. However, it is again observed for ammonia plasma that direct contact with the particle flux is necessary for changes in surface chemistry to occur.

4.2.3. Plasma Etch Rate Studies

Etch rate studies on poly(pyromellitimide) films were carried out by utilizing thin films spin-coated on ferrotype from the poly(amic-acid) precursor of Kapton®. The results of these experiments are shown in Figure 4.14.

As was seen in the case of LaRC-TPI, oxygen is the most ablative plasma, followed closely by argon. Again, ammonia plasma is seen to be negligibly ablative in comparison to the other two plasmas. This can be correlated to the curve-fitted XPS results in which chain scission was observed to be induced by oxygen and argon plasmas, but not for the ammonia plasma (see Section 4.2.2.2).

The ablative effect of oxygen plasma, or more specifically atomic oxygen, on Kapton® polyimide films is well-documented, especially within the context of low earth orbit (LEO) applications. Kapton® has been proposed for use in spacecraft thermal control blankets, but the erosion effects observed after exposure to atomic oxygen present a long-term durability problem [79]. Residual gas analyses of the vacuum effluent during the oxygen plasma treatment of polymer materials reveal the presence of CO, CO_2, H_2 and H_2O, strongly indicating the decomposition of organic matter [27,54].

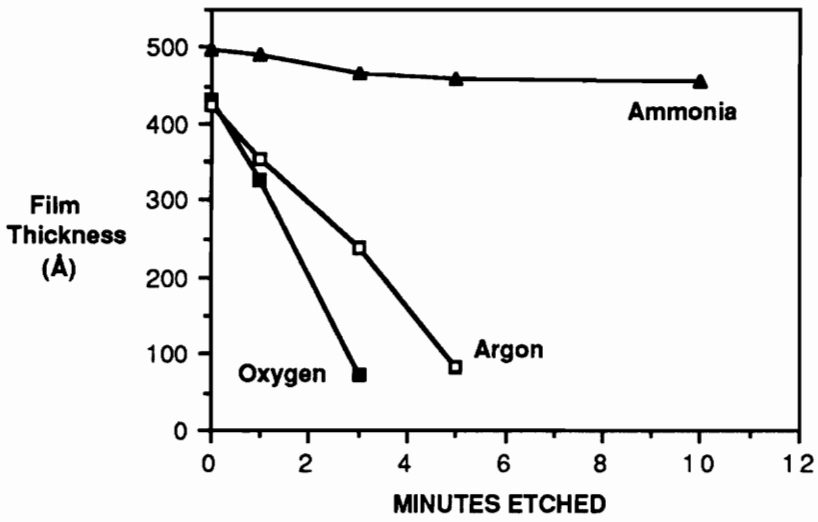

Figure 4.14: Comparison of etch rates of oxygen, argon and ammonia plasmas on Kapton®.

4.2.4. High Resolution Scanning Electron Microscopy (HR-SEM)

HR-SEM photomicrographs of Kapton® films subjected to 20 minutes of plasma exposure are shown in Figure 4.15. A distinct nodular morphology is clearly seen in the case of oxygen and argon plasmas, correlating with the ablative effects of these two plasmas documented in the etch rate experiments (Section 4.2.3). In contrast, the ammonia plasma-treated surface shows no features and is indistinguishable from the control even after 20 minutes of continuous plasma exposure. This result provides additional support of the negligible ablation observed for ammonia plasma seen in the etch rate experiments.

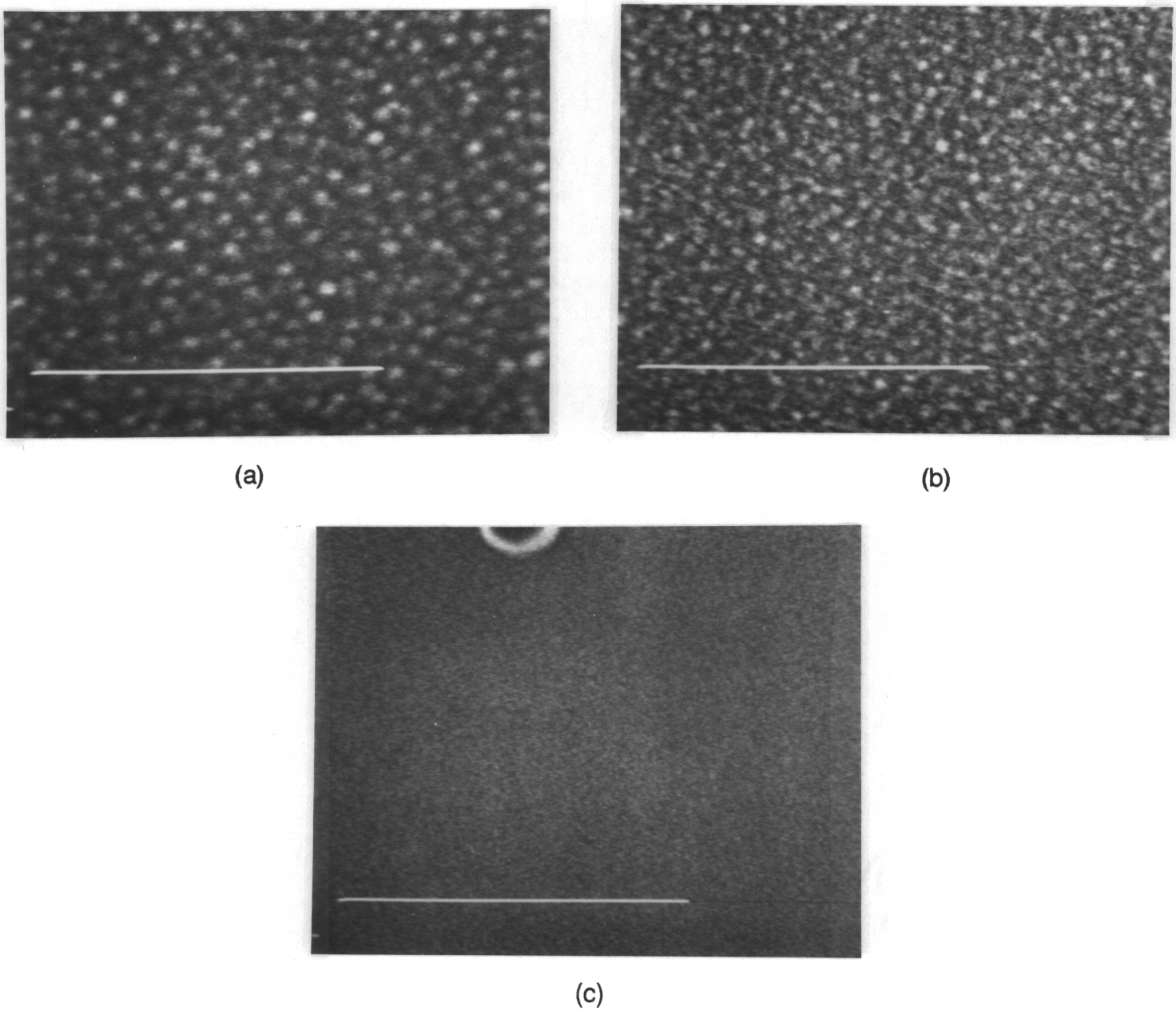

(a)

(b)

(c)

Figure 4.15: High resolution scanning electron micrographs of 20 minute plasma-treated Kapton® surfaces. (a) oxygen plasma (b) argon plasma (c) ammonia plasma. (——— = .5 μm)

4.3. Postulated Plasma Reaction Products

The purpose of this section is to justify the observed reaction products of oxygen, argon and ammonia plasma treatment of both LaRC-TPI and Kapton® polyimides. Both XPS and IR-RAS analyses revealed the presence of new species containing C-O (hydroxyl or ether), O-C=O (ester or carboxylic acid) and $O=C(O)_2$ (carbonate) functional groups. The feasibility of whether such reaction products can be produced in a plasma will be discussed.

It is difficult to fully understand the mechanisms involved in plasma reactions, due to the complexity of the plasma itself. The component species contained in a typical plasma - electrons, ions, radicals, excited state atoms and molecules, ultraviolet and vacuum ultraviolet radiation - are involved in a range of different reactions. The situation is further complicated due to the inclusion of variables such as reactor pressure, gas flow rate, wattage and temperature. As a result, few mechanisms have been studied in detail [27].

However, it is possible to propose reasonable reaction mechanisms from a comparison of plasma products from different reactions. Similarities have been observed between products of plasma reactions and reaction products from photochemistry, pyrolysis, radiochemistry and mass spectroscopy. It must also be reiterated that the environment within a plasma and the reactions taking place on a polymer surface exposed to plasma are primarily free radical in nature. The radical species in a plasma are capable of carrying out free radical abstractions and insertions similar to those encountered in conventional organic chemistry [27,29,32]. Thus, in the event that reaction products are identical, one may assume similarity of reaction mechanisms.

The presence of hydroxyl-containing species can be proposed to arise from reactions shown in Figure 4.16. Hydroxyl radicals are formed from the breakdown of residual water in the plasma system, or from the abstraction of hydrogen by atomic oxygen [30,145]. The addition of a hydroxyl radical to an aromatic ring results in the formation of an adduct radical which is stabilized by delocalization of the unpaired electron, as shown in Scheme A. This adduct radical can then either break down into a benzyl radical and water, or form a phenol-type product.

In Scheme B of Figure 4.16, the benzyl radical formed from the above reaction can also go on to further react with molecular oxygen to form hydroxyl products via a hydroperoxide intermediate. The hydrogen radical in the presence of molecular oxygen forms a reactive radical which attacks the benzene ring and forms a hydroperoxide which also breaks down to phenol [161,162]. Scheme C in Figure 4.16 shows the photo-oxidation of benzene, which ultimately leads to the formation of phenols, which may then be further oxidized to quinones [147,163].

The presence of the benzophenone group in LaRC-TPI is the starting point for several photochemical reactions. Benzophenone is a chromophore and hence photochemically labile, due to its strong absorption in the ultraviolet region. As shown in Scheme A in Figure 4.17, the excited benzophenone group can either abstract a hydrogen from a neighboring molecule forming a biradical or cleave via a Norrish Type I reaction and decarbonylate, yielding carbon monoxide and a benzyl radical [147,162,164]. If this carbonyl radical is exposed to oxygen species, ammonia species or the atmosphere before decarbonylation can occur , the observed presence of carboxylic acids, amides

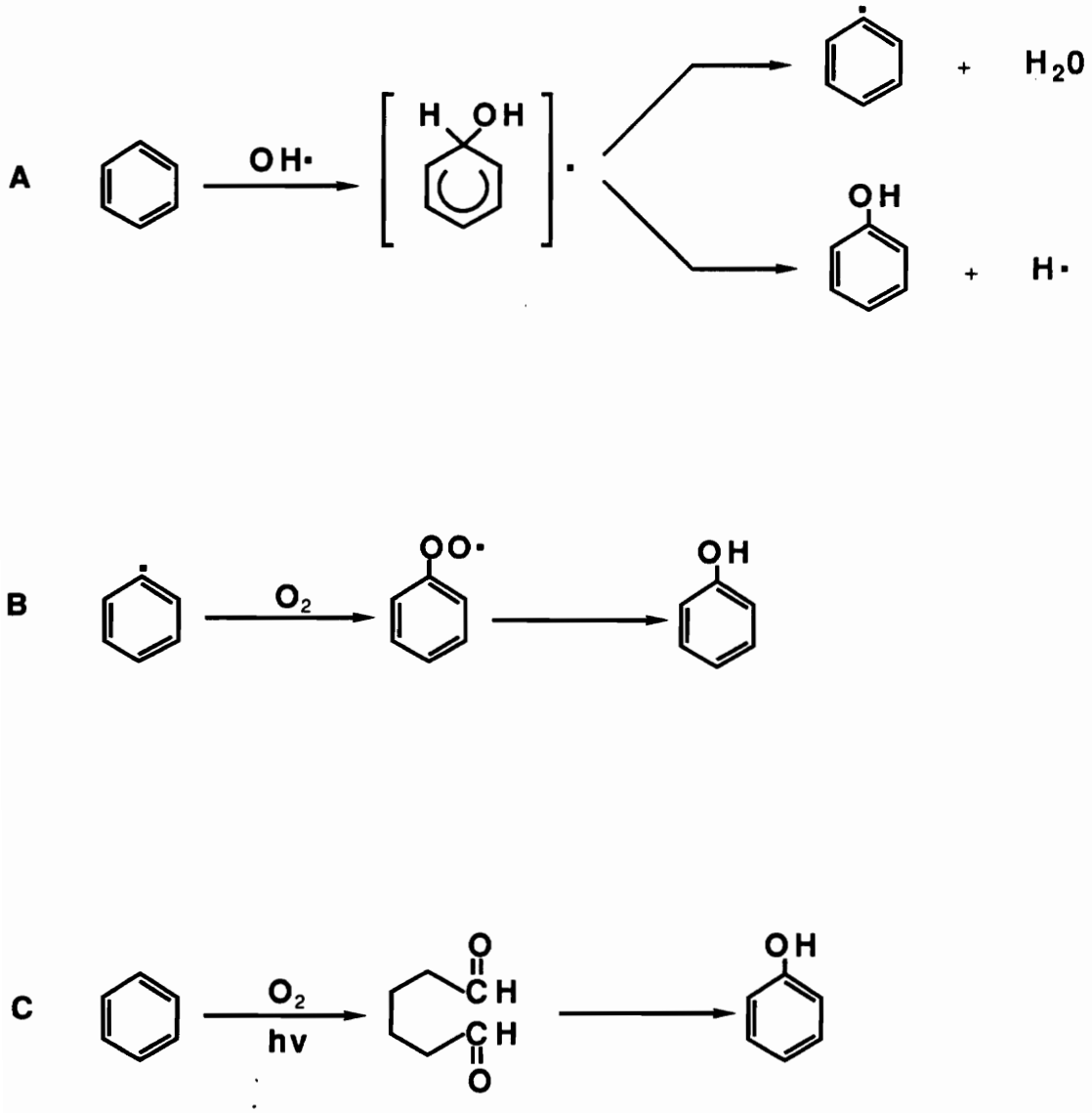

Figure 4.16: Postulated reaction mechanisms for the formation of hydroxyl groups in oxygen plasma-treated materials.

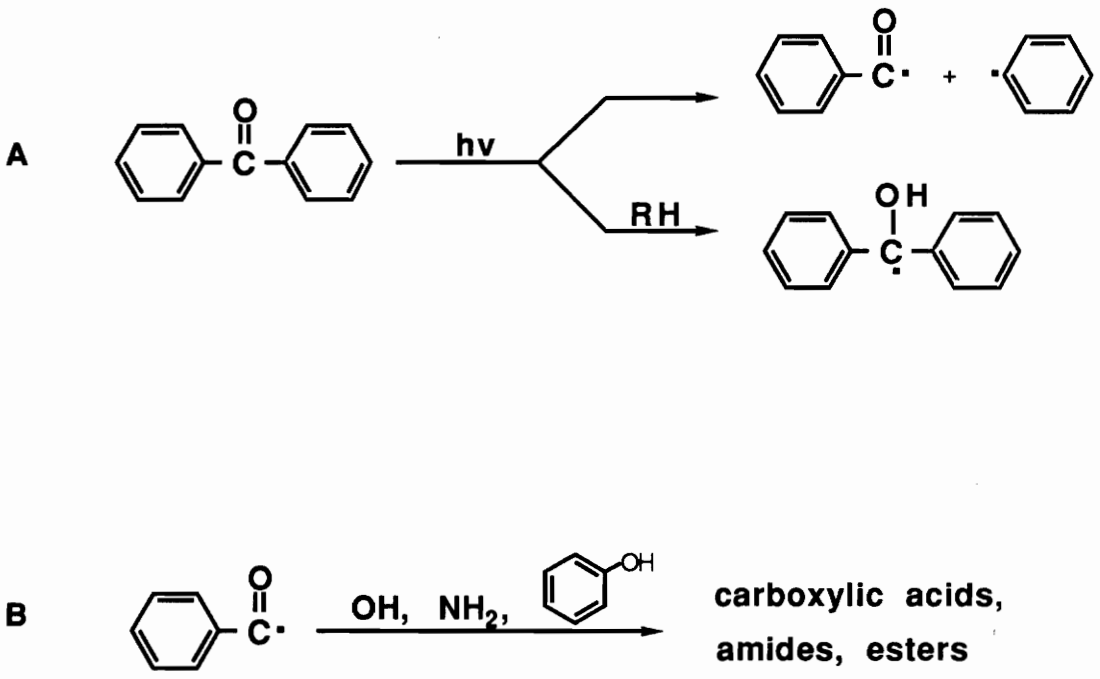

Figure 4.17: Photoreduction of benzophenone and subsequent plasma reactions to form carboxylic acids, amides and esters.

and esters by XPS and IR-RAS analyses can be rationalized, as depicted in Scheme B. This is also an obvious point for chain scission in LaRC-TPI.

Ester functionality can also be formed via several other pathways. The formation of a carboxylate species from benzophenone can terminate with an alkyl or aryl radical [162]. Also, in the presence of peroxy-carboxylic acid, benzophenone can undergo the Baeyer-Villager oxidation to form esters [164].

Carbonate-type structures observed in the oxygen and argon plasma-treated Kapton® films may be accounted for by the reaction of phenolic or hydroxyl radicals with atmospheric carbon dioxide, as hypothesized in Figure 4.18. These radicals may originate from oxygen addition to benzene rings as described above or via a cleavage reaction at the ether oxygen linkage.

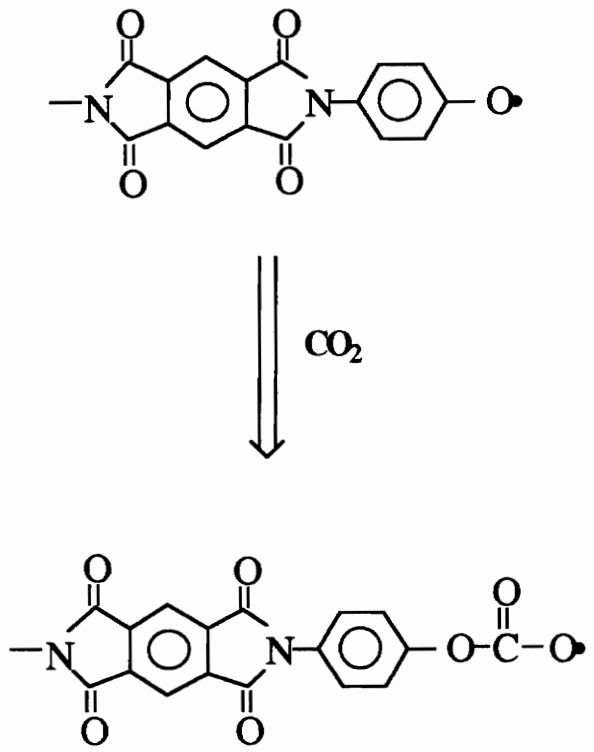

Figure 4.18: Formation of carbonate functionality through cleavage of the ether linkage in Kapton® polyimide.

4.4. Peel Testing

The interactions of the plasma-treated surfaces with other polymeric materials was investigated through peel testing with a pressure sensitive adhesive (PSA), as well as with a high performance thermoplastic polymer. It is understood that bonding with a PSA does not represent a realistic application of polyimide materials; however, it was expected that the use of a PSA would induce the least damage to the plasma-treated surface layer, in contrast to adhesives applied from solution or in a molten state. Thus, it becomes possible to probe the actual physical nature of the modified surface with the least possible disturbance. Bonding of Kapton® films with thermoplastic poly(ether sulfone) represents an application which is more likely to be encountered in practice and is also discussed in this section.

Although the experimental difficulties associated with peel testing are well-known and have been detailed in the Literature Review, it was hoped that it could serve as a test of practical adhesion and differentiate between the various plasma treatments.

4.4.1. Bonding with Scotch Magic Tape

Scotch Magic® tape was selected for these studies over other available pressure sensitive materials because of its polar character. The XPS C1s photopeak of Magic tape is shown in Figure 4.19, and is seen to contain two high binding energy shoulders at 286.2 and 288.6 eV, representative of C-O and O=C-O species, respectively. The atomic composition of the tape surface was found by XPS to be 84% C and 16% O, indicating a significant percentage of surface polar groups. It was expected that the polar groups in this particular

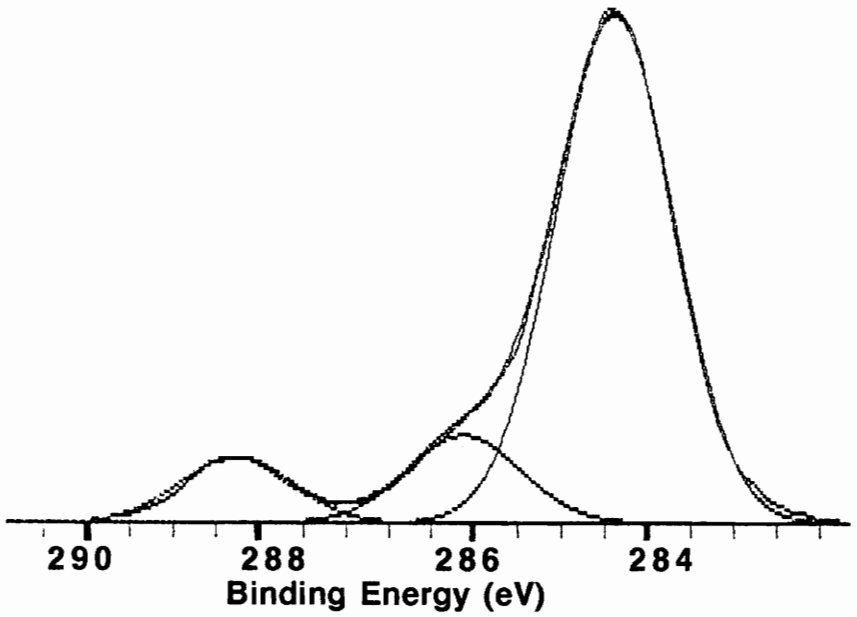

Figure 4.19: XPS C1s photopeak of Scotch® Magic® Tape.

PSA would be capable of interacting with the polar groups on the surface of the plasma-treated polyimides.

This form of peel testing has previously been used to study changes in the surface energy of a siloxane-modified polyimide after treatment with strong bases [165]. When a peel rate of 10 inches per minute is used, no cohesive failure within the PSA is observed. This conclusion was arrived at by auto-adhering two sections of the PSA together and peeling them apart in a 180° degree peel test at 10 inches per minute. Failure always occurred at the interface between the PSA and one of the backing materials, but never within the body of the adhesive.

Peel test results for the plasma-treated LaRC-TPI surfaces are shown in Figure 4.20. In order to determine the effect of treatment time, two sets of samples were made for each plasma treatment. One set was plasma-treated for 1 minute, the second set for 20 minutes. It is evident from the graph that in all instances, the peel strength of the PSA to the plasma-treated surfaces is lower than the peel strength to the control untreated surface. It is also noted that the 20 minute treatment samples show higher peel strengths than the 1 minute plasma-treated samples for all three plasmas. Figure 4.21 shows similar results for the peel strengths of the plasma-treated Kapton® films. Again, the peel strengths of the plasma-treated films are lower in all cases than the control samples, with the 20 minute plasma treatments being slightly higher than the 1 minute treatments.

A substrate heating effect was observed only for the samples which were plasma-treated for 20 minutes. When the samples were taken out of the plasma chamber after 20 minutes, they would be too hot to handle with bare hands.

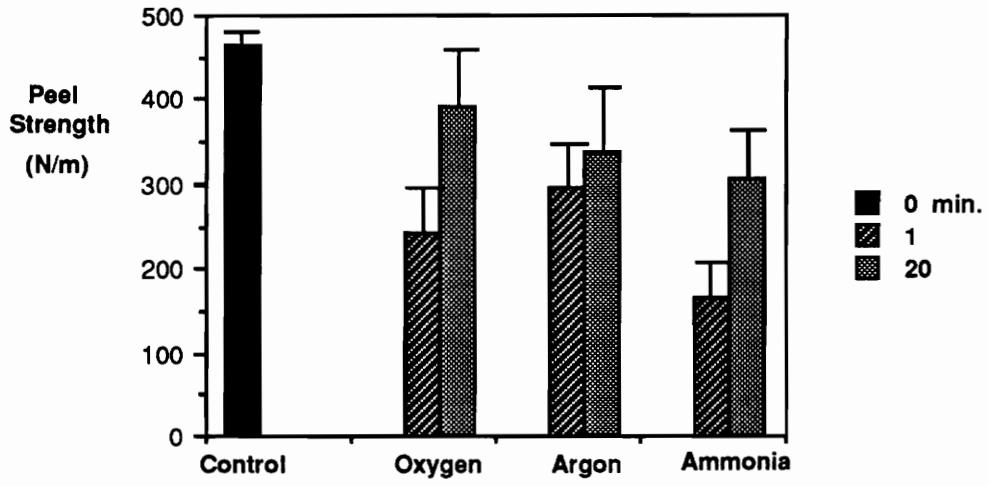

Figure 4.20: Peel test results for plasma-treated LaRC-TPI/Magic Tape.

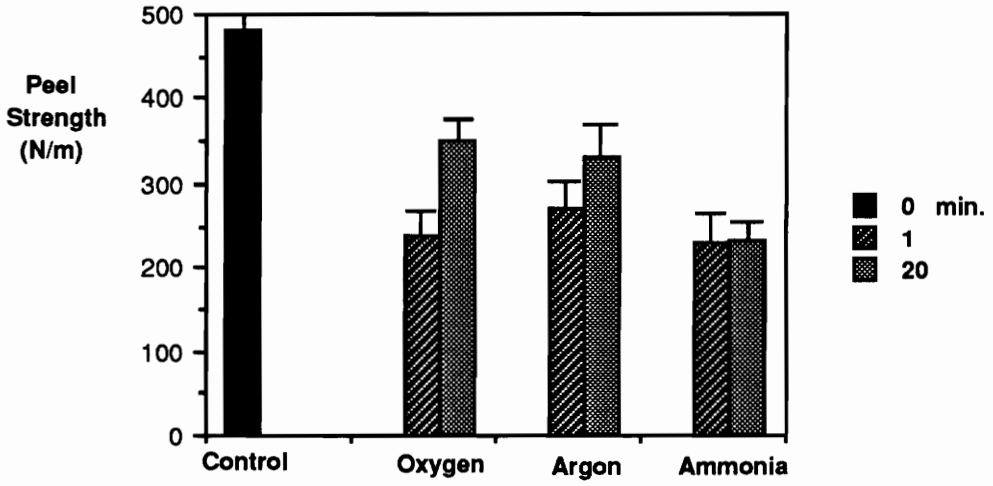

Figure 4.21: Peel test results for plasma-treated Kapton®/Magic Tape.

The effect of substrate heating was thought to be playing a role in the enhanced peel strength of the 20 minute plasma-treated samples by improving wetting, since the PSA was always applied within 30 seconds of removal from the plasma chamber.

Substrate heating was eliminated as a variable by removing the hot samples from the plasma chamber after a 20 minute treatment and placing them onto a large block of aluminum which acted as a heat sink. However, enhanced peel strengths were still observed even though the samples were cooled before the PSA was applied. This experimental result can then be explained by recalling the changes in surface topography of the polyimides after 20 minutes of plasma treatment as revealed by the HR-SEM photomicrographs (see Figures 4.10 and 4.15). Increases in surface roughness may lead to a greater degree of mechanical interlocking and hence increased peel strength. However, this does not explain the greater peel strength of the 20 minute ammonia plasma samples, since no changes in surface topography were observed even after 20 minutes of treatment. The 20 minute samples may have undergone more in-situ heating while in the plasma chamber than the 1 minute samples; which may also be affecting the nature of the plasma-modified layer. Also, even a slight increase in surface temperature relative to the 1 minute samples may be enough to enhance wetting of the PSA.

The overall decreased peel strengths of the plasma-treated controls are puzzling in light of the changes in polyimide surface chemistry after plasma treatment. Increases in surface wettability and polarity are usually indicative of higher surface free energy, a situation generally favorable toward adhesion. Other studies of plasma-modified polyimides have shown increased adhesion

toward chromium or copper deposited layers, due to what is generally accepted as increases in surface active sites [80,81,159].

It can be hypothesized that the ablative action of the plasma has created a loosely attached, highly oxidized layer on the surface of the bulk polymer. This overlayer acts as a weak boundary layer, preventing strong adhesion to the material below. Figure 4.22 shows a schematic representation of this weak boundary layer concept. The region denoted as "plasma zone" is the weakened polyimide which lies between the PSA and the bulk polyimide. During peel testing, the polar weak boundary layer does adhere strongly to the PSA; however, the cohesive strength of this layer as well as its adhesion to the underlying polyimide is weak. This results in a lower force to initiate peeling, with failure occurring either in the weak boundary layer or at the interface between this layer and the polyimide. This hypothesis is consistent with results from etch rate experiments, XPS curve-fitted data and HR-SEM analysis which clearly showed that ablation resulting from chain scission was occurring.

XPS analysis of the failure surfaces also provides additional evidence for this hypothesis. Tables 4.11 and 4.12 list the XPS analysis results for the tape sides and polyimide sides of the peel joint for both LaRC-TPI and Kapton. Because the PSA does not contain nitrogen, any nitrogen which is detected on the tape must originate from the surface of the polyimide. For both the as-received LaRC-TPI and Kapton® samples, no traces of nitrogen were found on the tape peel surface. For all of the plasma-treated samples, small quantities of nitrogen are detected on the tape side, indicating that the average plane of failure is cohesive within the plasma-treated polyimide surface. Only loosely attached material on the surface could be lifted off by the peeling action of the

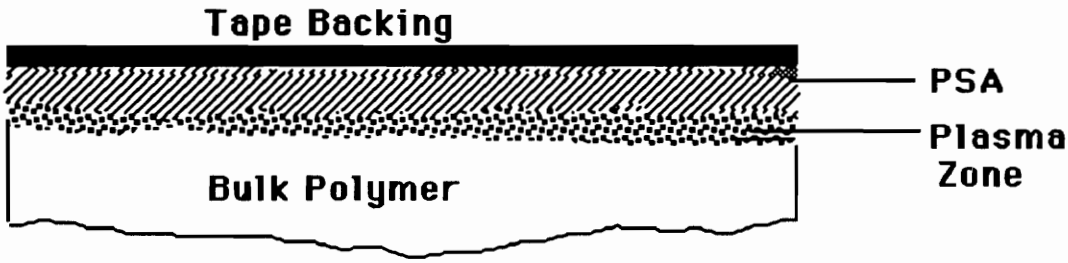

Figure 4.22: Proposed structure of weak boundary layer created by plasma.

Table 4.11: XPS Analysis of LaRC-TPI/Magic Tape peel surfaces, 15° take-off angle.

		Atomic Concentration(%)		
		C	O	N
Non-treated	Tape Side	86	14	0
	LaRC Side	82	15	3
1 min. Oxygen		85	13	2
		85	13	2
1 min. Argon		86	13	1
		85	13	2
1 min. Ammonia		84	15	1
		84	15	1
20 min. Oxygen		85	14	1
		71	26	3
20 min. Argon		84	15	1
		85	13	2
20 min. Ammonia		87	12	1
		82	16	2

Table 4.12: XPS analysis of Kapton®/Magic Tape peel surfaces, 15° take-off angle.

		Atomic Concentration(%)		
		C	O	N
Non-treated	Tape Side	86	14	0
	Kapton Side	81	17	2
1 min. Oxygen		85	14	1
		77	20	3
1 min. Argon		85	14	1
		83	15	2
1 min. Ammonia		85	14	1
		83	10	7
20 min. Oxygen		86	13	1
		84	15	1
20 min. Argon		85	14	1
		82	15	3
20 min. Ammonia		85	14	1
		84	10	6

PSA; the fact that no nitrogen was detected on the tape sides of the control samples shows that the polyimide surface is not inherently weak.

Lazare and Srinivasan also found that an oxidized layer was formed on polyimide after exposure to high energy vacuum ultraviolet radiation; they also observed that this layer was removable after contact with polar liquids [86]. The formation of low molecular weight material after corona discharge treatment of polypropylene was studied by Strobel et al. This low molecular weight material was also removed by washing with polar solvents, but was found to be completely insoluble in nonpolar solvents such as hexane [166]. Other researchers have also found reduced levels of adhesion which were thought to be a consequence of low molecular weight oxidized materials on the surface of corona or plasma-treated polymers [167,168].

4.4.2. Methanol Washing of Plasma-treated Surfaces

In light of the evidence presented above and references from the literature, solvent rinsing of the plasma-treated surfaces was carried out in an attempt to remove the weakly bound plasma-treated layer. Figures 4.23 and 4.24 show peel test results for plasma-treated LaRC-TPI and Kapton®, compared to the untreated control and samples which were rinsed in methanol immediately after plasma treatment. In all cases, samples which were washed with methanol following plasma treatment exhibited improved peel strengths over the plasma-treated samples, comparable to the peel strength of the control. This clearly shows that removal of the weak boundary layer created by plasma restores the original peel strengths by eliminating the weak point in the interphase region.

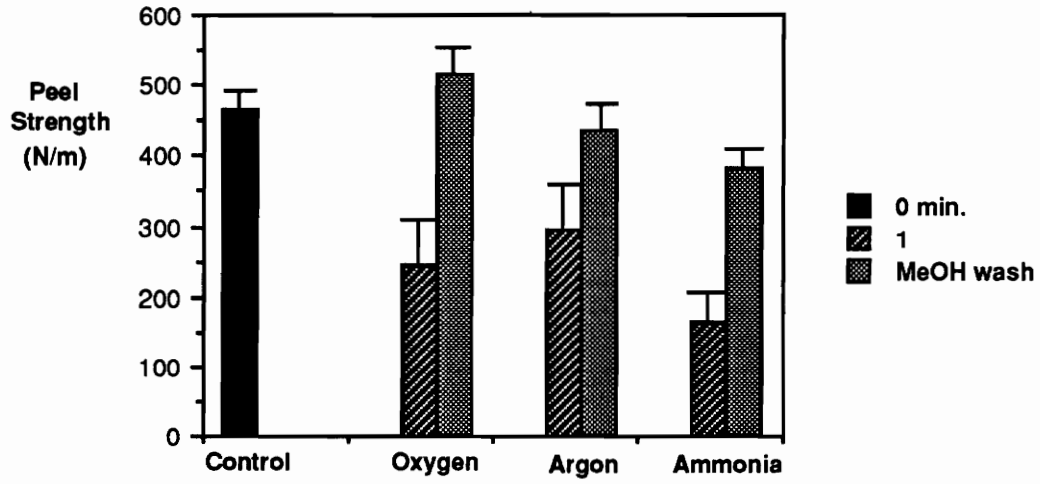

Figure 4.23: Peel test results for LaRC-TPI/Magic Tape, following plasma treatment and methanol washing.

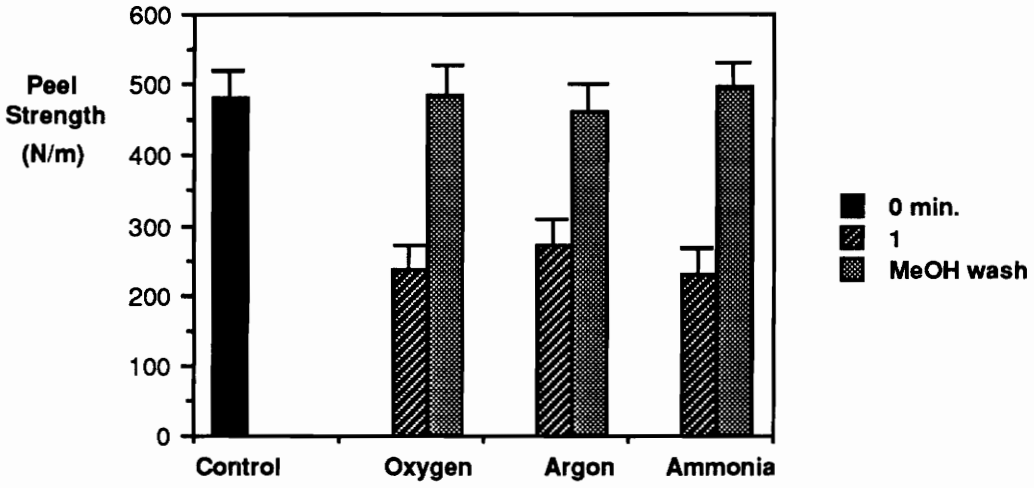

Figure 4.24: Peel test results for Kapton®/Magic Tape, following plasma treatment and methanol washing.

Figure 4.25 shows a comparison of the XPS C1s photopeak for the non-treated, oxygen plasma-treated and oxygen plasma-treated/methanol rinsed LaRC-TPI surfaces. The familiar high binding energy shoulder on the oxygen plasma-treated surface has first been observed in Figure 4.4b. This high binding energy material is apparently removed by the methanol rinse, as the resulting C1s photopeak is essentially identical to the original surface. A slight increase in intensity in the 286.0 eV region is likely due to residual surface methanol. This experiment showed that the methanol rinse did not drastically change the surface chemistry of the LaRC-TPI or Kapton® chemically, but simply removed an overlayer of loosely attached oxidized material.

Attempts were made to collect the methanol rinse residues in order to more fully chemically characterize the weak boundary layer material. UV-visible spectroscopy was used to analyze the rinse solutions. However, probably due to the very small amount of material which was collected, no signal was detected above the baseline.

4.4.3. Fluorine Contamination Experiments

It is shown in the following series of experiments that plasma treatments are not always detrimental to adhesion. In the case of a contaminated surface, plasmas are extremely useful in removing contamination layers and providing a fresh, activated surface for bonding. Moyer and Wightman have shown the utility of an oxygen plasma in removing fluoropolymer release cloth residues from LaRC-160 composites. Levels of adhesion greater than the control samples were observed following the plasma treatments due to the removal of low energy, non-wettable fluoropolymer layers [73].

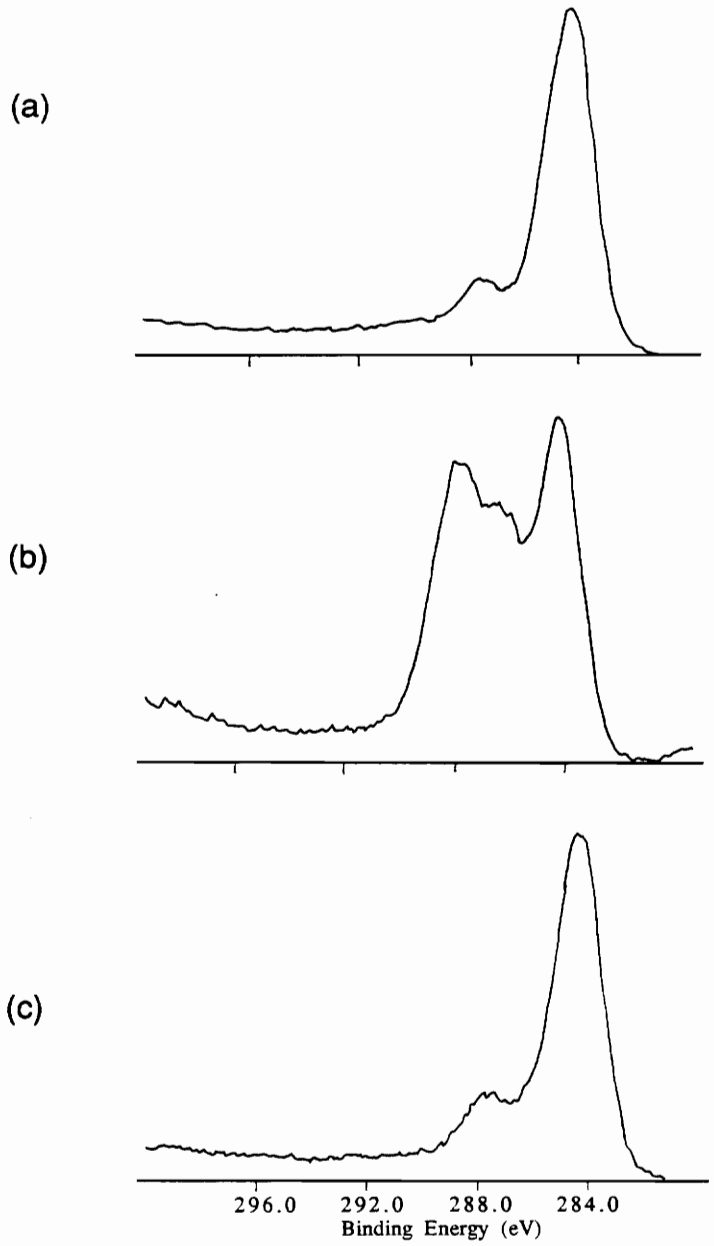

Figure 4.25: C1s photopeaks for (a) non-treated LaRC-TPI (b) oxygen plasma-treated LaRC-TPI (c) oxygen plasma-treated LaRC-TPI followed by methanol wash.

LaRC-TPI samples were deliberately contaminated with a fluorocarbon mold release agent to determine if it could be ablated in an oxygen plasma. Figure 4.26 shows the results of this experiment. It is seen that the fluorocarbon contamination greatly decreases the peel strengths as compared to the control. Oxygen plasma treatment improves the peel strength relative to the contaminated sample, but relative to the non-treated control, there is again seen a slight decrease in peel strength. Thus, the peel strength improvements which can be realized by removal of contamination can be great; however, what is considered to be an improvement depends on the baseline to which it is compared.

Figure 4.27 shows XPS C1s photopeaks for the oxygen plasma-treated LaRC-TPI samples contaminated with fluorocarbons. The intense high binding energy peak at ~292 eV is assigned to C-F species in the fluorocarbons. As the oxygen plasma treatment time increases, the intensity of this particular peak decreases until it is essentially non-detectable after 20 minutes, clearly showing the removal of the fluorocarbon residues. Correspondingly, the high binding energy region around ~288.0 eV increases in intensity due to the incorporation of oxygen into the surface.

4.4.4. Oxygen Plasma Treatment of High Density Polyethylene

Oxygen plasma treatment, contact angle analysis, XPS analysis and peel testing of high density polyethylene (HDPE) were carried out as a comparison to the polyimide materials. It was found for the polyimides that surface chain scission was the primary result of plasma treatment. In contrast, most polyolefin materials are known to undergo surface crosslinking as a consequence of

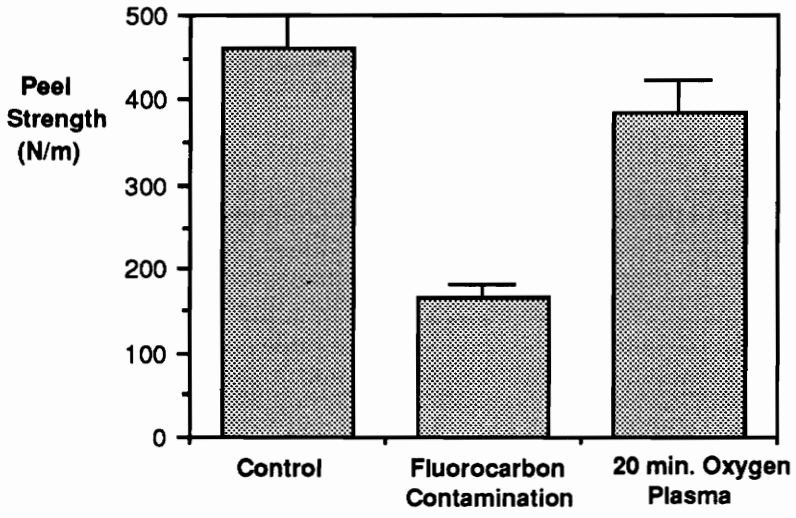

Figure 4.26: Peel test results for non-treated LaRC-TPI, fluorocarbon-contaminated LaRC-TPI, and fluorocarbon-contaminated LaRC-TPI followed by 20 minute oxygen plasma.

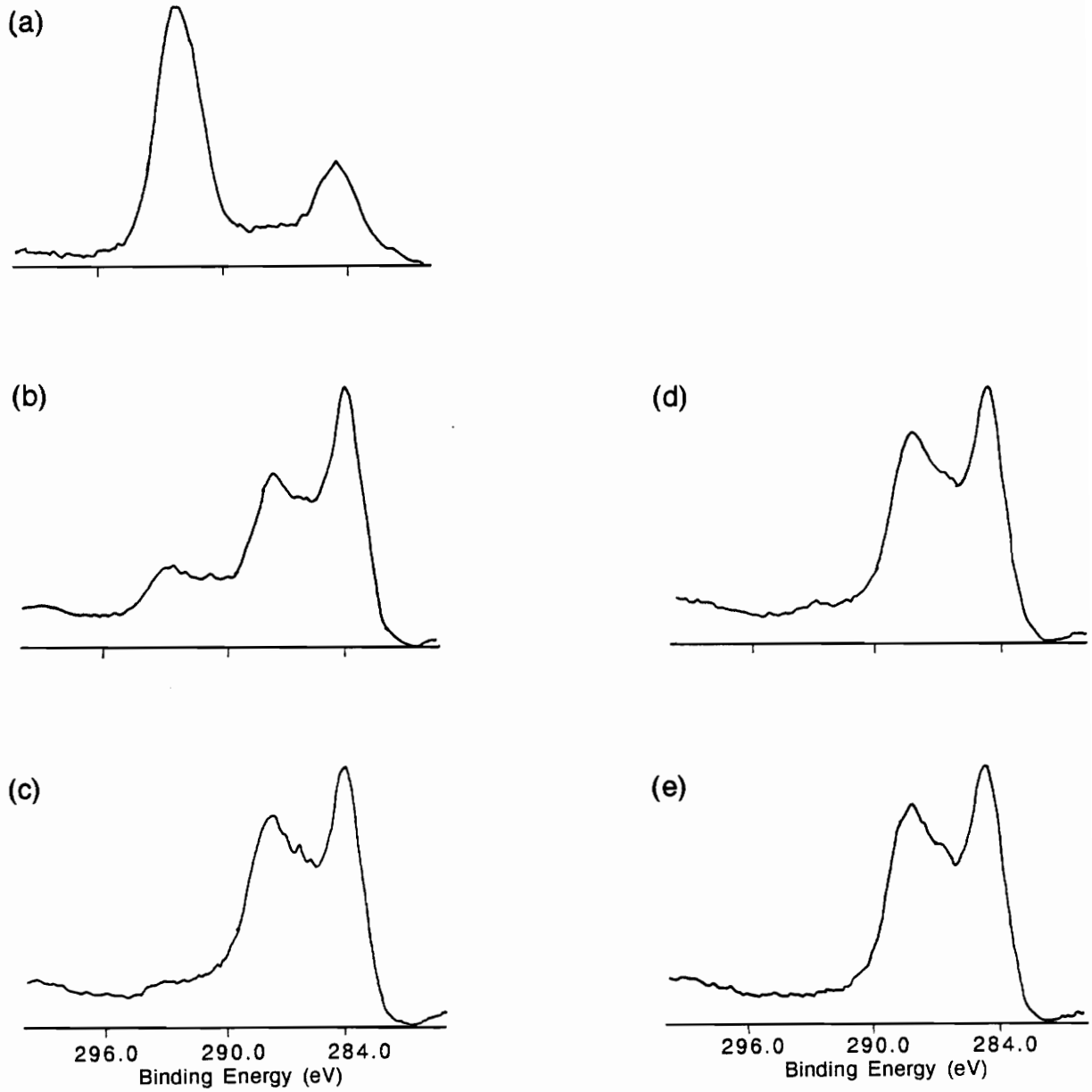

Figure 4.27: XPS C1s photopeaks of fluorocarbon-contaminated LaRC-TPI surface following oxygen exposure times of : (a) 0 minutes (b) 1 minute (c) 5 minutes (d) 10 minutes (e) 20 minutes.

irradiation with ionizing radiation [44,45,169-171]. It was expected that such differences in the physical state of the surface after crosslinking would cause differences in the level of adhesion.

Figure 4.28 shows the results of contact angle analysis for HDPE. HDPE, like the polyimides, also exhibits a high contact angle prior to plasma treatment. Wiping the surface with solvents actually causes the contact angle to increase. After oxygen plasma treatment, the contact angle decreases by more than 50%, indicating that a higher energy, more wettable surface has been created.

Changes in the C1s photopeak following oxygen plasma treatment of HDPE are shown in Figure 4.29. The oxygen atomic concentration on the surface increased from essentially zero before the plasma treatment to 26% after 5 minutes of treatment. Several new peaks are seen in the high binding energy region at 286.3, 287.7 and 289.3 eV, corresponding to the formation of C-O, C=O and O=C-O species, respectively.

When peel testing was carried out in the same manner as for the plasma-treated LaRC-TPI and Kapton® polyimides, the oxygen plasma-treated HDPE exhibited a 7-fold increase instead of a decrease in peel strength. These results are shown in Figure 4.30. Since polyethylene undergoes surface crosslinking instead of chain scission, no weak boundary layer is formed. Conversely, any low molecular weight material on the surface can be crosslinked into a more cohesively strong layer. The resulting increase in degree of surface oxidation is not accompanied by a decrease in the cohesive strength of the surface material and thus an increase in the level of adhesion is observed.

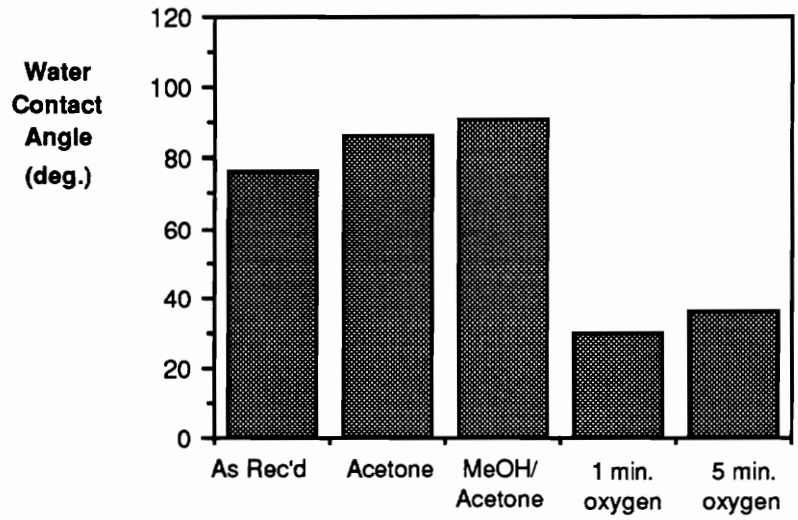

Figure 4.28: Contact angle analysis of as-received, solvent cleaned and oxygen plasma-treated high density polyethylene.

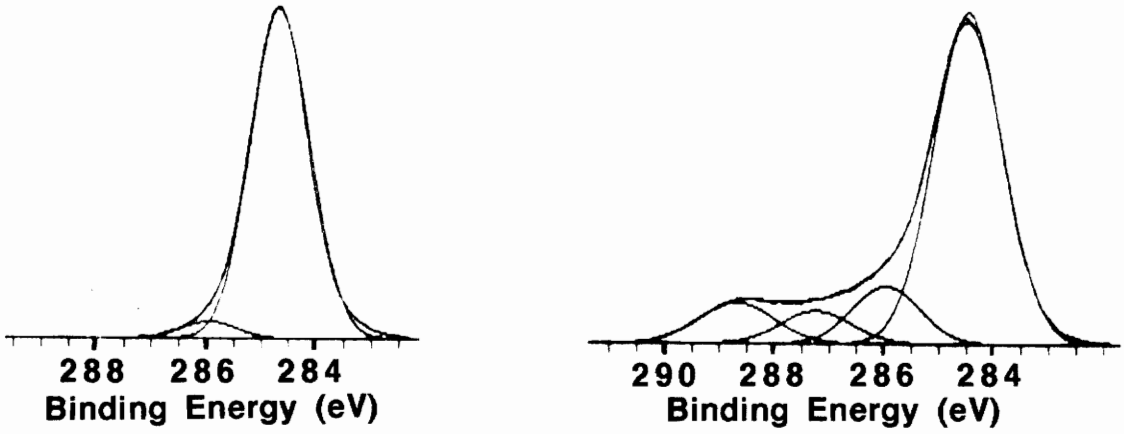

(a) (b)

Figure 4.29: XPS C1s photopeaks for (a) as-received and (b) oxygen plasma-treated high density polyethylene.

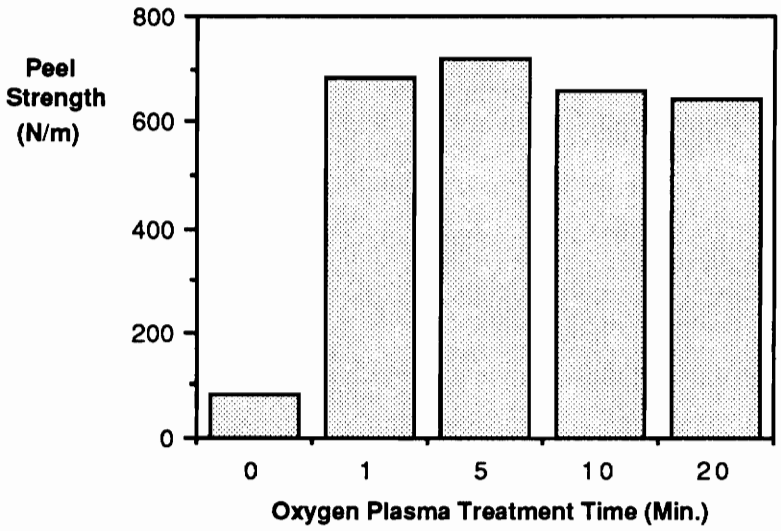

Figure 4.30: Peel test results for as-received and oxygen plasma-treated high density polyethylene.

Gleich et al. carried out lap shear bonding studies on plasma-treated polypropylene and polyimide coupons before and after plasma treatment [48]. It was found that for the polypropylene samples, increases in surface energy caused by the plasma treatment correlated with an increase in shear strength of the bonded samples. However, for the polyimide materials, there was no such correlation. Although the surface energies of the plasma-treated polyimides increased, no increases in lap shear strength were observed. This work supports the findings of this study, that is, the physical state of the surface plays a significant role in adhesive bonding.

4.4.5. Kapton® Bonding with Poly(ethersulfone)

A more realistic bonding situation involves the bonding of Kapton®, a high temperature polyimide film, with a high performance thermoplastic, poly(ethersulfone) (PES). The structure of PES is shown in Figure 4.31. It is an amorphous polymer and has a Tg in the vicinity of 223°C [172]. Since the formation of Kapton/PES joints involves melting the PES and heat-sealing the surfaces together, it is expected that this action might disrupt the low molecular weight fragments which result from plasma treatment. This disruption might cause the adhesion lowering effect seen with the PSA to be minimized.

Figure 4.32 shows the peel test results for the Kapton®/PES system. Two different thicknesses of Kapton® film were used, 2-mil and 5-mil. In all instances, the 2-mil film was peeled off the underlying 5-mil film. In contrast with the PSA bonding results, treatment in all three plasmas improves the peel strength of the Kapton®/PES joints. As mentioned above, it is possible that the

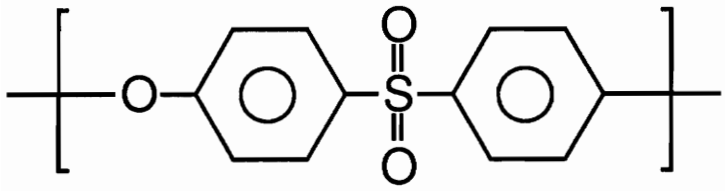

Figure 4.31: Structure of poly(ethersulfone).

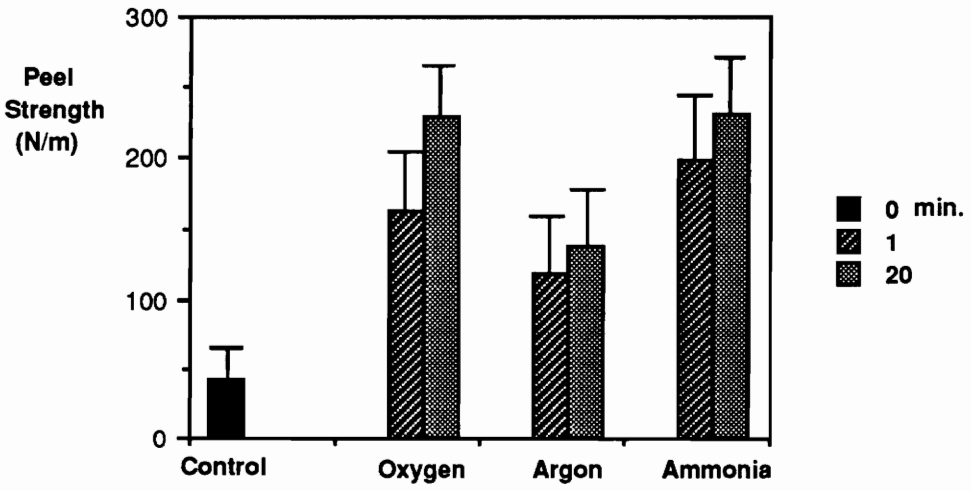

Figure 4.32: Peel test results for plasma-treated Kapton®/PES.

weak boundary layer has become disrupted or absorbed into the molten PES during bond formation, decreasing the dimensions of the fragile modified layer.

Results of XPS failure surface analysis are shown in Table 4.13. Both nitrogen and sulfur are used as tag elements to determine the average plane of failure, since the polyimide film contains no sulfur and PES contains no nitrogen. For the as-received control, failure has clearly taken place between the 2-mil film and the PES layer. No nitrogen is detected on the PES (5-mil film side) side of the failure surface. A surprising finding is that for all of the remaining plasma-treated samples, nitrogen and sulfur are detected on both peel surfaces. This could be indicative of an intermingling of low molecular weight material with the molten PES, forming a layer with intermediate properties through which failure propagates.

Table 4.13: XPS analysis of Kapton®/PES peel surfaces, 45° take-off angle.

		Atomic Concentration(%)			
		C	O	N	S
Non-treated	2-mil Side	75	18	6	1
	5-mil Side	77	17	0	6
1 min. Oxygen		76	16	7	1
		77	17	1	5
1 min. Argon		77	16	6	1
		75	18	1	6
1 min. Ammonia		77	15	7	1
		76	18	1	5
20 min. Oxygen		76	17	6	1
		75	17	2	6
20 min. Argon		77	16	6	1
		75	17	2	6
20 min. Ammonia		76	17	4	3
		76	16	7	1

V. Summary

As stated in the Introduction, the objective of this work was to characterize the surfaces of LaRC-TPI and Kapton® polyimides, two structurally dissimilar materials, after treatment with oxygen, argon and ammonia plasmas and to study the changes in the level of adhesion after plasma treatment. Surface-sensitive analytical techniques and peel testing were utilized to obtain information on the surfaces and interfaces involved.

Contact angle analysis revealed that the polyimide surfaces were more hydrophilic, as shown by a significant decrease in water contact angle, after treatment with each of the three plasmas. The reason for the increased wettability of the surface was shown by XPS and IR-RAS to be due to an increased concentration of surface polar groups. In the case of oxygen and argon plasmas, new species of oxygen-containing functional groups were created and the total atomic concentration of oxygen was increased. Also, higher than expected increases in the concentration of imide groups after oxygen and argon plasma treatment suggested a chain scission mechanism. Species in the ammonia plasma were determined to be attacking at carbonyl carbon sites, causing imide ring-opening and the subsequent formation of surface amide groups. The atomic concentration of surface nitrogen increased after ammonia plasma treatment. Shielding the polyimide surfaces with LiF windows showed that for oxygen and argon plasmas, the UV/VUV component of plasma is just as active as the entire plasma, whereas for the ammonia plasma direct contact with the particle flux is necessary for the observed changes in surface composition to occur.

XPS and IR-RAS were seen to be complementary techniques, in that the molecular bonding inferred by curve-fitting XPS photopeaks was confirmed by the presence of bands in the IR-RAS difference spectra. The results of XPS, HR-SEM and etch rate analysis by ellipsometry were also seen to be consistent in that the occurrence of chain scission inferred by XPS was supported by evidence from etch rate and HR-SEM analysis. Ablative effects and changes in surface topography shown by the etch rate experiments and HR-SEM photomicrographs, respectively, clearly revealed that for oxygen and argon plasma, significant molecular fragmentation was occurring.

Although LaRC-TPI and Kapton® are structurally dissimilar polyimides, many of the same changes in surface chemistry were observed after plasma treatments. Both showed increases in the concentration of oxygen-containing functional groups after oxygen and argon plasma treatments. Also, after ammonia plasma treatment, both polyimides showed strong evidence for amide functional group formation. The same mechanism for ammonia plasma reaction also appeared to be operative for both polyimides, as shown by the comparison of experimentally observed atomic concentrations and those of the hypothetical products.

Tape adhesion peel testing with a PSA as an adhesive was instrumental in showing the weak cohesive strength of the plasma-modified layer. These peel test results were related to the results of surface analysis in which all evidence suggested the formation of an oxidized, low molecular weight layer. The PSA tape did not disturb the plasma-modified layer but was able to distinguish between the non-treated, plasma-treated and plasma-

treated/methanol rinsed surfaces. In this particular instance, the PSA peel test was shown to be a sensitive probe of the interphase region.

Plasma treatment improved tape adhesion peel strengths in the specific cases of fluorocarbon-contaminated polyimide surfaces, high density polyethylene and in bonding with poly(ether sulfone). Adhesion was increased in the case of the fluorocarbon-contaminated surface due to the removal of the low energy fluorocarbon material. For high density polyethylene, although surface oxidation occurred, chain scission did not take place since polyolefins undergo surface crosslinking when bombarded with high energy radiation. Thus, no weak boundary layer was created on the surface of high density polyethylene. The results of Kapton® bonding with PES showed that the action of the molten thermoplastic during formation of the joint may have disrupted the plasma-modified layer sufficiently to allow increases in the level of adhesion.

In conclusion, the combined use of surface analysis techniques and peel testing has shown that the nature of the modified surface, both chemical and physical, is critical in potential adhesive bonding applications. The complementary nature of the various techniques shows the importance of characterizing the plasma-treated surface in a number of different ways. Finally, both the chemical and physical nature of the modified surfaces were seen to be important in the final level of adhesion which can be attained with a particular adhesive.

VI. References

1. T. Takekoshi, *Advances in Polymer Science*, vol. 94 (Springer-Verlag, Berlin, 1990).
2. G. Odian, *Principles of Polymerization*, 2nd ed. pp. 153-155 (John Wiley and Sons, New York, 1981).
3. S. Witzler, *Adv. Compos.,* p. 50 (Sept./Oct. 1990).
4. A.M. Thayer, *Chemical and Engineering News*, p. 37 (July 23, 1990).
5. J. King, M. Chaudhari and G. DiSalvo, *Proc. of the 32nd International SAMPE Symposium,* 59 (1987).
6. M.A. Chaudhari in *Looking Ahead for Materials and Processes*, J. de Bossu, G. Briens and P. Lissac, eds., p. 469 (Elsevier Science Publishers, Amsterdam, 1987).
7. J. Verbicky, Jr., "Polyimides" in *Encyclopedia of Polymer Science and Engineering,* 2nd ed., vol. 12, p. 364(John Wiley and Sons, New York, 1988).
8. F.W. Billmeyer, Jr., *Textbook of Polymer Science*, 3rd ed., pp. 427-428 (John Wiley and Sons, New York, 1984).
9. P.M. Hergenrother, *ChemTech*, 496 (Aug.1984).
10. C.E. Sroog, A.L. Endrey, S.V. Abramo, C.E. Berr, W.M. Edwards and K.L. Olivier, *J. Polym.Sci.*, **A3**, 1373 (1965).
11. C.E. Sroog, *J. Polym. Sci. - Macromol. Rev.*, **11**, 161 (1976).
12. J.A. Kreuz, A.L. Endrey, F.P.Gay and C.E. Sroog, *J. Polym. Sci.*, **A1(4)**, 2607 (1966).

13. R. Delasi, *J. Appl. Polym. Sci.*, **16**, 2909 (1972).

14. R.A. Dine-Hart and W.W. Wright, Jr., *J. Appl. Polym. Sci.*, **11**, 609 (1967).

15. M.C. Buncick and D.D. Denton, *J.Vac. Sci. Technol.*, **A9(2)**, 350 (1991).

16. H.J. Leary Jr. and D.S. Campbell, *Surf. Interface Anal.*, **1(3)**, 75 (1979).

17. "Kapton® Polyimide Film", DuPont Product Bulletin, 1985.

18. V.L. Bell, B.L. Stump and H. Gager, *J. Polym Sci. - Polym. Chem. Ed.*, **14**, 2275, 1976.

19. V.L. Bell, *"Process for Preparing Thermoplastic Aromatic Polyimides"*, U.S. Patent 4,094,862, June 13, 1978.

20. T.L. St. Clair and D.J. Progar, *Polym. Prepr.*, **16(1)**, 538 (1975).

21. A.K. St. Clair and T.L. St. Clair, *NASA Technical Memorandum 84516*, June 1982.

22. N.J. Johnston, T.L. St. Clair, R.M. Baucom and T.W. Towell, *NASA Technical Memorandum 101568*, March 1989.

23. N.J. Johnston and T.L. St. Clair, *SAMPE Preprints*, **18,** 53 (1986).

24. T.L. St. Clair, H.D. Burks, N.T. Wakelyn and T.H. Hou, *Polym. Prepr.*, **28(1)**, 90 (1987).

25. J.T. Mullerleille and G.L.Wilkes, *Polym. Prepr.*, **31(2)**, 211 (1990)

26. T.L. St. Clair, J.R. Pratt and D.J. Progar, *NASA Tech Briefs*, 55 (July 1990).

27. H.V. Boenig, *Plasma Science and Technology* (Cornell University Press, Ithaca, 1982).

28. "Plasma Technology", *Kirk-Ohmer Encyclopedia of Chemical Technology*, 3rd ed., vol. 18, p. 599 (John Wiley and Sons, New York, 1978).

29. F.K. McTaggart, *Plasma Chemistry in Electrical Discharges* (Elsevier, Amsterdam, 1967).

30. A.T. Bell and J.R. Hollahan, *Techniques and Applications of Plasma Chemistry* (John Wiley and Sons, New York, 1974).

31. S.L. Kaplan and P.W. Rose, *Plastics Engineering*, **44(5)**, 77 (1988).

32. E.M. Liston, *J. Adhes.*, **30**, 199 (1989).

33. D.T. Clark and A. Dilks, *J. Polym. Sci. - Polym. Chem. Ed.*, **15**, 2321 (1977)

34. J.R. Hollahan and B.B. Stafford, *J. Appl. Polym. Sci.*, **13**, 807 (1969).

35. A.T. Bell and K. Kwong, *AIChE J.* , **18(5)**, 990 (1972).

36. R.L. McCarthy, *J. Chem. Phys.*, **22,** 1360 (1954).

37. A.M. Mearns and A.J. Morris, *J. Phys. Chem.*, **74**, 3999 (1970).

38. H. Yasuda, *J. Macromol. Sci. - Chem.*, **10(3)**, 383 (1976).

39. N. Inagaki, S. Tasaka and H. Kawai, *J. Adhe. Sci. Technol.*, **3(8)**, 637 (1989).

40. B. Tung, D.M. Polynski and S.T. Terney, *SAMPE Quarterly*, **19(5)**, 36 (1988).

41. L.M. Siperko and R.R. Thomas, *J. Adhe. Sci. Technol.*, **3**, 157 (1989).

42. Y. Momose, T. Ohaku, H. Chuma, S. Okazaki, T. Samta, M. Masui and M. Takeuchi, *J. Appl. Polym. Sci. - Appl. Polym. Symp.*, **46**, 153 (1990).

43. R.H. Hansen and H. Schonhorn, *J. Polym. Sci. - Polym. Letters Ed.*, **4**, 203 (1966).

44. M. Hudis and L.E. Prescott, *J. Polym. Sci. - Polym. Letters Ed.*, **10**, 179 (1972).

45. R.H. Hansen and H. Schonhorn, *J. Appl. Polym. Sci.*, **11**, 1461 (1967).

46. D.M. Brewis and D.J. Briggs, *Polymer,* **22**, 7 (1981).

47. E. Occhiello, M. Morra, G. Morini, F. Garbassi and P. Humphrey, *J. Appl. Polym. Sci.*, **42**, 551 (1991).

48. H. Gleich, R.M. Criens, H.G. Mosle and U. Leute, *Int. J. Adhes. Adhes.*, **9(2)**, 88 (1989).

49. N. Inagaki, S. Tasaka, H. Kawai and Y. Kimura, *J. Adhe. Sci. Technol.*, **4(2)**, 99 (1990).

50. H. Yasuda, H.C. Marsh, S. Brandt and C.N. Reilley, *J. Polym. Sci. - Polym. Chem. Ed.*, **15**, 991 (1977).

51. B.L. Chow and D.J. Whittle, *J. Adhe. Sci. Technol.*, **2(5)**, 363 (1988).

52. T. Vargo, J.A. Gardella and L. Salvati, *Polym. Prepr.*, **28(1)**, 31 (1987).

53. H.F. Webster and J.P. Wightman, *J. Adhe. Sci. Technol.*, **5(1)**, 93 (1991).

54. G.M. Porta, Ph.D. Dissertation, Virginia Polytechnic Institute and State University, 1989.

55. Y. Yasuda, H.C. Marsh, S. Brandt and C.N. Reilley, *J. Polym. Sci. - Polym. Chem. Ed.*, **15**, 991 (1977).

56. D.S. Dunn and D.J. McClure, *J. Vac. Sci. Technol.*, **A5(4)**, 1327 (1987).

57. J.H. Cross, M.W. LeMay and D.J. McClure, *J. Vac. Sci. Technol.*, **A3(3)**, 49 (1985).

58. T.A. Giroux and S.L. Cooper, *J. Colloid Interface Sci.*, **139(2)**, 351 (1990).

59. G. Joseph and C.P. Shama, *J. Biomed. Mater. Res.*, **20**, 677 (1986).

60. S.L. Kaplan, T.S. Dunn and P.W. Rose, *"Medical Polymers and Plasma Technology"*, Plasma Science Technical Note 8/88 No. 5.

61. C.G. Golander and W.G. Pitt, *Biomaterials*, **11**, 32 (1990).

62. M.R. Wertheimer and H.P. Schreiber, *J. Appl. Polym. Sci.*, **26**, 2087 (1981).

63. L.S. Penn, T.J. Byerley and T.K. Liao, *J. Adhes.*, **23,** 163 (1987).

64. Y.I. Mitchenko, V.A. Fenin and A.S. Chegolya, *J. Appl. Polym. Sci.*, **41**, 2561 (1990).

65. E.L. Lawton, *J. Appl. Polym. Sci.*, **18**, 1557 (1974).

66. C. Jones and E. Samman, *Carbon*, **28(4)**, 509 (1990).

67. Ibid., 515 (1990).

68. A. Benatar and T.G. Gutowski, *Polym. Compos.*, **7**, 84 (1981).

69. R.E. Allred and L.A. Harrah, *Proc. of the 34th Intl. SAMPE Symp.*, 2559 (1989).

70. J.G. Dillard and I.M.Spinu, *J. Adhes.*, **31**, 137 (1990).

71. A.J. Kinloch, B.R.K. Blackman and J.P. Dear, U.S. Army Research Development and Standardization Group (UK), 4th Interim Report, March 1990.

72. S.L. Kaplan, P.W. Rose and D.A. Frazer in *How To Apply Advanced Composites Technology,* Proc. of the Advanced Composites Conference IV, p. 193 (ASM International, Dearborn, 1988).

73. D.J.D. Moyer and J.P. Wightman, *Surf. Interface Anal.*, **14**, 496 (1989).

74. P. Bodo and J.E. Sundgren, *J.Vac. Sci. Technol.*, **A6(4)**, 2396 (1988).

75. Kyung W. Paik and A.L. Ruoff, *J. Adhe. Sci. Technol.*, **4(6)**, 465 (1990).

76. R.G. Nuzzo, Y.H. Wong and G.P. Schwartz, *Langmuir*, **3**, 1136 (1987).

77. K.W. Lee, S.P. Kowalczyk and J.M. Shaw, *Macromolecules*, **23(7)**, 2097 (1990).

78. P.C. Stancil, E.R. Long, S.A.T. Long and W.L. Harries, *Polym. Prepr.*, **32(1)**, 644 (1991).

79. G.S. Arnold and D.R. Peplinski, *AIAA J.*, **23(10)**, 1621 (1985).

80. T.S. Oh, S.P. Kowalczyk, D.J. Hunt and J. Kim, *J. Adhe. Sci. Technol.*, **4(2)**, 119 (1990).

81. A.D. Katnani, A. Knoll and M.A. Mycek, *J. Adhe. Sci. Technol.*, **3(6)**, 441 (1989).

82. B.J. Bachman and M.J. Vasile, *J. Vac. Sci. Technol.*, **A7(4)**, 2709 (1989).

83. R. Flitsch and D.Y. Shih, *J. Vac. Sci. Technol.*, **A8(3)**, 2376 (1990).

84. D.S. Dunn, J.L. Grant and D.J. McClure, *J. Vac. Sci. Technol.*, **A7(3)**, 1712 (1989).

85. F.D. Egitto, F. Emmi and R.S. Horwath, *J. Vac. Sci. Technol.*, **B3(3)**, 893 (1985).

86. S. Lazare and R. Srinivasan in *Recent Advances in Polyimide Science and Technology*, W.D. Weber and M.R. Gupta, eds., p. 407 (Society of Plastics Engineers, 1987).

87. W.C. Wake, *Adhesion and the Formulation of Adhesives*, 2nd ed. (Applied Science Publishers, London, 1982).

88. K.L. Mittal, *J. Vac. Sci. Technol.*, **13(1)**, 19 (1976).

89. P.J. Hine, S. El. Mudarris and D.E. Packham, *J. Adhe. Sci. Technol.*, **1(1)**, 69 (1987).

90. D.E. Packham in *Adhesion Aspects of Polymeric Coatings*, K.L. Mittal, ed. (Plenum Press, New York, 1983).

91. G.D. Bucci and R.D. Savage, *PC Fab.*, p. 22 (July 1986).

92. D.J. Arrowsmith, *Trans. Inst. Met. Finish.*, **48**, 88 (1970).

93. J.J. Bikerman, *The Science of Adhesive Joints*, 2nd ed. (Academic Press, 1982).

94. D.M. Brewis and D. Briggs, *Polymer*, **22**, 7 (1981).

95. W.A. Duke and A.J. Kinloch in *Developments in Adhesion* - 1, W.C. Wake, ed., p. 251 (Applied Science Publishers, London, 1977).

96. G.L. Schneberger, *Adhesives Age*, p. 18 (May 31, 1985).

97. R.J. Good, *J. Adhes.*, **4**, 133 (1972).

98. D. Tabor and R.H.S. Winterton, *Proc. R. Soc. London*, **A312**, 435 (1969).

99. K.W. Allen, *J. Adhes.*, **21**, 261 (1987).

100. S.S. Voyutskii, *Autohesion and Adhesion of High Polymers*, V. Vakula, ed. (Wiley Interscience, New York, 1963).

101. D.L. Allara, F.M. Fowkes, J. Noolandi, G.W. Rubloff and M.V. Tirrell, *Mater. Sci. Eng.*, **83**, 213 (1986).

102. B.V. Derjaguin and V.P. Smilga, *J. Appl. Phys.*, **38**, 4609 (1967).

103. M. Zhenyi, F. Jiawen and J.T. Dickinson, *J. Adhes.*, **25**, 63 (1988).

104. H. von Harrach and B.N. Chapman, *Thin Solid Films*, **13**, 157 (1972).

105. V. N. Kestelman, S.S. Negmatov and Y.M. Evdokimov, *Int. J. Adhes. Adhes.*, **8(3)**, 171 (1988).

106. F.M. Fowkes in *Physicochemical Aspects of Polymer Surfaces*, vol. 2, K.L. Mittal, ed., p. 583 (Plenum Press, New York, 1983).

107. F.M. Fowkes, *J. Adhe. Sci. Technol.*, **4(8)**, 669 (1990).

108. J.C. Bolger in *Adhesion Aspects of Polymeric Coatings*, K.L. Mittal, ed., p. 3 (Plenum Press, New York, 1983).

109. A.W. Adamson, *Physical Chemistry of Surfaces,* 5th ed. (John Wiley and Sons, New York, 1990).

110. E.M. Petrie, *Adhesives Age*, p. 6 (May 15, 1989).

111. D.J. Zalucha in *High Performance Adhesive Bonding*, G. DeFrayne, ed., p. 60 (Society of Manufacturing Engineers, Michigan, 1983).

112. G.P. Anderson, S.J. Bennett, K.L. DeVries, *Analysis and Testing of Adhesive Bonds* (Academic Press, New York, 1977).

113. *1990 Annual Book of ASTM Standards*, vol 15.06 Adhesives (American Society for Testing and Materials, Philadelphia, 1990).

114. A.N. Gent and G.R. Hamed, *Polym. Eng. Sci.*, **17(7)**, 462 (1977).

115. A.N. Gent and S.Y. Kaang, *J. Adhes.*, **24**, 173 (1987).

116. J.R. Huntsberger in *Treatise on Adhesion and Adhesives* - 6, R.L. Patrick, ed., p. 1 (Marcel Dekker, New York, 1989).

117. A.J. Kinloch, *J. Adhes.*, **10**, 193 (1979).

118. T. Igarashi in *Adhesive Joints: Formation, Characteristics and Testing,* K.L. Mittal, ed., p. 419 (Plenum Press, New York, 1984).

119. G.R. Hamed in *Treatise on Adhesion and Adhesives* - 6, R.L. Patrick, ed., p. 33 (Marcel Dekker, New York,1989).

120. J. Kim, K.S. Kim and Y.H. Kim, *J. Adhe. Sci. Technol.*, **3(3)**, 175 (1989).

121. J. Johnston, *Adhesives Age*, p. 30 (Dec. 1990).

122. A.N. Gent and G.R. Hamed, *Rubber Chem. Technol* ., **55**, 483 (1982).

123. J.J. Aklonis and W.J. MacKnight, *Introduction to Polymer Viscoelasticity*, 2nd ed. (John Wiley and Sons, New York, 1983).

124. J.D. Ferry, *Viscoelastic Properties of Polymers*, 3rd ed. (Wiley, New York, 1980).

125. D.W. Aubrey in *Adhesion* - 3, K.W. Allen, ed., p. 191(Applied Science Publishers, London, 1979).

126. A.J. Kinloch and M.L. Yuen, *J. Adhes.*, **30**, 151 (1989).

127. G.R. Hamed, *J. Adhes.*, **13,** 101 (1981).

128. A.W. Czanderna, ed., *Methods of Surface Analysis* (Elsevier, New York, 1975).

129. D. Briggs in *Practical Surface Analysis by Auger and X-ray Photoelectron Spectroscopy*, D. Briggs and M.P. Seah, eds., p. 359(John Wiley and Sons, London, 1983).

130. R. Holm and S. Storp, *Surf. Interface Anal.*, **2(3)**, 96 (1980).

131. A. Dilks in *Electron Spectroscopy - Theory, Techniques and Applications,* vol. 4, C.R. Brundle and A.D. Baker, eds., p. 277 (Academic Press, London,1981).

132. R.T. Conley, *Infrared Spectroscopy* (Allyn and Bacon, Inc., Boston, 1966).

133. P.R. Griffiths and J.A. deHaseth, *Fourier Transform Infrared Spectrometry* (John Wiley and Sons, New York, 1986).

134. H. Ishida, *Rubber Chem. Technol.,* **60(3)**, 497 (1987).

135. J.F. Rabolt, M. Jurich and J.D. Swalen, *Appl. Spectrosc.,* **39(2)**, 269 (1985).

136. F. Boerio, C.A. Gosselin, R.G. Dillingham and H.W. Liu, *J. Adhes.*, **13**, 159 (1981).

137. M. Morra, E. Occhiello and F. Garbassi, *Adv. Colloid Interface Sci.*, **32**, 79 (1990).

138. J. Brandrup and E.H.Immergent, eds., *The Polymer Handbook* , 3rd ed. (John Wiley and Sons, New York, 1989).

139. H.J. Leary and D.S. Campbell, *Surf. Interface Anal.*, **1(3)**, 75 (1979).

140. H.J. Leary and D.S. Campbell in *Photon, Electron and Ion Probes of Polymer Structure and Properties*, vol. 162, p. 419, D.W. Dwight, T.J. Fabish and H.R. Thomas, eds. (American Chemical Society, Washington, 1981).

141. J. Russat, *Surf. Interface Anal.*, **11(8)**, 414 (1988).

142. M.C. Buncick and D.D. Denton, *J.Vac. Sci. Technol.*, **A9(2)**, 350 (1991).

143. L.P. Buchwalter, *J.Vac.Sci. Technol.*, **A7(3)**, 1772 (1989).

144. P.L. Buchwalter and A.I. Baise in *Polyimides: Synthesis, Characterization and Applications,* vol. 1, p. 537, K.L. Mittal, ed. (Plenum Press, New York, 1974).

145. J.K. Kochi, *Free Radicals* , vol. 2 (John Wiley and Sons, New York, 1973).

146. C.D. Wagener, W.M. Riggs, L.E. Davis and J.F. Moulder, *Handbook of X-ray Photoelectron Spectroscopy*, G.E. Muilenberg, ed. (Perkin-Elmer Corp., Eden Prairie, 1979).

147. J.K. Rabek, *Mechanisms of the Photophysical Processes and Photochemical Reactions in Polymers: Theory and Applications* (John Wiley and Sons, New York, 1987).

148. OptoVac, Inc. product information for Lithium Fluoride single crystal material.

149. S. Lazare and R. Srinivasan in *Recent Advances in Polyimide Science and Technology*, W.D. Weber and M.R. Gupta, eds., p. 407 (Society of Plastics Engineers, 1987).

150. R.M. Silverstein, G.C. Bassler and T.C. Morrill, *Spectrometric Identification of Organic Compounds*, 4th ed. (John Wiley and Sons, New York, 1981).

151. L.M. Harwood and C.J. Moody, *Experimental Organic Chemistry: Principles and Practice* (Blackwell Scientific Publishers, Oxford, 1989).

152. L.J. Bellamy, *The Infra-red Spectra of Complex Molecules* (John Wiley and Sons, New York, 1975).

153. R.T. Morrison and R.N. Boyd, *Organic Chemistry*, 4th ed. (Allyn and Bacon, Inc., Boston, 1983).

154. C.J. Pouchert, *The Aldrich Library of Infrared Spectra*, edition III (Aldrich Chemical Company, Milwaukee, 1981).

155. P.R. Young, M.A. Druy, W.A. Stevenson and D.A.C. Compton, *Proceedings of the 20th International SAMPE Technical Conference*, Minneapolis, MN, 1988.

156. P.D. Frayer in *Polyimides: Synthesis, Characterization and Applications*, vol. 1, K.L Mittal, ed. (Plenum Press, New York, 1984).

157. H. Ishida, S.T. Wellinghoff, E. Baer and J.L. Koenig, *Macromolecules*, **13**, 826 (1980).

158. D.S. Dunn, J.L. Grant and D.J. McClure, *J. Vac. Sci. Technol.*, **A7(3)**, 1712 (1989).

159. R. Flitsch and D.Y. Shih, *J. Vac. Sci. Technol.*, **A8(3)**, 2376 (1990).

160. A. Toth, I. Bertoti, T. Szekely, J.N. Sazanov, T.A. Antonova, A.V. Shchukarev and A.V. Gribanov, *Surf. Interface Anal.*, **8**, 261 (1986).

161. G.H. Williams, *Homolytic Aromatic Substitution* (Pergamon Press, New York, 1960).

162. E.S. Huyser, *Free Radical Chain Reactions* (John Wiley and Sons, New York, 1970).

163. K.P.C. Vollhardt, *Organic Chemistry* (W.H. Freeman and Co., New York, 1987).

164. F.A. Carey and R.J. Sundberg, *Advanced Organic Chemistry*, 2nd ed. (Plenum Press, New York, 1985).

165. T.D. Lin, M.S. Thesis, Virginia Polytechnic Institute and State University, 1990.

166. M. Strobel, C. Dunatov, J.M. Strobel, C.S. Lyons, S.J. Perron and M.C. Morgen, *J. Adhes. Sci. Technol.*, **3(5)**, 321 (1989).

167. D.M. Brewis, *Prog. Rubber Plast. Technol.*, **1**, 1 (1985).

168. C.Y. Kim, J. Evans and D.A.I. Goring, *J. Appl. Polym. Sci.*, **15**, 1365 (1971).

169. H. Schonhorn, F.W. Ryan and R.H. Hansen, *J. Adhes.*, **2**, 93 (1970).

170. D. Briggs and C.R. Kendall, *Int. J. Adhes. Adhes.*, **2(1)**, (13)1982.

171. D. Briggs, *J. Adhes.*, **13**, 287(1982).

172. Stabar S100 Technical Data, August 1989.

APPENDIX: XPS Analysis of Standards

In order to make more definitive determinations of the identity of surface functional groups following plasma treatment, various standards containing functional groups of interest were analyzed by x-ray photoelectron spectroscopy. Samples were obtained in film, fiber, pellet or powder forms and analyzed as received by the procedure described in the Experimental section. C1s, O1s and N1s (if applicable) photopeaks were curve-fitted to obtain information on functional groups.

Figure A.1 shows the chemical structures of the compounds which were analyzed. Nylon 6,6, and poly(methylmethacrylate) were obtained in film form. Phenyl benzoate, phthalimide, terephthalic acid and poly(vinyl phenol) were analyzed as powders which were deposited on the XPS mounts using double-sided tape. Polycarbonate was analyzed as a pellet and Kevlar® as a fiber tow. Table A.1 shows the functional groups and their corresponding curve-fitted binding energies.

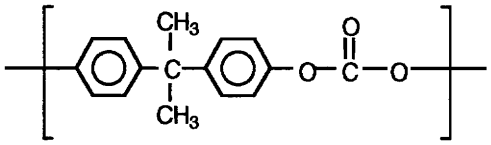

(A)

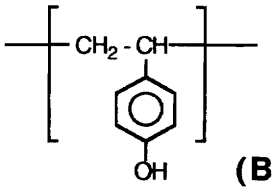

(B)

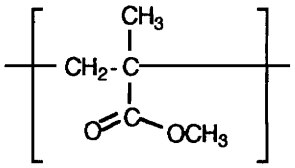

(C)

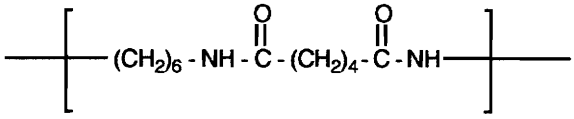

(D)

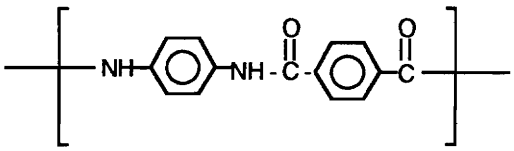

(E)

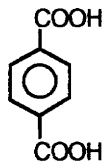

(F)

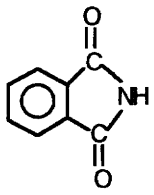

(G)

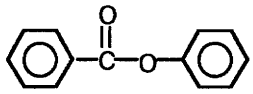

(H)

Figure A.1: Chemical structures of XPS standards. (A) bisphenol A polycarbonate (B) poly(vinyl phenol) (C) poly(methyl methacrylate) (D) nylon 6,6 (E) Kevlar®, poly(imino-1,4-phenylene imino terephthaloyl) (F) terephthalic acid (G) phthalimide (H) phenyl benzoate

Table A.1: Functional groups and binding energies of XPS standards.

		Binding Energy (eV)		
Standard	Functional Group	C1s	O1s	N1s
polycarbonate	$O=C(O)_2$ (carbonate)	285.9, 290.4	533.7, 534.3	------
poly(vinyl phenol)	C-OH (hydroxyl)	286.2	533.4	------
poly(methyl methacrylate)	O=C-O-C (ester)	286.1, 288.4	531.7, 533.2	------
nylon 6,6	O=C-NH-C (aliphatic amide)	285.7, 287.6	531.3	399.6
Kevlar®	O=C-NH-C (aromatic amide)	286.1, 287.9	531.4	399.7
terephthalic acid	O=C-OH (carboxylic acid)	289.1	532.0, 533.4	------

		Binding Energy (eV)		
Standard	Functional Group	C1s	O1s	N1s
phthalimide	O=C-N-C=O (imide)	288.3	531.7	399.9
phenyl benzoate	O=C-O-C (ester)	286.0, 288.9	531.4, 533.5	------

VITA

The author, Joannie W. Chin, was born in Pingtung, Taiwan, R.O.C. on April 7, 1965 to Dr. and Mrs. Hsien Chang Wang. Her family moved to Cleveland, Ohio in 1966 and she graduated from Richmond Heights High School in 1982. In the fall of that year, she entered Case Western Reserve University, majoring in polymer science and engineering. While attending CWRU, she participated in the Society of Women Engineers and the Society of Plastics Engineers. She also took part in undergraduate research with Dr. Hatsuo Ishida. During the summers of 1984 and 1985 she worked as a summer intern at the Dow Chemical Company in Granville, Ohio and the Standard Oil Company in Cleveland, Ohio, respectively. She graduated from CWRU in 1986 with high honors.

The author married Albert B. Chin in July of 1986 and began working as a research scientist in the research and development laboratories of Gould, Inc., Foil Division in Eastlake Ohio. She was employed there for three years, working in the areas of polymer/metal adhesion, adhesives for electronic applications and copper foil processing. In the fall of 1989, she entered the graduate program in chemistry at Virginia Polytechnic Institute and State University, working under the guidance of Dr. James P. Wightman. She was awarded an Adhesive and Sealant Council Fellowship in 1991 to study plasma modification of polyimides. The author is also a member of Tau Beta Pi, Sigma Xi, the Adhesion Society and the American Chemical Society.